Additional MSc thesis

Bi-stable interlocks of sutured ABS geometries- A numerical study in Abaqus

Sofia Papoulidou

October 2022

An additional thesis submitted to the Delft University of Technology in partial fulfillment of the requirements for the degree of Master of Science in Civil Engineering

Supervisors: Dr. Ir. M. Lukovic
Dr. Branko Šavija

Abstract

Concrete elements, partially or entirely prefabricated are becoming more and more popular in engineering practice. The biggest challenge in this process is the realization of connections between components. These connections fall within two categories: Precast-to-precast connections with hardened parts and precast-to-in situ connections, where an in-situ concrete element needs to adhere to a precast element. Some kind of interlocking surface might be effectual in both situations. Geometrical interlocking that exists in natural materials (turtle shells, diatoms) is the main inspiration for interlocking mechanisms in engineering practice. The concept of bistable interlocks has been introduced in the past few years to theoretical mechanics. These interlocks could allow many stable positions before the connection collapses, and may provide an additional "safety boundary" in brittle concrete-to-concrete connections by spreading the nonlinear deformations through the material and making the transformed material less brittle and more damage tolerant. In this research, the properties of bistable interlocked materials will be explored based on the numerical models built. These properties are immediately correlated to the experiments performed. Sensitivity analyses are performed to investigate the parameters that can lead to the optimal behavior of the sutured geometries.

Acknowledgments

The previous year at Delft University of Technology was difficult yet great. I've learned a lot that I'll keep with me for the rest of my life, not just the coming year of my master's program. So I want to thank TU Delft for this wonderful experience.

First and foremost, I would want to express my gratitude to the Civil Engineering Department, in particular the Concrete Structures department, for allowing me to enroll in the MSc. Additional thesis course. It has been an incredibly educational journey and a great preparation for my thesis.

I am appreciative of my supervisors for this Additional thesis, Professor dr. Mladena Lukovic and Dr.Branko Šavija. Professor Mladena Lucovic with her enthusiasm over the subject motivated me to move forward and was always there to support me with her guidance and advice during this additional thesis. Dr. Branko was always available to check my progress and gave me great input during this project. I want to thank them both deeply for their help and understanding during this journey.

I also want to mention the support and help regarding Abaqus of the PhD candidate Yading Xu. I am forever grateful to my friends and classmates for sharing with me this incredible year at TU Delft. Special thanks are in order to my friend Androniki Pavlidou who helped me and motivated me to compose this report.

I am grateful to my mum for her unwavering belief in me. My partner Antonis Tzioumakas deserves a special mention for his encouragement and support during my most difficult days.

Contents

List of Figures

Acronyms

BIM Bistable Interlocked Material

ABS Acrylonitrile Butadiene Styrene

1 Introduction

1.1 Mechanical Interlocking in Interfaces

Geometric interlocking mechanisms are important in engineering materials like adhesives, metals, composites, and natural materials like diatoms and shells. The mechanisms of geometrical interlocking in nature acted as inspiration for geometries and materials in engineering with ”enhanced” attributes.

In the paper (Mirkhalaf and Barthelat, 2017) a new form of sutured material was developed based on jigsaw-like morphologies that geometrically can be designed to lock into two stable states **(equilibrium positions)**.

In this research (Mirkhalaf and Barthelat, 2017), is shown that with careful modification of the architecture of the tabs, the mechanical response of these bi-stable materials can be engineered. This modification was made possible by the use of 3D printing and design exploration. A main benefit of the mechanical interlock mechanism is that without visible damage accumulation, the system can be cycled between two equilibrium points multiple times. Staying in the linear elastic regime is really important to ensure **reversible deformations**. It is also explained how to make the second equilibrium position more stable than the first, essentially offering a **geometric hardening mechanism** to postpone the localization of strains and to spread nonlinear deformations. Additionally, another enhanced property was the significantly improved **toughness** of the bi-stable interlocked material (compared to the polymer they are made of).

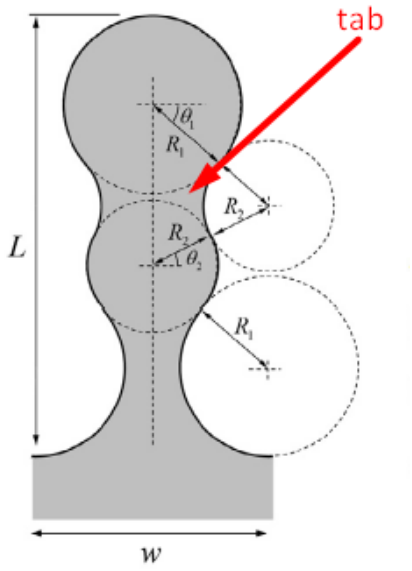

Figure 1.1: Overview of the suture geometry and tabs

This leads to the main research question of this additional thesis which is to validate the results of the BIM (Bistable interlocked materials) model presented in the paper, with numerical models in Abaqus and to explore different variations of the initial model and their properties in comparison with the initial one. This main research question can be divided into subquestions:

1. How the sutured material can be modeled?
2. How the sutured geometries behave under tensile tests?
3. Could the experimental results presented in the paper (Mirkhalaf and Barthelat, 2017) be verified with the use of numerical models?
4. Could the initial numerical model be optimized by the examination of models with different critical parameters?

1.2 Sutures and geometry

Sutures with elaborate geometries interlocking, can ensure the strong and frequently compliant connection of structural parts and this can also be seen in nature: Some examples are ammonite shells, the beak of red-bellied woodpeckers and the shell of sea turtles.

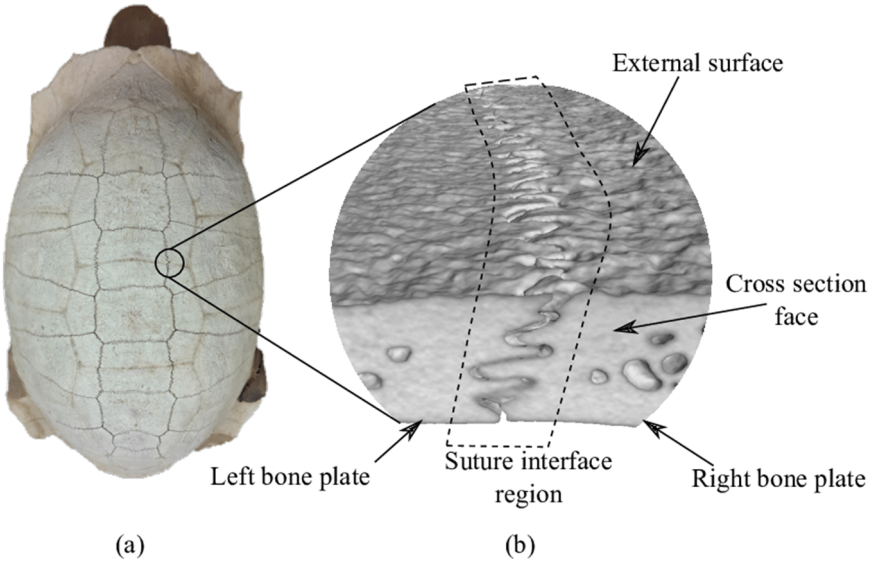

Figure 1.2: Sutured geometries in nature (Alheit et al., 2021)

As mentioned before, sutures can produce significant deformations, toughness, and damping in ordinarily brittle systems and materials. This principle can be implemented for the design of sutured geometries in engineering to create materials with enhanced properties.

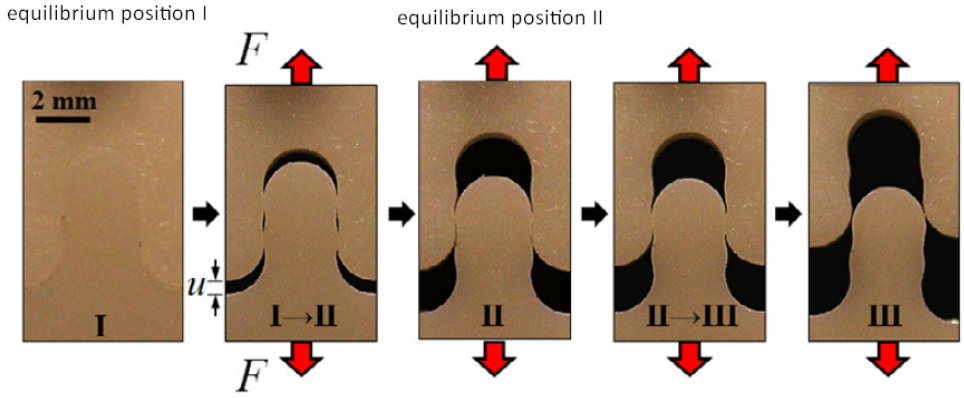

Figure 1.3: Sutured geometries under tensile test (Mirkhalaf and Barthelat, 2017)

For the model examined in the paper (Mirkhalaf and Barthelat, 2017) the non-linear traction behaviour is generated by the frictional pull-out of the jigsaw tabs, and this mechanism can act as a source of progressive locking and ”geometric hardening,” which delays deformation localization and disperses non-elastic deformations over wide areas of the material.

1.3 Material -ABS

The material used for this research was **ABS** (Acrylonitrile Butadiene Styrene). ABS is an engineering plastic with a homogeneous distribution of butadiene part over an acrylonitrile-styrene matrix. It has outstanding toughness, dimensional stability, processing ease, chemical resistance, and affordability. It does, however, have inherent weaknesses in terms of mechanical strength, fragility and conductibility (Olivera et al., 2016).

The specific type of ABS used as the foundation material was a UV-curable acrylonitrile butadiene styrene (ABS, EnvisionTech Perfactory, MI, US) (Mirkhalaf and Barthelat, 2017). ABS is a stiff and strong polymer (flexural strength = 118±12 MPa, tested empirically with flexural tests), but it is also brittle, with a flexural strain at failure of 0.112±0.18 (Mirkhalaf and Barthelat, 2017). The interlocking tab's two solid components, were 3D printed separately and then they were connected. To make the connection, they were slid together along the out-of-plane axis.

For a brittle material as ABS, the benefit of this hardening mechanism is that massive deformations can be spread and this can ensure delocalization of strains. As a result the fracture toughness can be severely improved.

Additionally, this approach is used in fiber-reinforced composites, topologically interlocked materials and glass. Glass, which is also a stiff and hard material but with brittle behavior and low toughness showed promising results. Specifically modified glass can resist about two to four times more impact energy than plain glass panels by embedding internal architectures engraved into the material by using three-dimensional laser engraving (Mirkhalaf et al., 2016). Similar mechanisms (topologically interlocked materials) have already shown very interesting results in ceramics such as improving the strength and toughness (Mirkhalaf et al., 2018).

2 Project Framework

2.1 Design of sutures

In this chapter the complex suture geometry used is going to be explained along with the mechanism of friction activated due to the tensile forces. The theory behind this mechanism is crucial to understand and to use as a foundation for the numerical analysis that will be performed in a later stage.

2.1.1 Mechanism & Equilibrium Positions

The bi-stable interlocking materials investigated in this paper are built from sutures with precisely-defined geometries. The suture's shape is based on jigsaw-like pieces created by tangentially blending a sequence of arcs of circles with radii R_1 and R_2 at positions indicated by angles θ_1 and θ_2 as can be observed in figure 2.1. The two parts of the interlocked tab were first manufactured one by one, using 3D printing, and then were slid together in the out of plane direction.

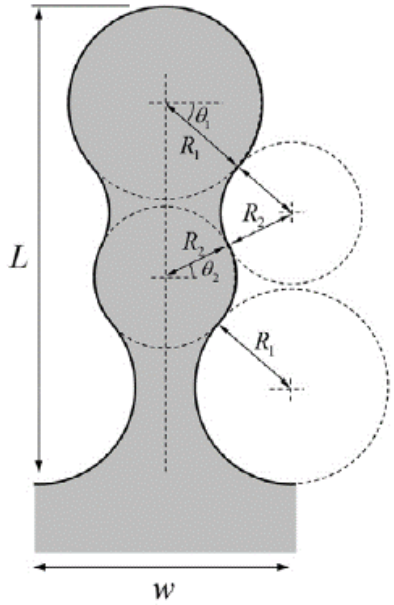

Figure 2.1: Geometry of one interlocked tab (Mirkhalaf and Barthelat, 2017)

The tabs and their parameters are of primal importance for the behavior of the total geometry. No adhesive was used in this process, to highlight the mechanical interlocking effect (with contact mechanics and friction) that is governing the interaction (Mirkhalaf and Barthelat, 2017).

The interlocking mechanism works as follows:

As the initial configuration is at equilibrium, it provides the system with the first stable position (**stage I**). Then, as the tabs are pulled out of their starting position due to tensile stresses applied across the suture line (**stage I**→ **stage II**), the pull-out is resisted by geometric interference, contact stresses, and friction acting at two pairs of contact points (Malik et al., 2017).

With more pull-out stresses applied, the tabs' ends move to the second cavity-like position, locking the system in the second stable state (**stage II**).

At this point, if compression is applied to the tabs, the system returns to the first stable position (**stage II**→ **stage I**), as can be seen in figure 2.2. This is the benefit mentioned before, that with cycling of the system between 2 stable positions, reversible deformations can be achieved and the system can stay in the linear regime.

Alternatively, if more tension is applied to the tabs (**stage II**→ **stage III**) it will be pulled out completely (**stage III**)(Mirkhalaf and Barthelat, 2017). This case is going to be examined in this research.

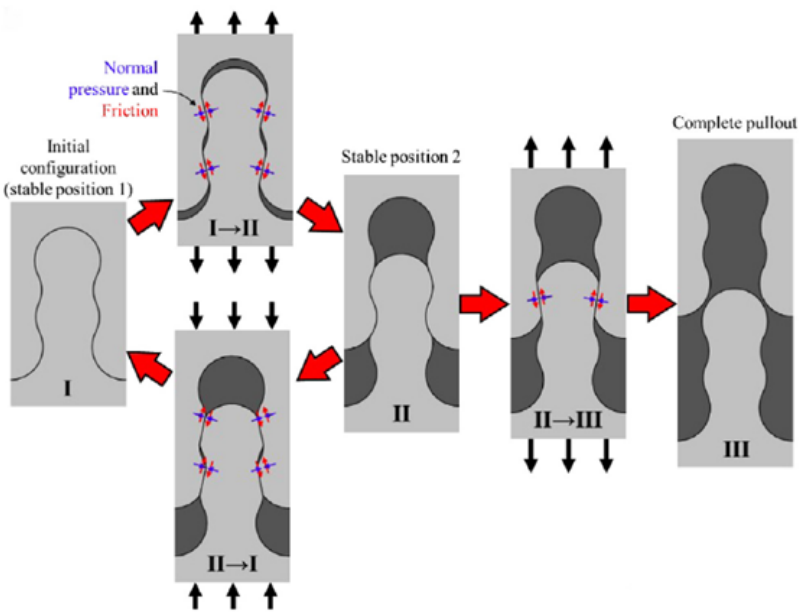

Figure 2.2: Equilibrium positions while tensile stresses are applied to the specimen (Mirkhalaf and Barthelat, 2017)

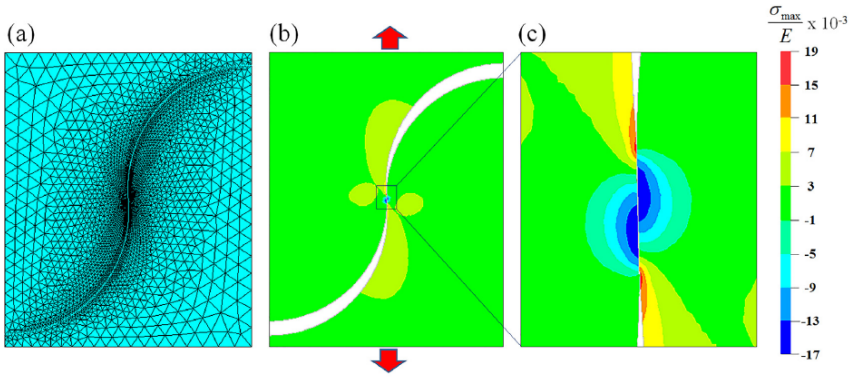

Figure 2.3: Contact stresses as a function of normalized pullout distance (Malik et al., 2017)

2.1.2 Design variations & parameters

A small number of geometric parameters can be used to program the system's mechanical reaction across its various states. Higher locking angles, for example, increase the geometric interference and the required force for pull-out. Additionally, the radius R_1 can be made bigger than R_2 to increase the force required for the complete pull-out. Because all of the mechanisms rely on bulk material elasticity and friction, there is no specific length scale connected with them, hence the non-dimensional R_1/R_2 was employed. Furthermore, a closer look at the geometry reveals that the four parameters (R_1, R_2, θ_1 , θ_2) are not independent of each other.
In the paper (Mirkhalaf and Barthelat, 2017) the parameters used for 3D printing of the samples were different combinations of interlocking angles (θ_1 = 5°, 15°, 25°, 35°) and different radii ratio (R_1/R_2 = 1, 1.03, 1.05, 1.06) to investigate the design and performance of this interlocked suture. All the samples had a thickness t = 2 mm.

By defining the main parameters θ_1 and R_1/R_2, it was possible to find other parameters of interest that depend on the main parameters. The most important are:

- the angle θ_2
- the length L
- the width w

The formulas below show how they are connected to the main parameters:

$$\theta_2 = cos^{-}1 * [1/2 * (R_1/R_2 + 1) * cos(\theta_1)] \tag{2.1}$$

$$L = 2 * [R_1 * (1 + sin(\theta_1) + R_2 * (sin(\theta_1) + sin(\theta_2))] \tag{2.2}$$

$$w = 2 * (R_1 + R_2) * cos(\theta_1) \tag{2.3}$$

Here it should be mentioned that the parameters should be chosen from an admissible range, that ensures the interlocking effect is working. For example, the cases where $R_1/R_2 < 1$ can result in loose and unstable second equilibrium locations, and hence only the cases with $R_1/R_2 \geq 1$ are mechanically and functionally significant. It is expected to have excessive loads and tab fracture in circumstances where the interlocking angle θ_1 and/or the ratio R_1/R_2 are too high, which would be an undesirable failure mode for the suture since it can result in tab fracture. In the figure below, the admissible domain for the main parameters R_1/R_2 and θ_1 is depicted:

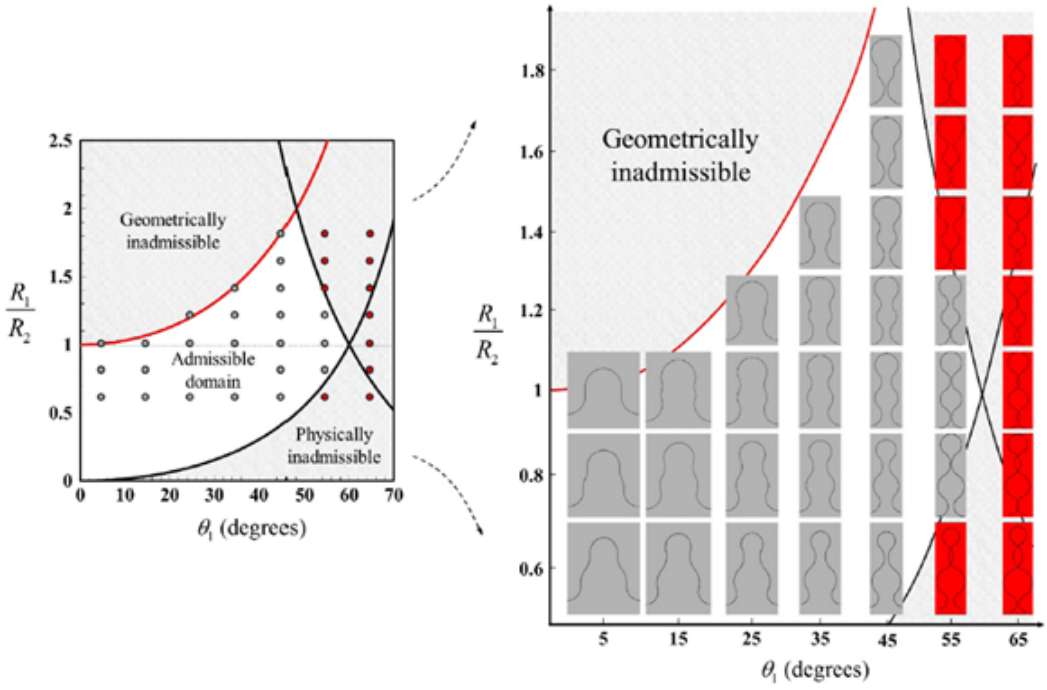

Figure 2.4: Admissible domain for the design of the tabs (Mirkhalaf and Barthelat, 2017)

Figure 2.5 makes even more clear the relationship between the geometry of the tabs and the stresses generated in them. It is clear that higher ratio $R_1/R_2 > 1$ and θ_1 result in stronger tabs as the interlocking effect is more pronounced, but there may be fracture of the solid material.

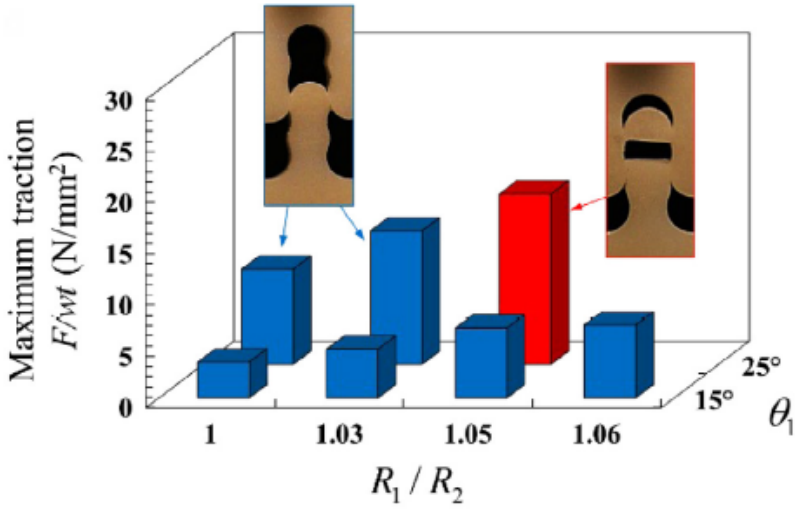

Figure 2.5: Effect of R_1/R_2 and θ_1 on the maximum pullout traction (Mirkhalaf and Barthelat, 2017)

2.2 Execution & testing of sutures (3D printing)

As mentioned before, during the execution, the parameters tested for 3D printing of the samples were different combinations of interlocking angles (θ_1 = 5°, 15°, 25°, 35°) and different radii ratio (R_1/R_2 = 1, 1.03, 1.05, 1.06). All the samples had a thickness of t = 2 mm.

The 3D printer used, was a high-resolution 3D printer (EnvisionTech's Micro HiRes Machine) that uses Digital Light Processing (DLP) technology. This method allows for the printing of pore-free, homogeneous, and mechanically isotropic components. The printer's high spatial resolution (80 μ m) allowed for great morphological fidelity and smooth surfaces, which were necessary for a consistent friction coefficient and minimization of stress concentrations (Mirkhalaf and Barthelat, 2017) .

The two solid parts that made up the interlocking tabs were 3D printed separately before being combined by sliding them together in an out-of-plane motion. The assembly was performed smoothly and required very little force in the out-of-plane direction (Mirkhalaf and Barthelat, 2017).

The gap at the interfaces after assembly was roughly 8 μ m, according to detailed microscopy of the individual pieces with various combinations of θ_1 and R_1/R_2. This distance was broad enough to assure that the formed solid tabs were free of stresses before testing, but small enough to assume that the tabs were initially in contact for the sake of the analysis.

To minimize in-plane bending and deformation modes that are not representative of a long suture line, the total width of the sample was approximately six times the width of the individual tabs (after experimental verification that the total width of the sample was large enough to have no effect on the mechanical response of the individual tabs) (Mirkhalaf and

Barthelat, 2017). A tiny loading machine was used to perform tensile testing on the tabs in quasi-static circumstances (displacement rate = 5 μ m/s).

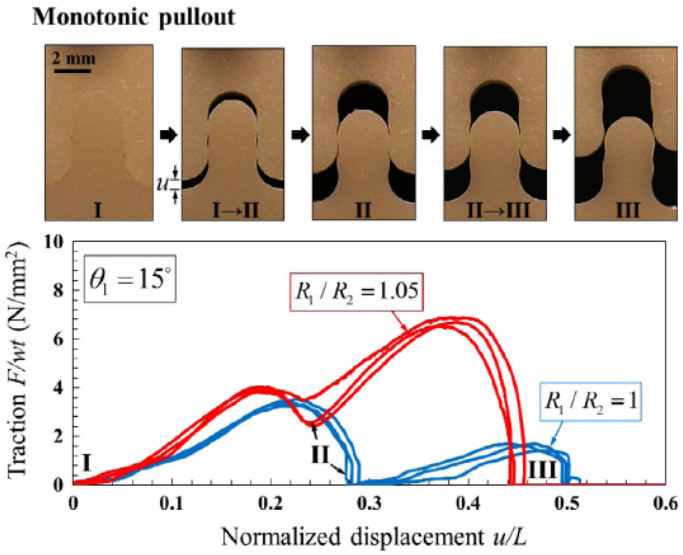

Figure 2.6: Force traction relation for different parameters of samples (Mirkhalaf and Barthelat, 2017)

For each arrangement (set of parameters θ_1 and R_1/R_2), three samples were tested and the figure 2.6 displays a collection of typical tensile responses. F/wt is used for traction and u/L is used for pullout displacement, to derive a measure of the effective traction and deformation for the suture. Initially, the pullout traction grew, with normal and frictional forces at two pairs of contact points resisting the tab's removal. The traction reached the first maximum and as the tab was approaching its second stable point, it dropped to a local minimum on the curve, **(stage II)**. When the tab was pulled out even more (between **stage II** and **stage III**) the same mechanism took place (governed by contact and friction). In that stage, there was a single pair of contact points but the friction mechanism worked in the same way.

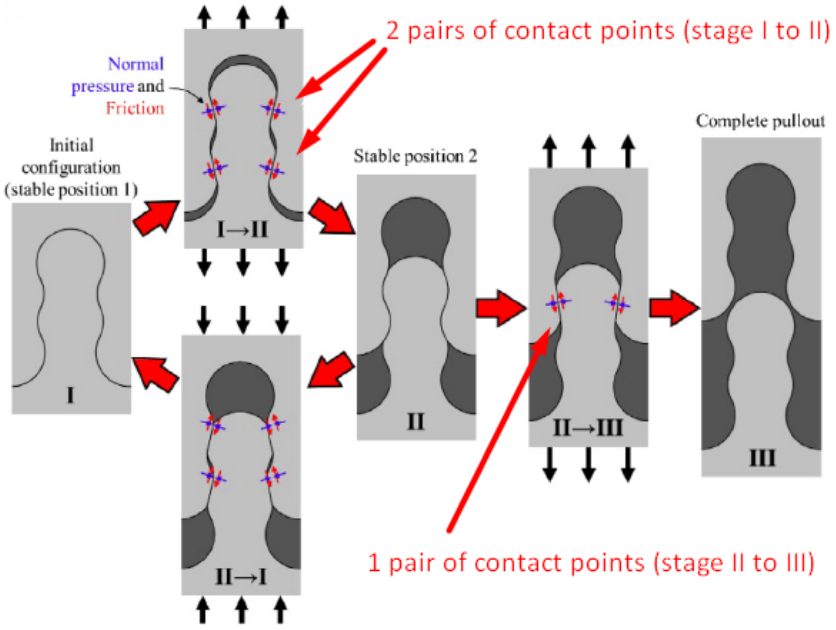

Figure 2.7: Contact points pairs during the pull-out test (Mirkhalaf and Barthelat, 2017)

Two basic geometry cases were investigated and are going to be the main cases for the numerical models:

- $R_1/R_2 = 1$
- $R_1/R_2 = 1.05$

As it can be seen in 2.6 these cases although with a very similar geometry have quite different responses.

- In the case of $R_1/R_2 = 1$ the traction begins to increase until it reaches a local maximum due to the contact stresses generated from the tensile forces applied to the suture. Then the traction at the equilibrium position II was zero because the interlocking parts fitted without any stresses. Then the second peak was *lower than the first* as it can be seen in figure 2.6. Specifically, the second peak was only half of the traction at the first peak. This makes the system more vulnerable to tension (once the second equilibrium position is reached) and it does not help with the general stability.
- In the case of $R_1/R_2 = 1.05$ the traction increased until it reached a local maximum due to the contact stresses generated from the tensile forces applied to the suture (between **stage I** and **stage II**). Then as the equilibrium position II was reached the traction was higher than the previous case (where it was zero) because there were some contact stresses even in the interlocked position between the tabs since the R_1 should fit in a smaller cavity (radius R_2). Then as expected since the second tab had a larger radius than the first, the second peak was higher than the first as can be seen in figure 2.6.

It is obvious from the figure that a slight change in the geometry of the tabs (from $R_1/R_2 = 1.0$ to $R_1/R_2 = 1.05$) can increase the first peak and greatly increase the second peak. This

means that a higher force was required to displace the tab from equilibrium position II and to complete pullout. This property can be particularly important for improving the stability of materials made up of many suture lines.

Also another benefit is if the suture is subjected to cyclic loading the system can be cycled multiple times between positions I and II. The mechanical response of the tab is the same along numerous cycles, indicating that bringing the system back and forth between positions I and II does not diminish the overall performance (Mirkhalaf and Barthelat, 2017) . This conclusion suggests that the system, is totally driven by elastic deformations of the tabs, contact mechanics, and friction, and has no permanent damage.

The bistable interlocking materials (BIMs) exhibit improvements in toughness and strain at failure of up to 10 folds when compared to normal ABS, but a 10–30 fold reduction in strength and modulus (for instance, bistable cellular materials are two to four orders of magnitude softer than the solid materials from which they are made (Restrepo et al., 2015)). This method can be utilized to make customized sutures using other kinds of materials, other interfaces, and various length scales. The final material will be more ductile due to a hardening mechanism since deformations and strains can spread along the element.

3 Model & Variations

3.1 General

In this chapter, it is going to be thoroughly presented the step-by-step approach on how the numerical models were built in Abaqus in order to be compared with the experimental results of the paper (Mirkhalaf and Barthelat, 2017). All the design choices are paramount to make a numerical model as close as the physical models to verify them but also to find the key parameters on how to optimize them in a later stage.

3.2 Model geometry in Autocad

To create a complex geometry in Abaqus was challenging and the accuracy of the interlocking features (R_1/R_2, θ_1, θ_2) was expected to be quite high so the geometry of one suture (with specific R_1/R_2 ratio and specific θ_1 and θ_2 angles as of in the paper (Mirkhalaf and Barthelat, 2017)) was created in Autocad.

In total, *3 different geometries* were employed and these variations will be mentioned in the sub-chapter 3.4. The aim of these variations is to make a solid comparison with the initial model and highlight how the force and displacement relation is affected but the changes of the geometrical parameters of the tabs.

The *main model geometry* that was used was $R_1/R_2 = 1.05$, and according to the formulas (see Chapter "Project Framework" formulas 2.1, 2.2, 2.3) was found $\theta_1 = 15^\circ$, $\theta_2 = 8^\circ$, $w = 3.96$ mm and $L = 3.44$mm.

The 3 different geometry models are presented in the following figures:

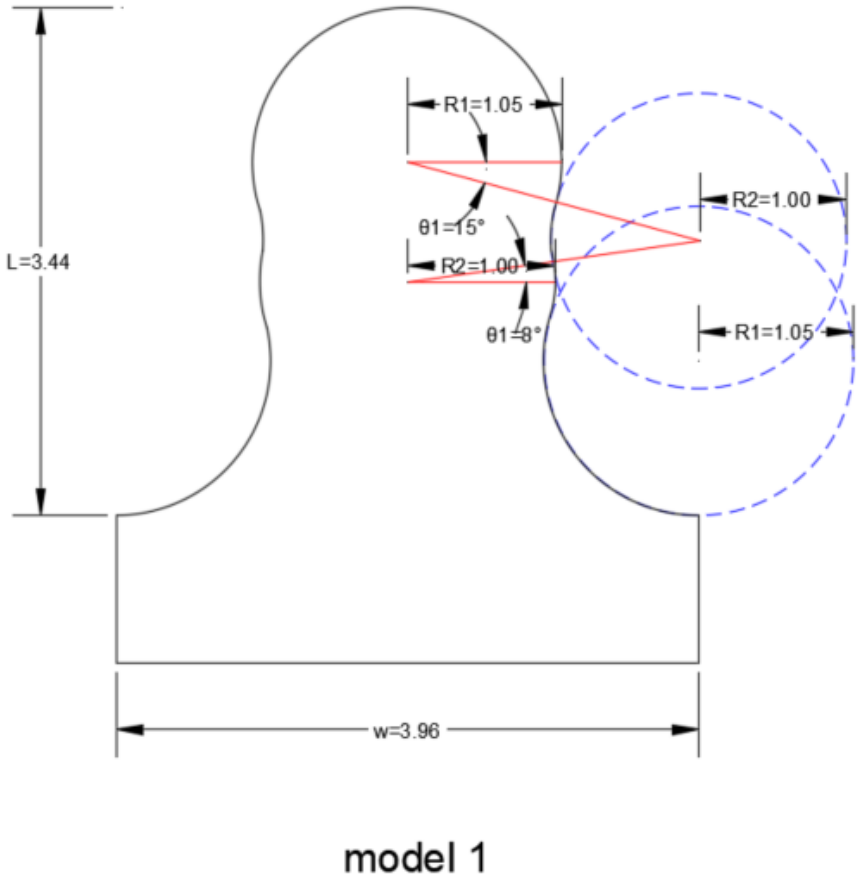

Figure 3.1: Initial model (Geometry 1)

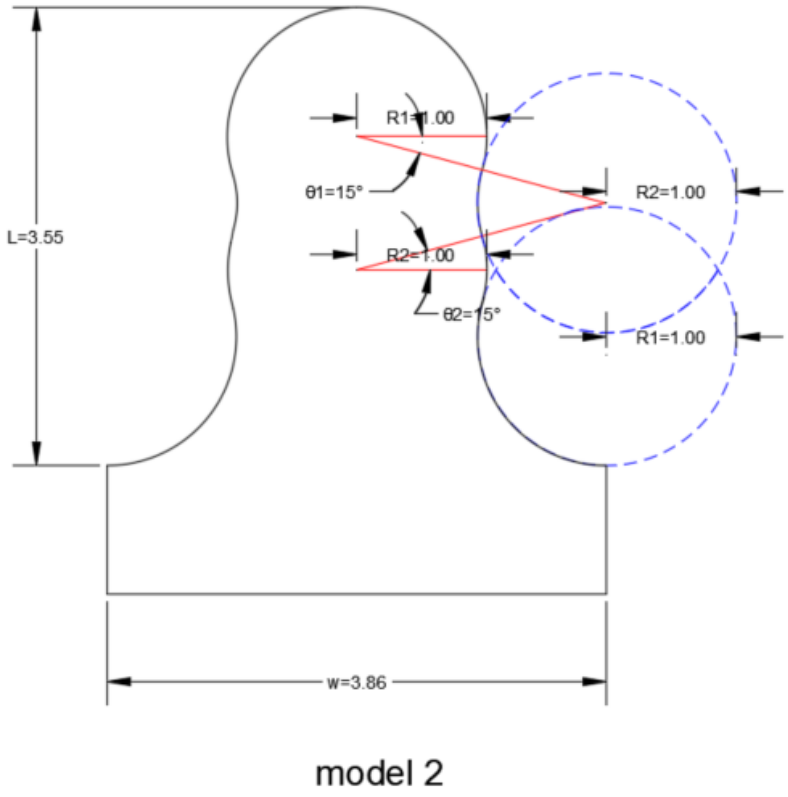

Figure 3.2: Geometry 2

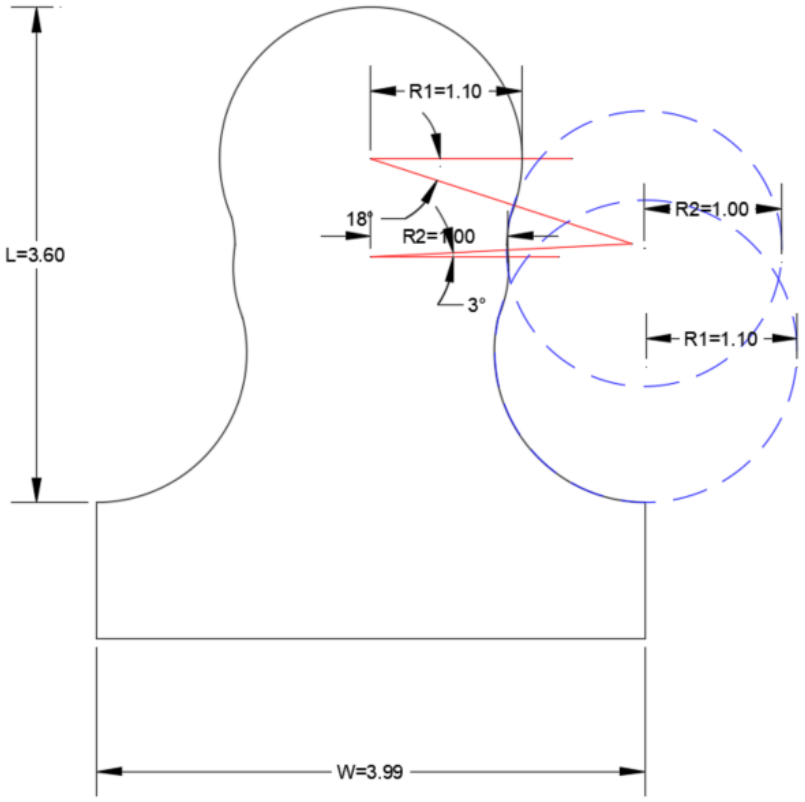

Figure 3.3: Geometry 3

3.3 Model in Abaqus

Abaqus CAE modelling software is a software that is used for both pre-processing (modeling and analysis of mechanical parts and assemblies) as well as for viewing the outcome of finite element analysis. For more info visit Abaqus CAE website.

For this particular application Abaqus CAE software was chosen to model the complex interface of the 2 pieces that the suture is made of. Abaqus is quite efficient when it comes to nonlinear problems with several contact interactions. In this case the complexity of the geometry of the tab composed of 2 arcs of different radii ratio and angles was high and sensitive to even small changes of these parameters.

The modelling procedure in Abaqus follows the model database or ”tree”. This model tree contains all the information about the simulation as different modules. This is presented in more detail in the flowchart 3.4.

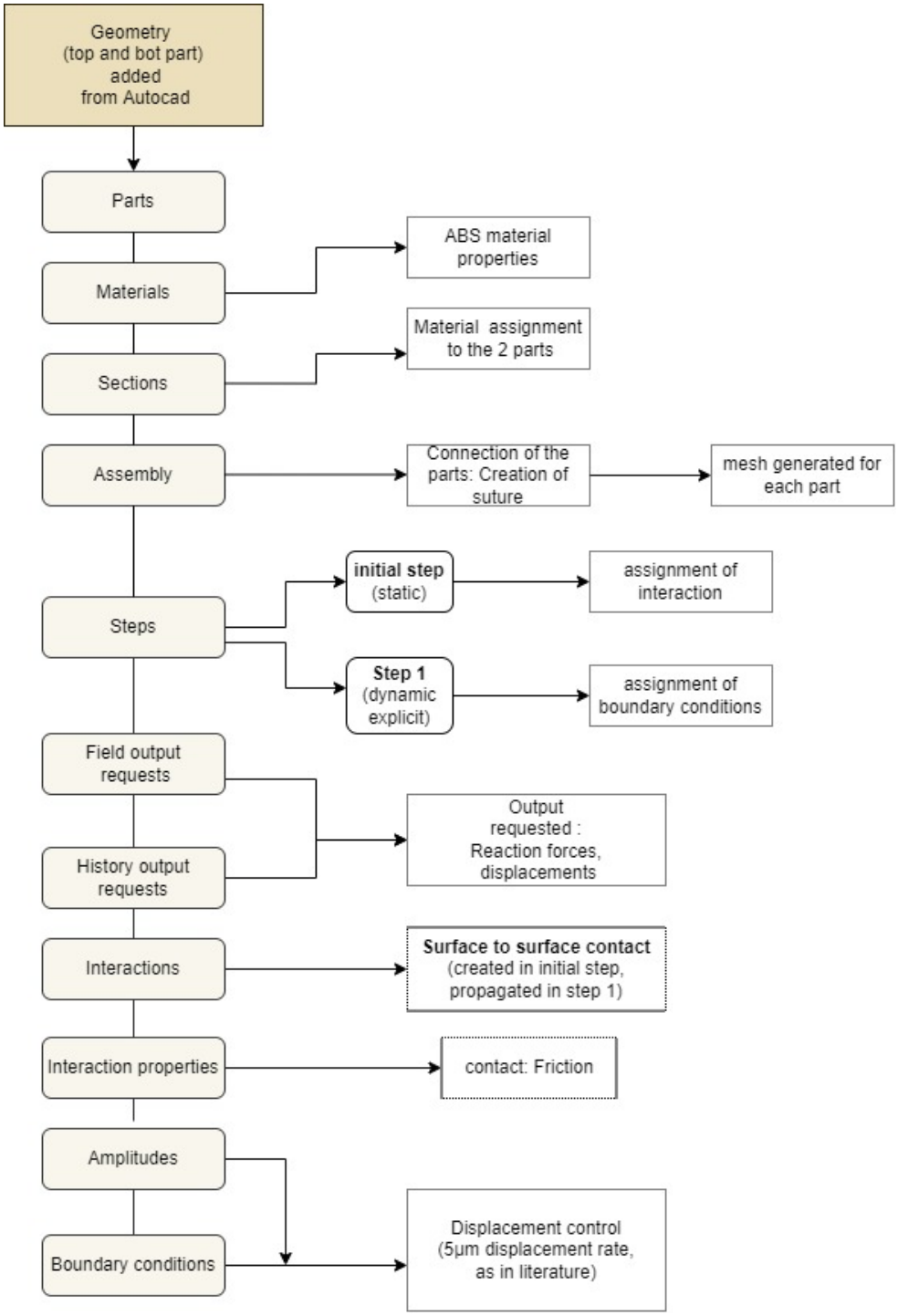

Figure 3.4: Modelling step-wise approach

3.3.1 Module: Parts

First the suture was imported in Abaqus as *two different parts* (top and bottom part). These parts were defined as *2D planar deformable* parts. The parts were used to create the assembly of the suture and to enable to test the whole suture under tension.

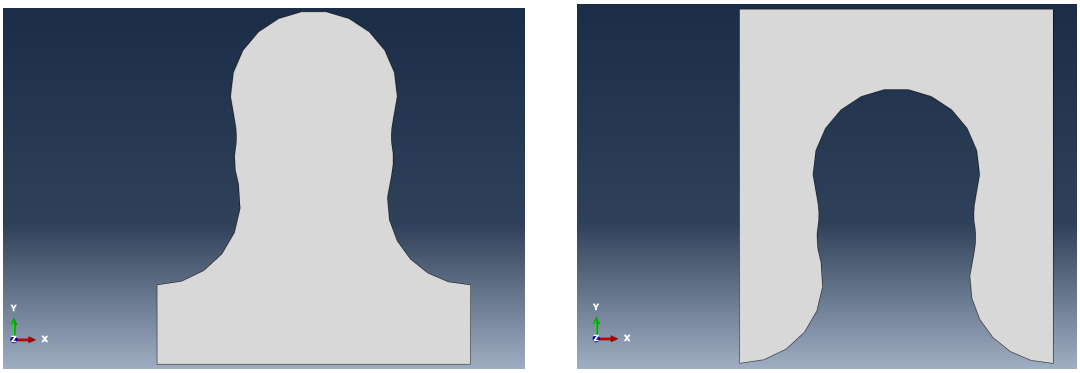

(a) bottom part (b) top part

Figure 3.5: Model parts

For each part, a section was assigned. This section contains all the information about the material type and properties.

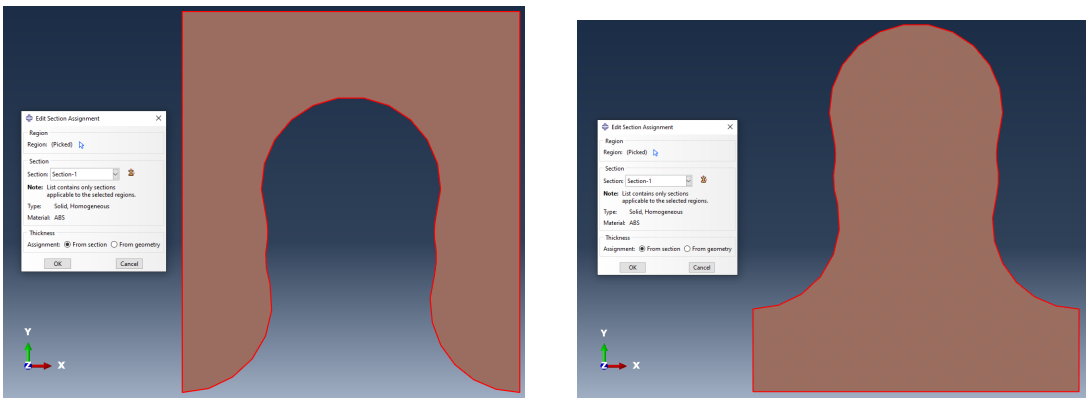

(a) Section properties top part (b) Section properties bottom part

Figure 3.6: Section properties

3.3.2 Module: Assembly

To bring the top and bottom part together, the instances were translated in respect to the global coordinate system and to each other. The assembly of the suture and local/global coordinate systems, are shown in Figure 3.7. In the assembly module the *mesh* of each part, the *sets* that will determine where the output will be taken from and the *surfaces* on the top and the bottom of the suture are defined.

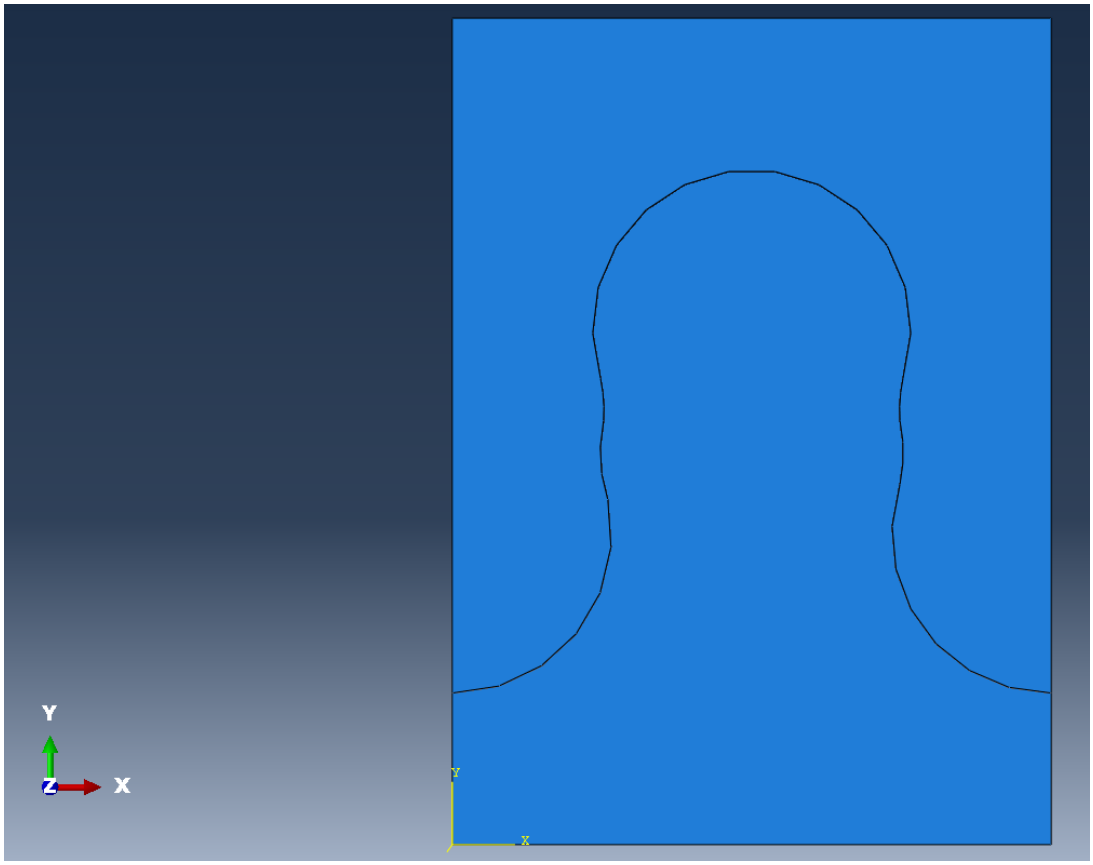

Figure 3.7: Assembly of the top and bottom part

3.3.3 Module: Material

The stress-strain curve of usual ABS specimens shows a relatively large elastic regime and a small plastic regime after yielding. This describes a common curve for ABS, although it can alternate with the consistency of the material, temperature, angle of printing and more. Some typical stress-strain graphs from different experiments of ABS are presented below:

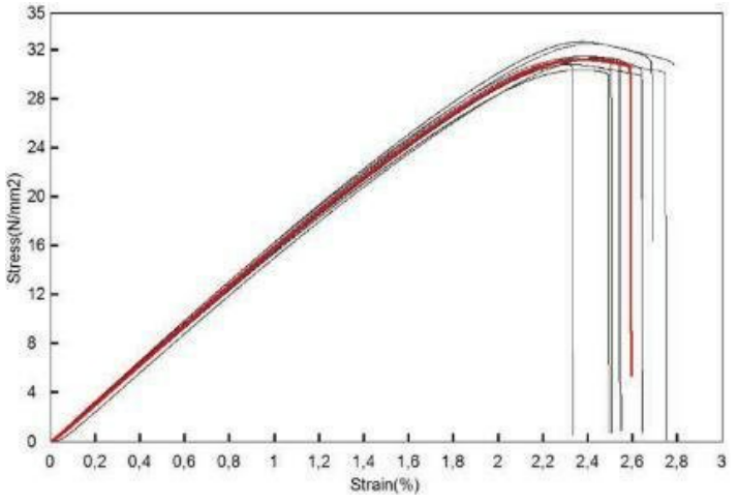

(a) ABS stress-strain relation [1] (Banjanin et al., 2018)

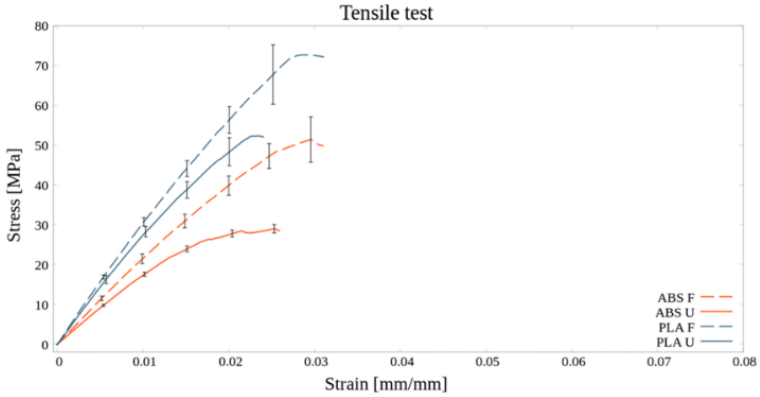

(b) ABS stress-strain relation [2] (Vukasovic et al., 2019)

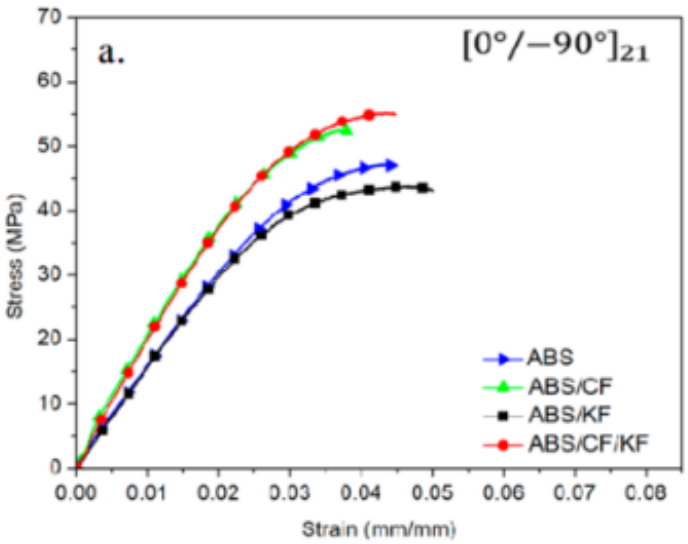

(c) ABS stress-strain relation [3] (Wang et al., 2019)

Figure 3.8: ABS typical stress-strain curves

To model the material behavior, *three approaches* were followed. First, an **elastoplastic material model**, following closely the parameters given in the paper (Mirkhalaf and Barthelat, 2017), then a simple **linear elastic** material, and then an **elastic-brittle** material were modelled. The assumptions behind each choice will be presented further below (see paragraphs Elastoplastic material model, Linear elastic material model, Elastic-brittle material model).

For the reference model and its variations it was judged best that the **linear elastic** material model will be implemented (Chapter 4). The **elastoplastic material model** and the **elastic-brittle** material results will be presented further in the material study (subschapter 4.5) and a comparison of the results of all different material models will be performed.

Elastoplastic material model

In the paper (Mirkhalaf and Barthelat, 2017) parameters of the ABS material were measured experimentally with flexural tests. A material model following these parameters was built. ABS is described as a relatively stiff and strong polymer with E = 1.7 ± 0.2 GPa, strength = 118 ± 12 MPa, but also relatively brittle, with a strain at failure ε= 0.112 ± 0.18. Also, with a three-point bending configuration, the 0.2% offset yield strength of ABS was measured as σy = 109.8 ± 8.7 MPa. The density of the ABS used was $1.07E-09$ ton/mm3, the Young's modulus was 1700 MPa and the Poisson's ratio $\nu = 0.2$. For this material model the parameters used are shown in detail at figure 3.9.

yield stress=	109.8	Mpa
stress at failure=	118	Mpa
yielding strain=	6.65	%
strain at failure=	11.2	%
E modulus =	1700	Mpa

Figure 3.9: Elastoplastic material model parameters according to the paper (Mirkhalaf and Barthelat, 2017)

The constitutive relation plotted in Excel, is shown in the figure 3.10. A simple hardening plasticity model was applied according to the data given.

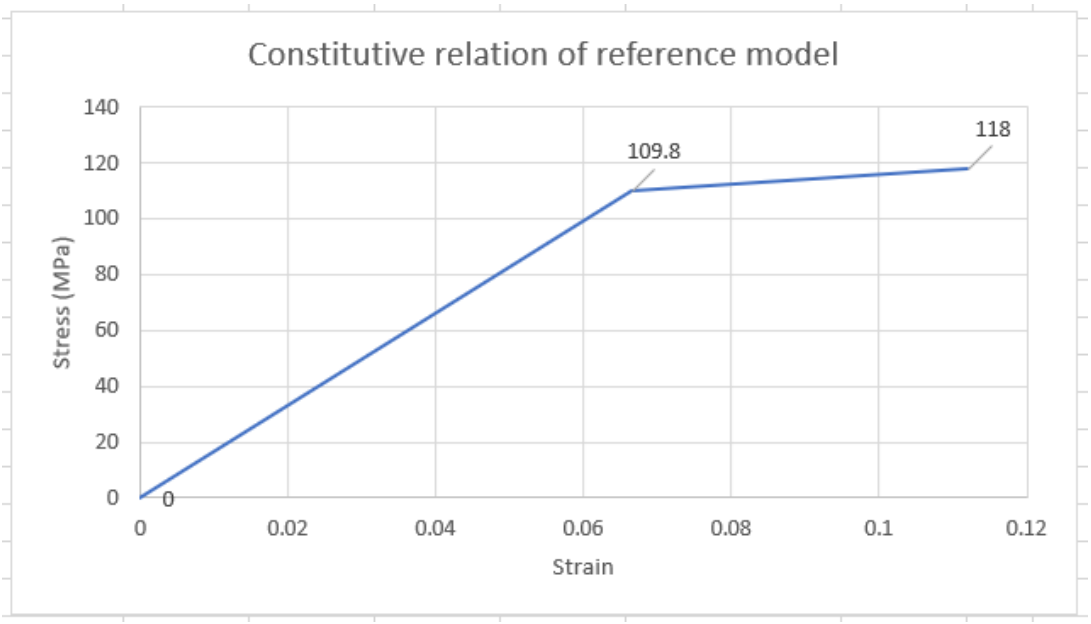

Figure 3.10: Constitutive relation for elastoplastic material

Linear elastic material model

An assumption regarding linear elasticity is a simplification but could be considered satisfactory here since the plain ABS in general is a brittle and tough material. The elastic branch is governing and only a small portion near failure would not be "accurately" captured.

The density of the ABS used, was $1.07E-09$ ton/mm3 (literature). The Young's modulus was 1700 MPa (literature) and the Poisson's ratio $\nu = 0.2$ (assumption).

Elastic-brittle material model

For the material model that included cracking, the density of the ABS used was $1.07E-09$ ton/mm3, the Young's modulus was 1700 MPa and the Poisson's ratio $\nu = 0.2$, as before. The property *brittle cracking* was added (alongside with *brittle shear* and *brittle failure*). This option is used to define cracking and post-cracking properties.

Brittle cracking model in Abaqus/Explicit can be used for applications in which the material behavior is dominated by tensile cracking and compressive failure is not important (Systemes, 2008). Here, it is a good assumption since the tensile cracking dominates the behavior of the model.

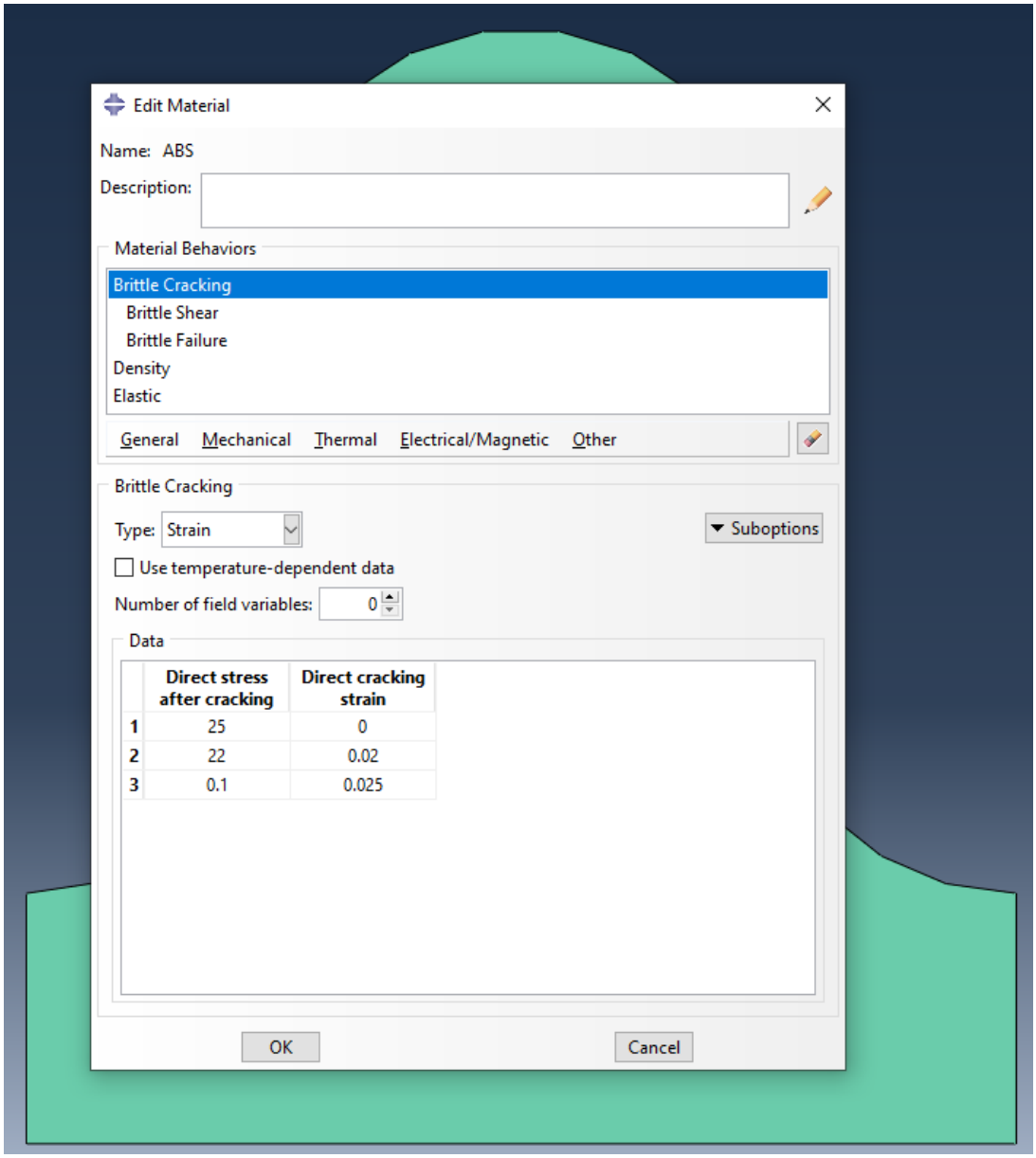

Figure 3.11: Properties - brittle cracking

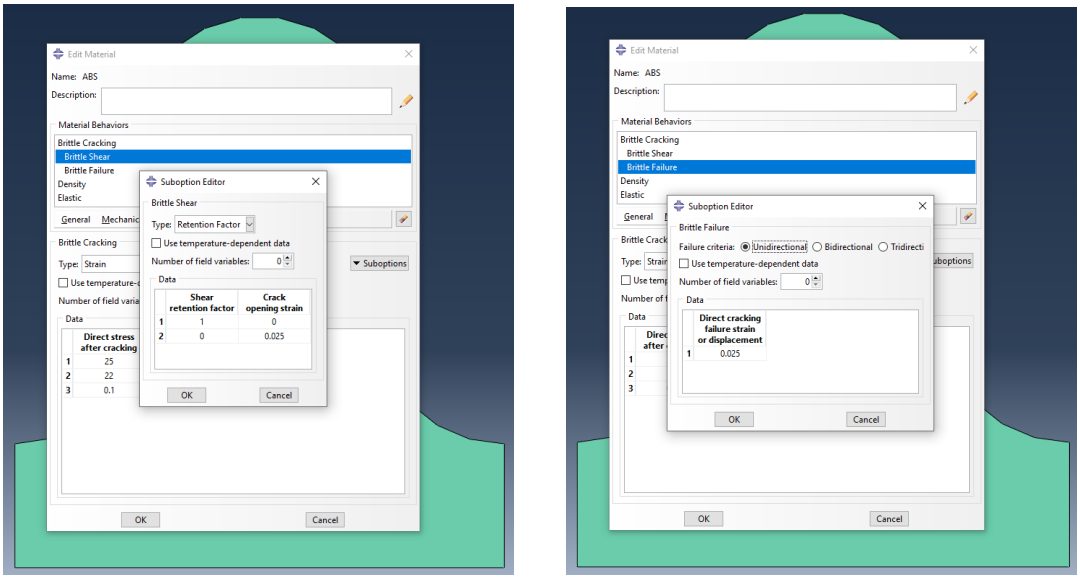

(a) Properties-Brittle shear

(b) Properties- brittle failure

Figure 3.12: Properties- brittle shear and failure

3.3.4 Module: Mesh

The mesh was created in the module Assembly. The part instances became *independent* in meshing to make possible to mesh the parts and to give freedom for performance of a variety of operations that are not possible in dependent parts (such as to add partitions and more) (Systemes, 2022h).

To create the mesh, the following commands were used:

- Seed Part Instance
- Mesh controls
- Element type

Seed Part Instance

The seeding tools allow to adjust the mesh density in selected regions. Specifically the seeds act like markers that are placed along the margins of a zone to set the target mesh density for that region. The seeds along the region's boundaries determine both the mesh density along the region's perimeter and the mesh density in the region's interior (Systemes, 2022i).

Different mesh densities were considered. First a coarse mesh was considered and then a finer mesh. The coarse mesh had approximate global seed size 0.2 and the refined mesh 0.1. Also a locally refined mesh at the curved areas was employed.

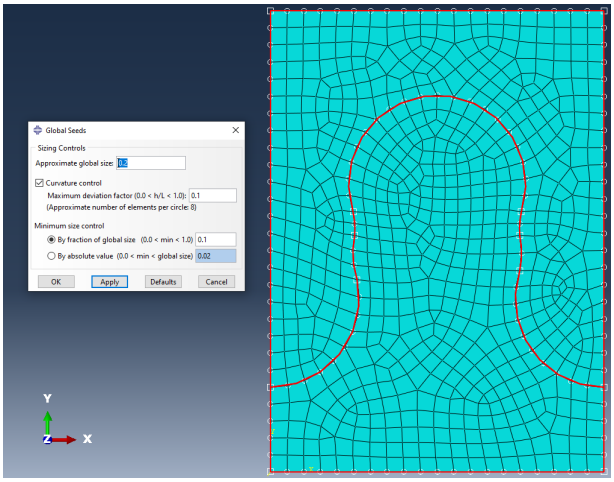

(a) coarse mesh - global seed size 0.2

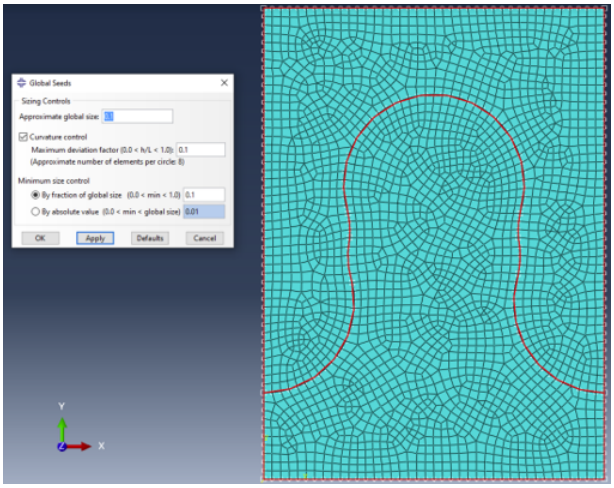

(b) fine mesh - global seed size 0.1

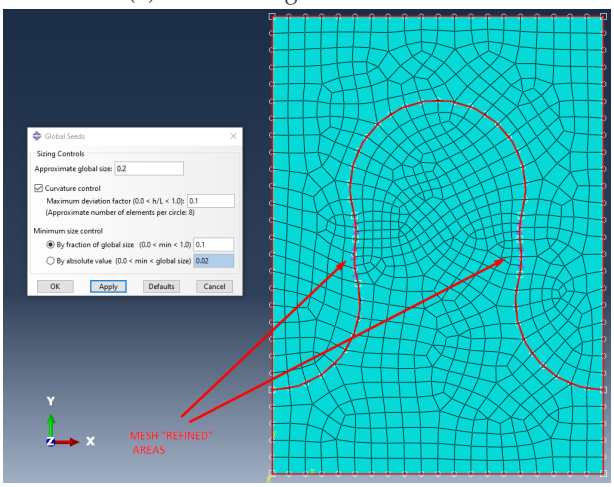

(c) Refined mesh locally

Figure 3.13: Mesh variations

Mesh controls

Free meshing was employed that uses no pre-established mesh patterns. This means that it is not possible to predict the pattern of the mesh based on the region topology. Since it is unstructured, free meshing allows more flexibility than structured meshing (Systemes, 2022e). The topology of regions that are meshed with the free mesh technique can be very complex. Due to the curves and the relatively complex geometry of the sutures a free mesh was implicated, to cover for the curvature of the tabs. The mesh controls implicated are presented in the figure 3.14.

In this case the shape of the implemented mesh elements was quad-dominated (default). This means that primarily quadrilateral elements were used, but triangles were also allowed in transition regions.

When suitable, Abaqus/CAE uses *mapped meshing* with advancing front method (see figure 3.14). Mapped meshing is identical to structured meshing but it only applies to regions with four sides, so in this case although it was used as a default option, it would not be beneficial for this type of geometry.

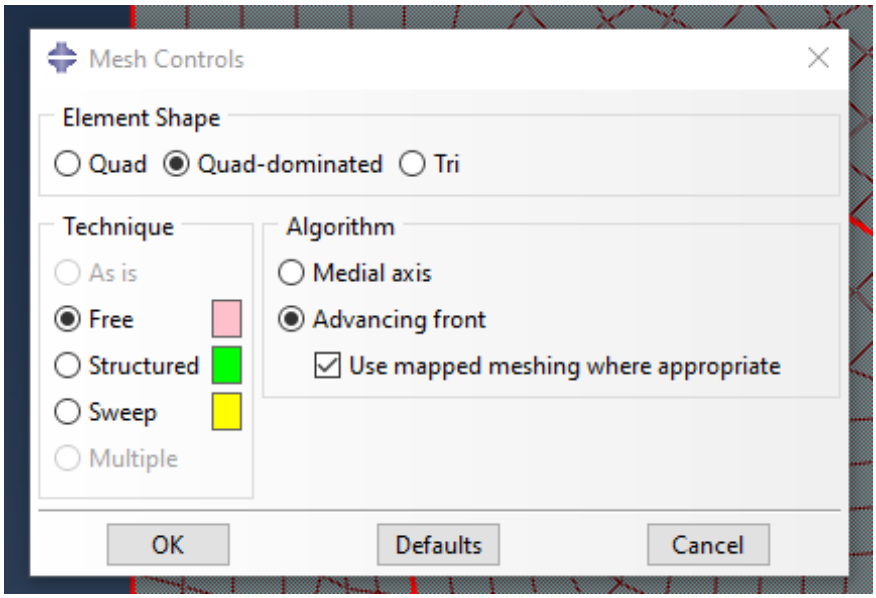

Figure 3.14: Mesh controls properties

Element type

Plane stress elements were used for the modelling of the sutures in 2D, from the explicit library. The rest of the properties were the defaults options of Abaqus.

3.3.5 Module: Interaction

As mentioned before, the mechanism of interlocking is governed by friction. Therefore in the model, **no adhesion or ties were considered**. The sliding of surfaces in respect to one another is of importance here. In this sub-chapter it is explained how this mechanism can be modelled in Abaqus.

Possible contact is defined in an Abaqus/Standard simulation by either naming the surfaces involved in a contact interaction **(contact pair approach)** or by specifying an automatically generated element-based surface as the contact domain **(general contact approach)** (Systemes, 2022a). The *contact pair approach* was chosen for this type of interaction.

Similar to how each element must refer to an element property, each contact interaction for both contact approaches must refer to a **contact property**. These properties can be mechanical, thermal or electrical. The contact property can contain constitutive behavior like friction, cohesive behavior and more (Systemes, 2022a).

Interaction: Surface to surface contact

The surface to surface contact was used here and it was defined in the initial step (step 0), then propagated to the next step (step 1). Initially, the primary and secondary surfaces were chosen (figure 3.15) denoted with red and magenta colors respectively. For the dynamic analysis performed explicit surface to surface contact was used while for the static analysis standard surface to surface contact was used.

The constraint formulation chosen was the **penalty contact method** over the kinematic formulation. This algorithm searches for node-into-face and edge-into-edge penetrations in the current configuration. The penalty contact algorithm is less stringent when it comes to the enforcing of contact constraints than the kinematic contact algorithm (Systemes, 2022b), (Systemes, 2015). In addition, the penalty contact technique can model some cases of contact that the kinematic method cannot. When the penalty contact formulation is applied, the main and secondary nodes at the penetration points experience equal and opposing contact forces with magnitudes equal to the penalty stiffness times the penetration distance (Systemes, 2022c). The sliding between them was finite.

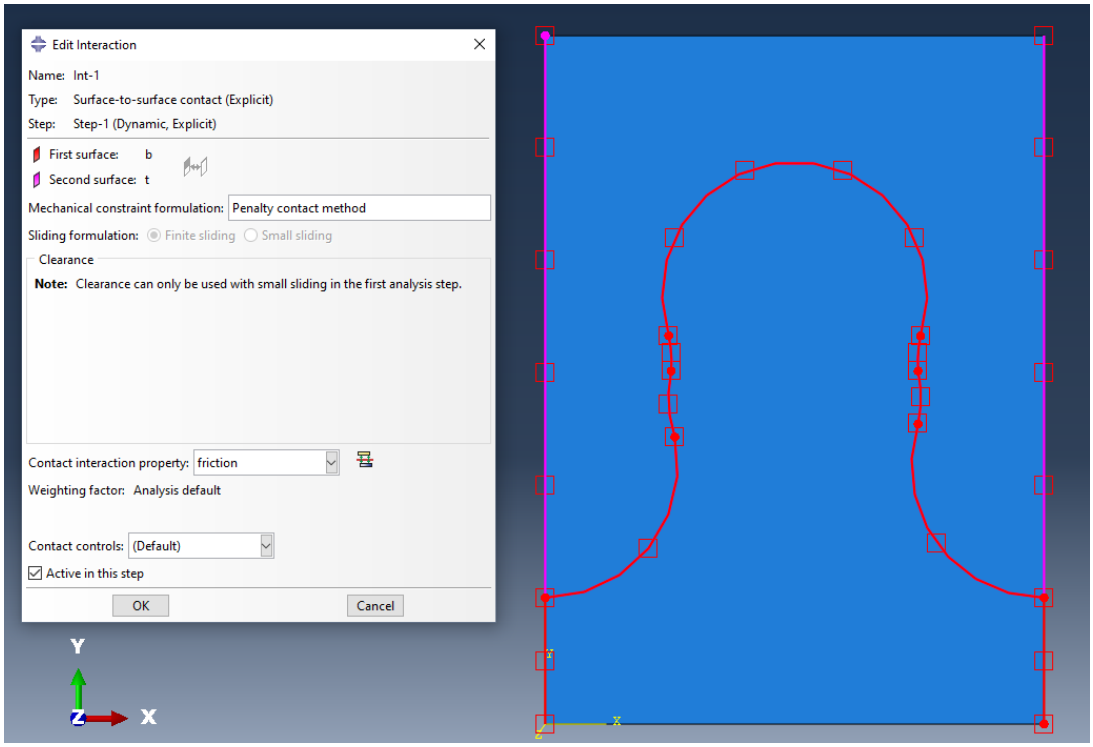

Figure 3.15: Master-Slave surface and interaction properties

As seen in figure 3.15, the sides of the top and the bottom part were chosen as well as the curved interface of the top and the bottom part. This choice ensured that the nodes at the edges that belong to the interfaces, will be included for the interaction.

3.3.6 Module: Interaction Property

Friction

When two surfaces come into contact, shear and normal forces are transmitted across their interface. Between these two force components, there is usually a connection and this is the *friction* between the adjacent surfaces. In Abaqus, friction can be defined as an interaction property and the friction's contact property options are **normal** and **tangential behavior** (see figure 3.17). There, more properties (as friction coefficient, contact stiffness, elastic slip) are defined (Systemes, 2022f).

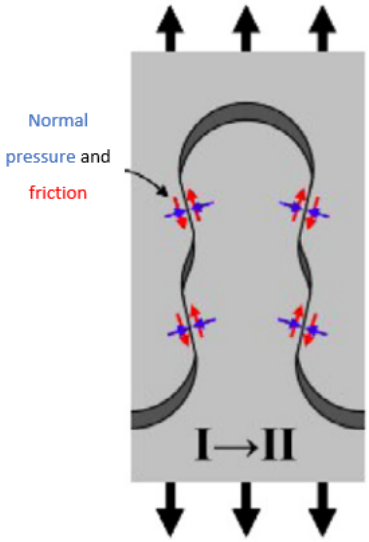

Figure 3.16: Normal pressure and friction (Mirkhalaf et al., 2016)

In the tangential behavior input tab, the *friction coefficient* was defined as **0.35** (as measured in literature) and it can be seen at figure 3.17. Also the *penalty friction formulation* was used to permit some relative motion of the surfaces (an "elastic slip"). In the normal behavior, the contact stiffness was chosen as 1700MPa (which is the same stiffness as the rest of the material).

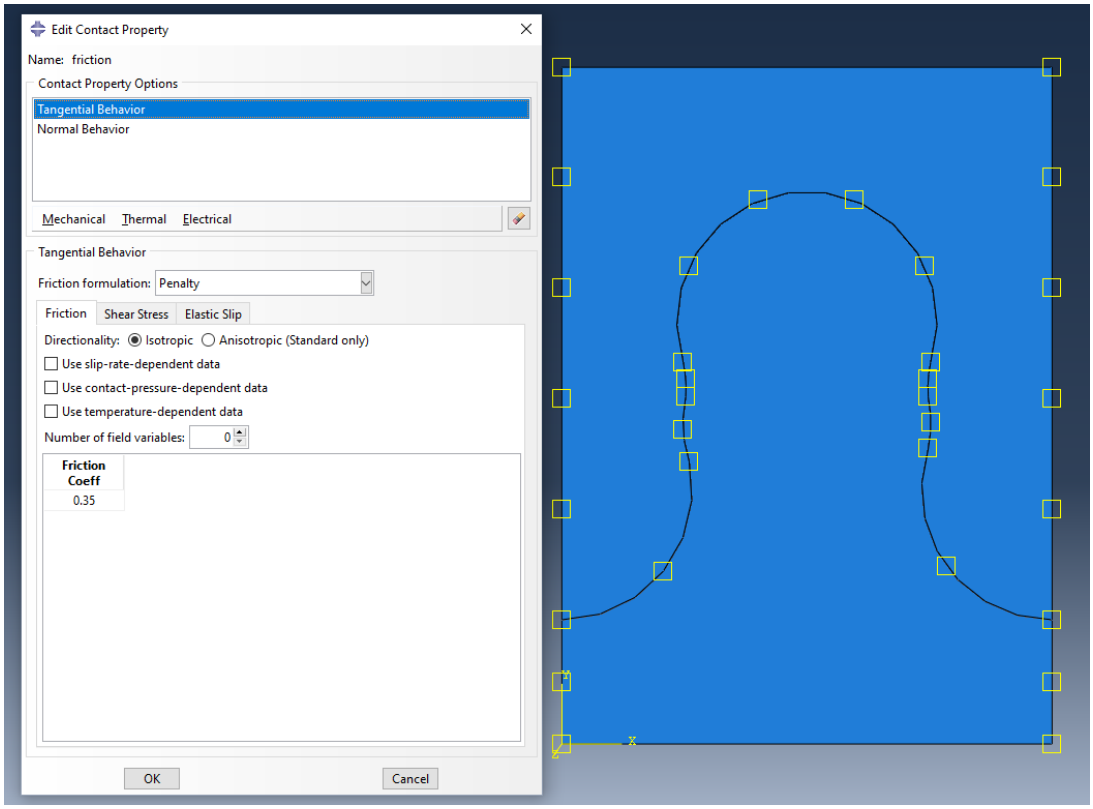

Figure 3.17: Friction tangential behavior-Friction coefficient and properties

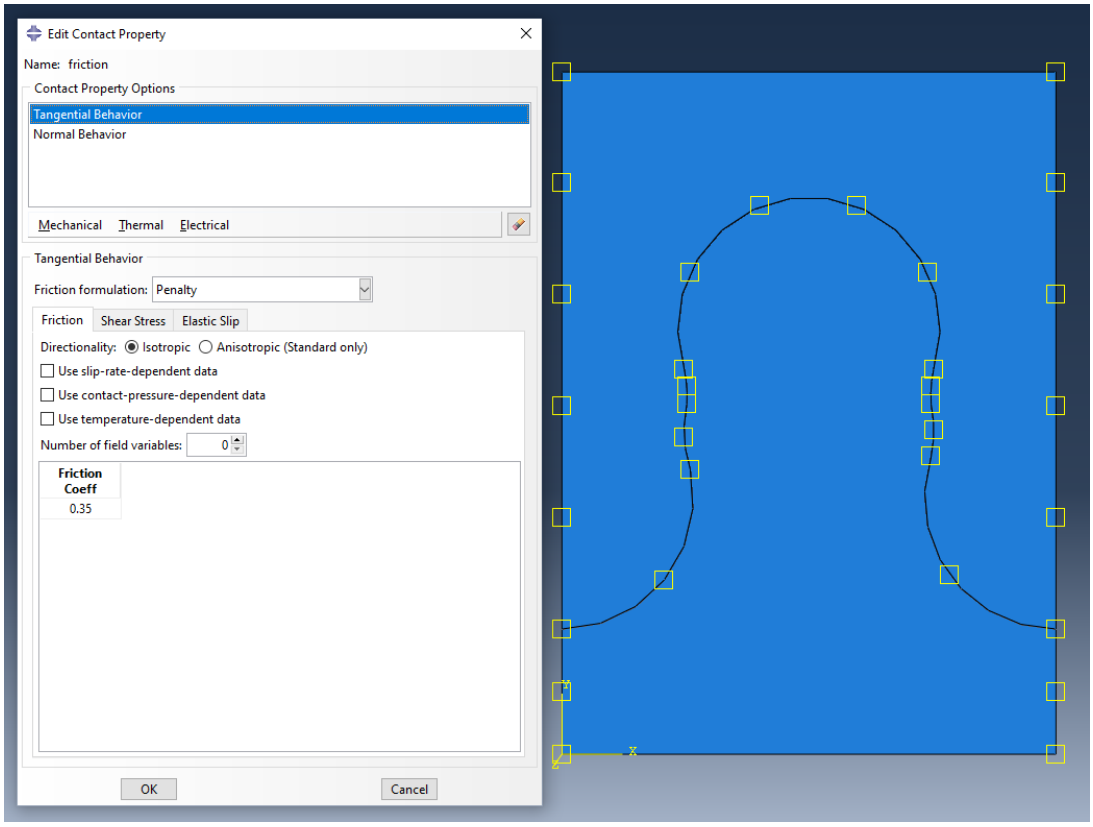

Figure 3.18: Friction normal behavior-Contact stiffness and properties

3.3.7 Module: Boundary Conditions

As mentioned in the literature, tensile tests were performed on the tabs in quasi-static conditions with a displacement rate of 5 μm. To model this behavior, the tensile force was applied at the top part and the bottom part was completely fixed.

These boundary conditions were enforced as restrains of displacements in x, y direction and rotation in xy plane. At the bottom part, all degrees of freedom were restrained. At the top part, the tension force was applied as a *displacement rate of 5μm*, with all the other degrees of freedom restrained. For the analysis, a time period of 500 seconds was used so the total displacement obtained at the end of the analysis with this displacement rate, was 2.5 mm. This is shown in figures 3.19a, 3.19b.

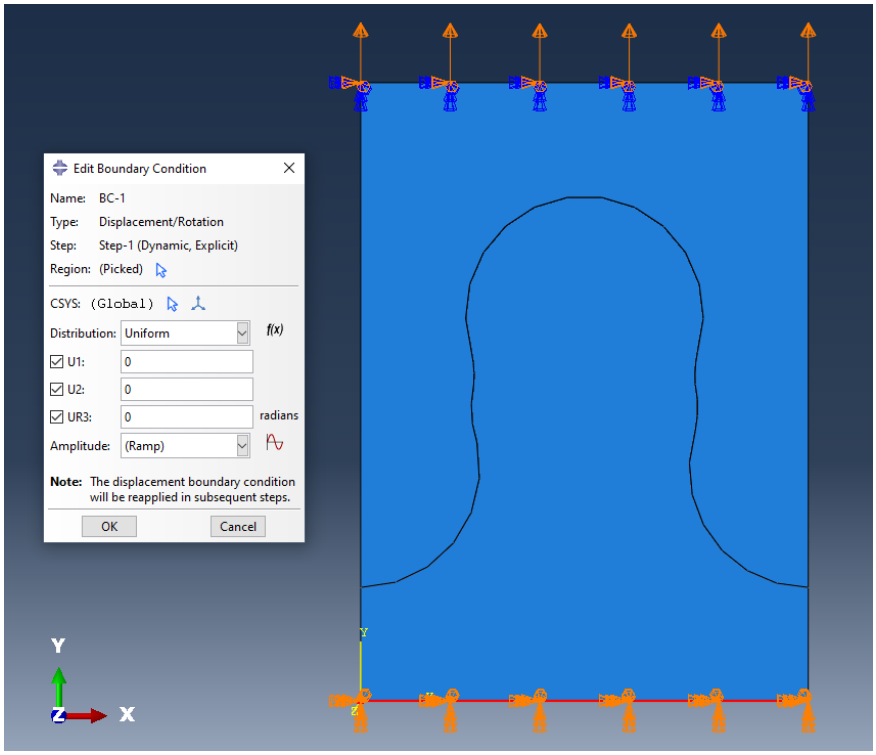

(a) Boundary conditions at the bottom part

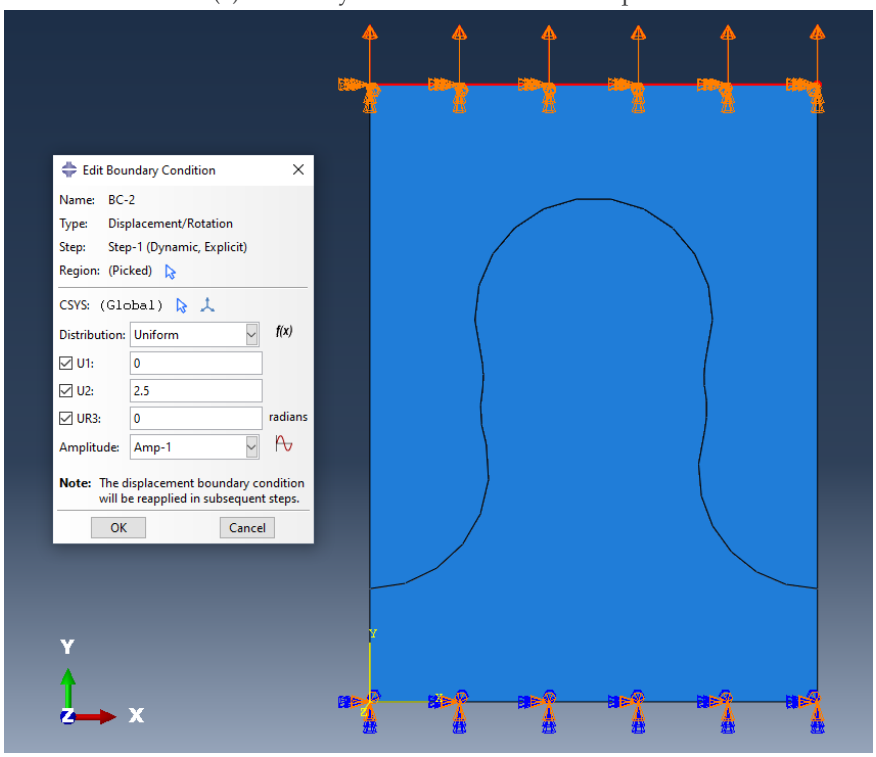

(b) Boundary conditions at the top part

Figure 3.19: Boundary conditions at the top and bottom parts

3.3.8 Module: Steps

Analysis

A basic concept in Abaqus is the implementation of steps. Steps are phases of the loading timeline. Each step uses a defined analysis procedure (static, dynamic, etc) (Systemes, 2022d). Two steps were included for the analysis. The initial one *(static)* was existent already and the interface conditions were defined in that step. The second one was a *dynamic (explicit)* step to take into account the inertia effects. The loading (applied as boundary conditions with a displacement rate of 5 μm) was defined in this step. In addition, the history output requests were defined in this step. The requested outputs were the displacements and the summation of reaction forces on the top set of the suture (figures 3.21, 3.22). The interface conditions were propagated from the initial step to the second step. NLGEOM, an option that takes into account material and geometrical non linearities was used to account for large displacements.

In the initial model, dynamic analysis was performed but at a later stage also static analysis, to see how the results were affected by the loading procedure. Since the displacement rate was 5 μm (constant) it was considered a sufficient assumption. The parameters of the static analysis were the same (time period t=500 sec, which would give a total displacement of 2.5 mm in the end of the analysis). NLgeom was again kept on to account for non linearities.

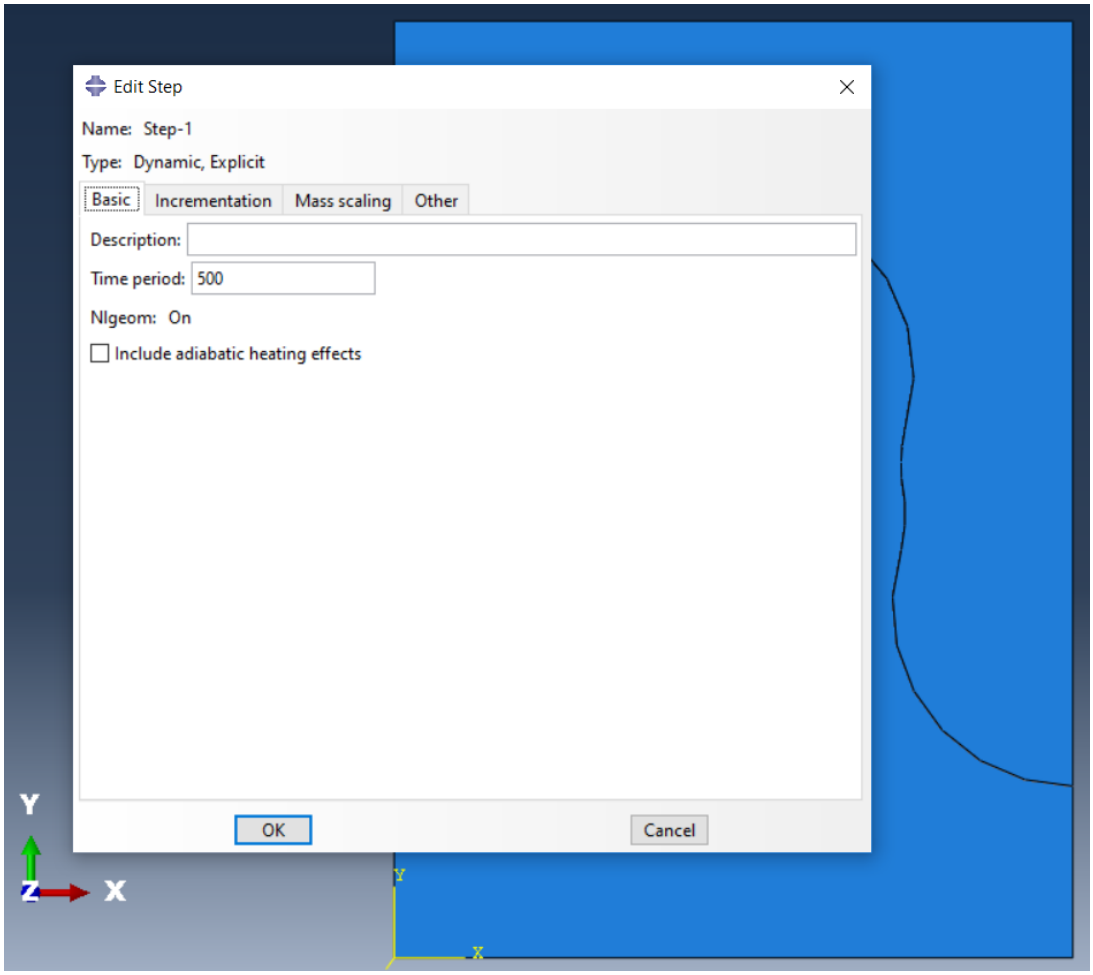

Figure 3.20: Dynamic explicit step

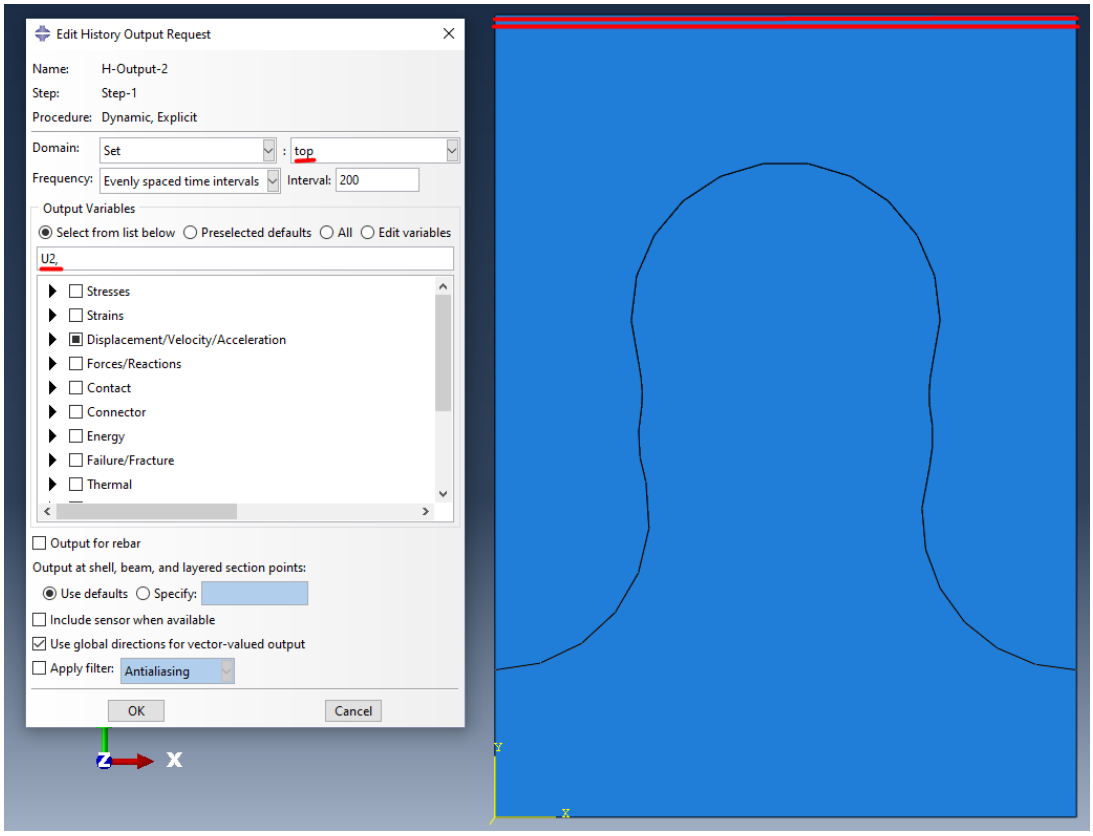

Figure 3.21: Output request-Displacements on the top set

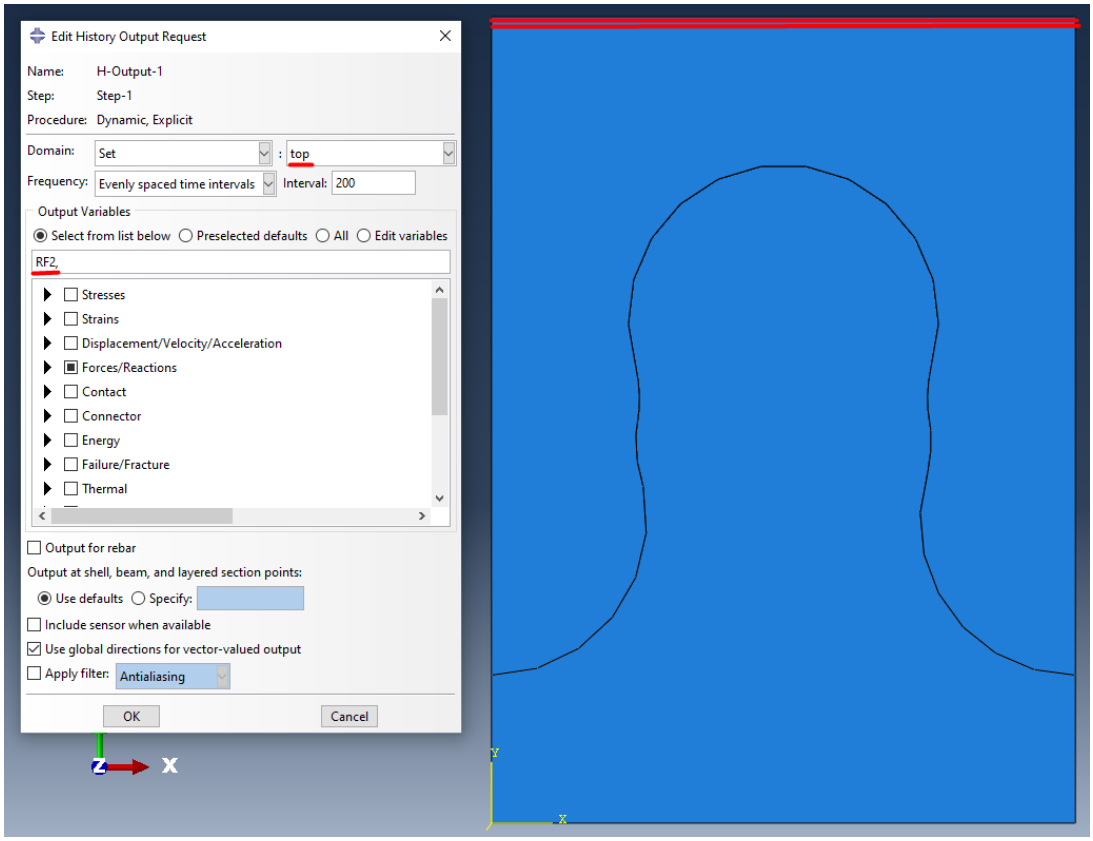

Figure 3.22: Output request-Reaction forces at the top set

Mass Scaling

Mass scaling is frequently used in Abaqus/Explicit for computational efficiency in quasi-static analyses and in some dynamic analyses that contain a few very small elements that are governing for the stable time increment (Systemes, 2022g). Scaling the mass density in some cases may have the potential to improve the effectiveness of the analysis since it affects the stability limit. For instance, the complicated discretization of several models frequently results in regions where the stability limit is controlled by tiny or irregularly shaped elements. These "governing elements" are often few in number and may only be found in specific locations. The stability limit can be greatly enhanced by raising the mass of only these regulating parts and the calculation time will be less, while the impact on the model's overall dynamic behavior may be minimal.

With the application of a mass scaling factor, the mass of the elements with a time increment below a certain value is scaled. In this case the desired element-by-element stable time increment was defined for the whole model for semi-automatic mass scaling (Systemes, 2022g). Abaqus/Explicit then determined the necessary mass scaling factors. The scale was chosen to target a time increment of $1e-06$ as also seen in the figure 3.23.

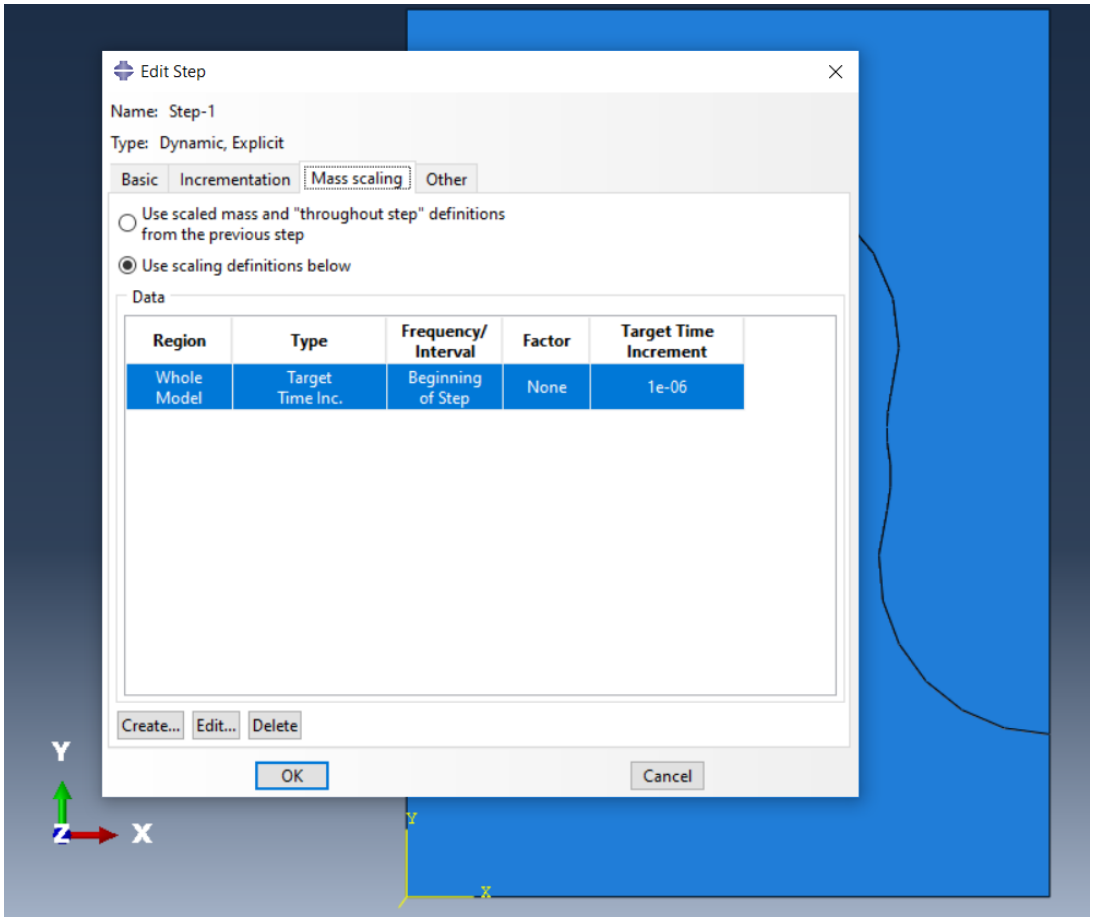

Figure 3.23: Mass scaling

3.4 Variations of the model

The initial model that was created and presented above, was the one with parameters "closest" to the ones given in the literature (Mirkhalaf et al., 2016). In this way, the experimental model could be validated with the numerical model and then compared with other numerical models having a critical variable changed, for the sake of optimization.

The variables that were judged critical to explore the difference in behavior of the models, were the **geometry of the tabs**, the **contact stiffness of the interface** and the **friction coefficient**.

The simulations performed are presented below with numbers, to make it easier to refer to each one of them. These simulations include the initial model *(simulation 1)*, six variations with different contact stiffness parameters *(simulation 2 - 7)*, two variations with different geometry *(simulation 8, 9)* and two variations with different friction coefficients *(simulation 10, 11)*. Additionally a simulation featuring a sutured line with multiple tabs, was performed. The results of these simulations are going to be presented in detail in the chapter 4.

Simulations	Parameters				
Number of simulation	Geometry (R1/R2 ratio)	Contact stifness of interface (MPa)	Friction coefficient of interface	Contact Pressure (MPa)	Material model
1	**1.05**	**1700**	**0.35**	-	linear elastic
2	1.05	1000	0.35	-	
3	1.05	3000	0.35	-	
4	1.05	1.7E+10	0.35	-	
5	1.05	1.7E+10	0.35	124.5 (literature)	
6	1.05	1.7E+10	0.35	1.245E+11	
7	1.05	1.7E+10	1	1.245E+11	
8	1.00	1700	0.35	-	
9	1.10	1700	0.35	-	
10	1.05	1700	0.15	-	
11	1.05	1700	0.55	-	

Figure 3.24: Simulation overview

For the simulations with varying geometry parameters *(simulation 8, 9)* the different parameters are shown in figure 3.25. For all the rest (simulations 1-7 & 10-11), **geometry 1** was used with R_1 / R_2=1.05.

Parameters	Geometry 1	Geometry 2	Geometry 3
θ1 (degrees)	15	15	18
θ2 (degrees)	8.02	14.89	3.02
R1 (mm)	1.05	1.00	1.10
R2 (mm)	1.00	1.00	1.00
R1/R2	1.05	1.00	1.10
w (mm)	3.96	3.86	3.99
L (mm)	3.44	3.55	3.60

Figure 3.25: Geometry parameters

4 Results

4.1 Reference model- Simulation 1

4.1.1 Parameters used

The initial model *(simulation 1)* was the one used as a reference with parameters closest to the literature, as they appear in figure 2.6. The basic parameters of interest that influence the results of the analysis are $\mathbf{R_1/R_2}$, $\boldsymbol{\theta_1}$, **the contact stiffness of the interface and friction coefficient**. For simulation 1 the parameters used were:

- $\mathbf{R_1/R_2 = 1.05}$, as seen in the paper (Mirkhalaf and Barthelat, 2017),
- $\boldsymbol{\theta_1 = 15}\ ^\circ$, as seen in the paper (Mirkhalaf and Barthelat, 2017),
- **contact stiffness 1700 MPa**, as was measured in the paper (Mirkhalaf and Barthelat, 2017)),
- **friction coefficient f=0.35**, as was measured in the paper (Mirkhalaf and Barthelat, 2017).

Simulations	Parameters				
Number of simulation	Geometry (R1/R2 ratio)	Contact stifness of interface (MPa)	Friction coefficient of interface	Contact Pressure (MPa)	Material model
1	**1.05**	**1700**	**0.35**	-	linear elastic
2	1.05	1000	0.35	-	
3	1.05	3000	0.35	-	
4	1.05	1.7E+10	0.35	-	
5	1.05	1.7E+10	0.35	124.5 (literature)	
6	1.05	1.7E+10	0.35	1.245E+11	
7	1.05	1.7E+10	1	1.245E+11	
8	1.00	1700	0.35	-	
9	1.10	1700	0.35	-	
10	1.05	1700	0.15	-	
11	1.05	1700	0.55	-	

(a) Basic parameters

Parameters	Geometry 1	Geometry 2	Geometry 3
θ1 (degrees)	**15**	15	18
θ2 (degrees)	**8.02**	14.89	3.02
R1 (mm)	**1.05**	1.00	1.10
R2 (mm)	**1.00**	1.00	1.00
R1/R2	**1.05**	1.00	1.10
w (mm)	**3.96**	3.86	3.99
L (mm)	**3.44**	3.55	3.60

(b) Geometry parameters

Figure 4.1: Parameters used for simulation 1

4.1.2 Numerical Results

The Force - displacement graph of the reference model (simulation 1) is presented in Figure 4.2. The graph presents many similarities with the experimental results, that are going to be further analysed in subchapter 4.1.5. Three points (A, B, C) are noted in the graph, where stresses and reaction forces are extracted for further investigation.

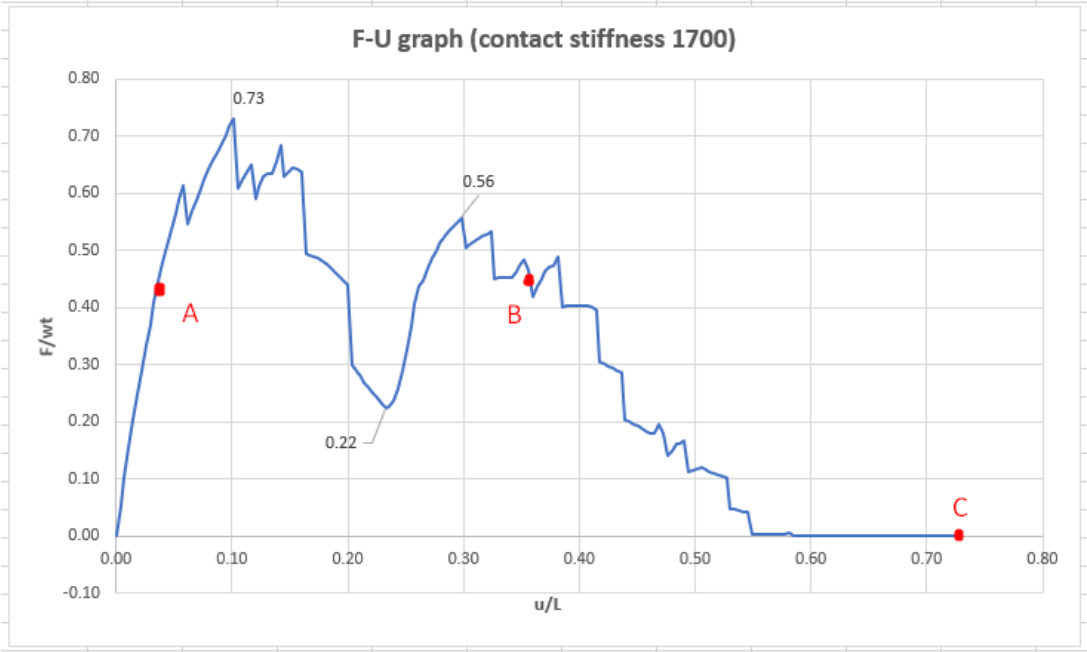

Figure 4.2: Force - Displacement plot normalized- Simulation 1

4.1.3 Reaction forces

The summation of reaction forces was the output of interest to investigate if the response of the numerical model is similar to the experiments. *Two analyses* were performed in the same model, one requesting the output (reaction force summation) at the *top set* (see Figure 4.3a) and one requesting the output at the *bottom set* (see Figure 4.3b). The reason behind investigating both sets is to make sure that the reaction forces are the same at the top and bottom, as they should be in a linear elastic model without permanent deformation.

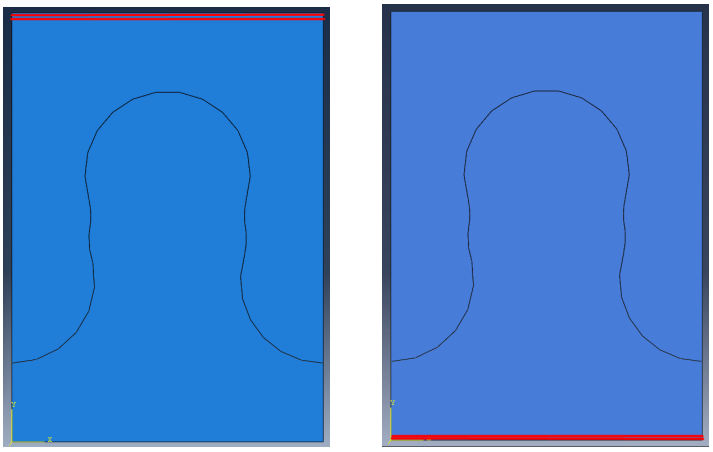

(a) Top set of the suture (b) Bottom set of the suture

Figure 4.3: Top and bottom sets of the suture

Indeed, the reaction forces are almost identical on the top set and on the bottom set (the graph is almost mirrored), so this result can be considered satisfying.

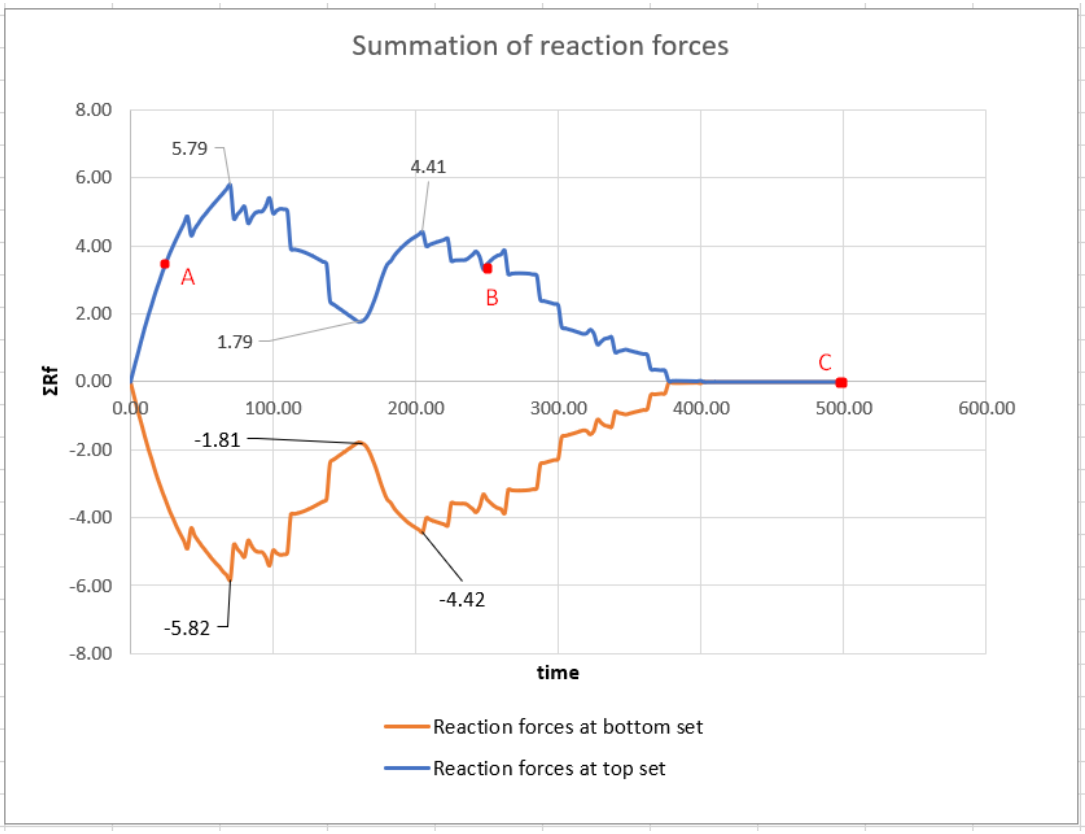

Figure 4.4: Comparison of reaction forces on top and bottom sets

The changes in the reaction forces as the time of the analysis proceeds are shown in figure 4.5. In the very beginning of the analysis the reaction forces are generated at the *top* since the tensile forces, as a displacement rate of 5μm, are applied there and as the analysis proceeds reaction forces are generated at the bottom as well.

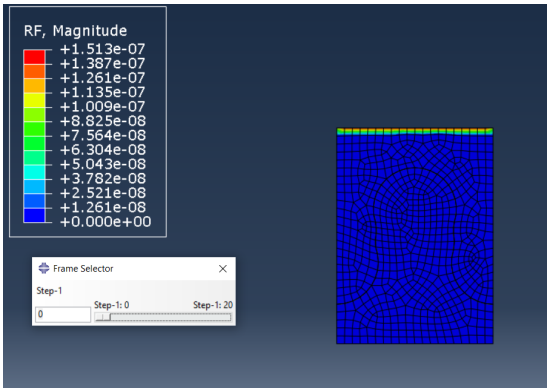

(a) Reaction forces- Point A

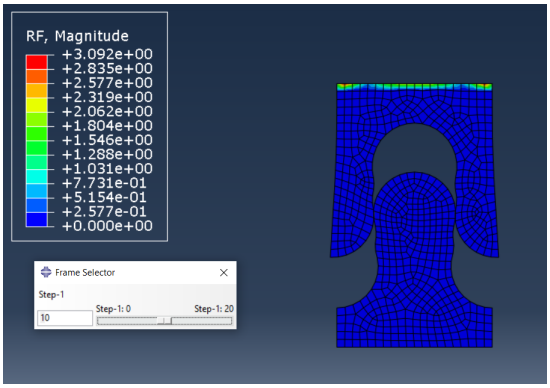

(b) Reaction forces- Point B

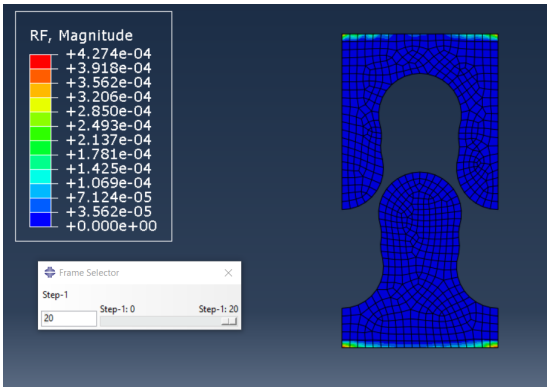

(c) Reaction forces- Point C

Figure 4.5: Reaction forces- simulation 1

4.1.4 Stress propagation

The stress propagation during the analysis is shown in the Figure 4.6. The stresses are going to be analyzed separately for the top and bottom parts of the suture.

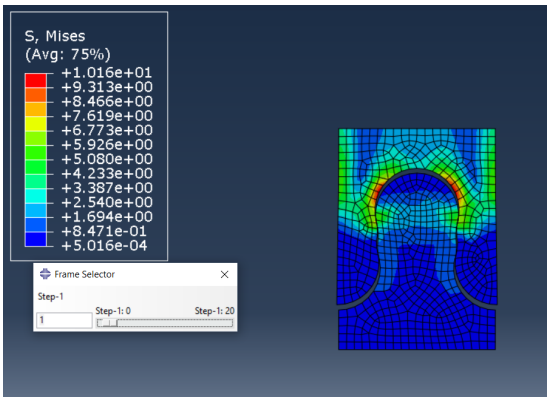

(a) Stresses- Point A

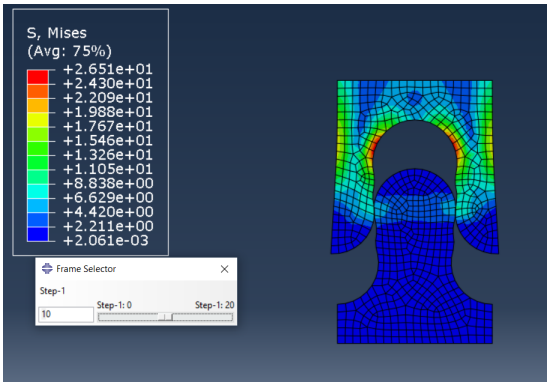

(b) Stresses- Point B

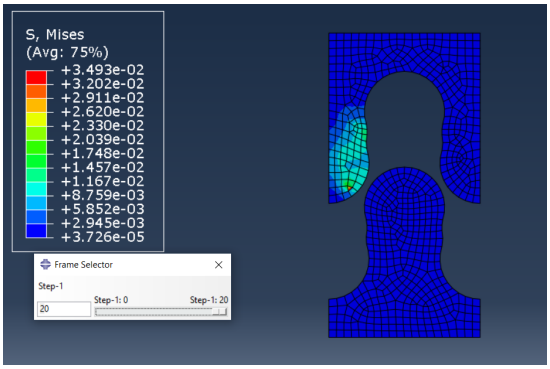

(c) Stresses- Point C

Figure 4.6: Stress propagation - simulation 1

Bottom part: The larger stress values (concentration of stresses) are generated at the places where the top part is coming in contact with the bottom part while it is being pulled out. These are frictional and normal stresses as reactions to the pull-out forces. This is highlighted in figure 4.7.

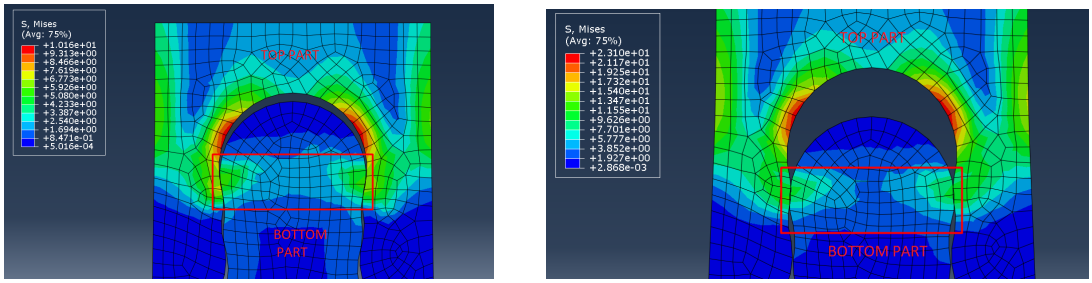

(a) Stress detail 1 (b) Stress detail 2

Figure 4.7: Stress concentrations at the bottom part

Top part: There are stress concentrations in the areas where the top part comes in contact with the bottom part (friction and normal stresses due to the pull-out). While the tab is being pulled out, the zones at the top part (highlighted in figure 4.8) are more susceptible to cracking since the edges of the top part displace laterally.

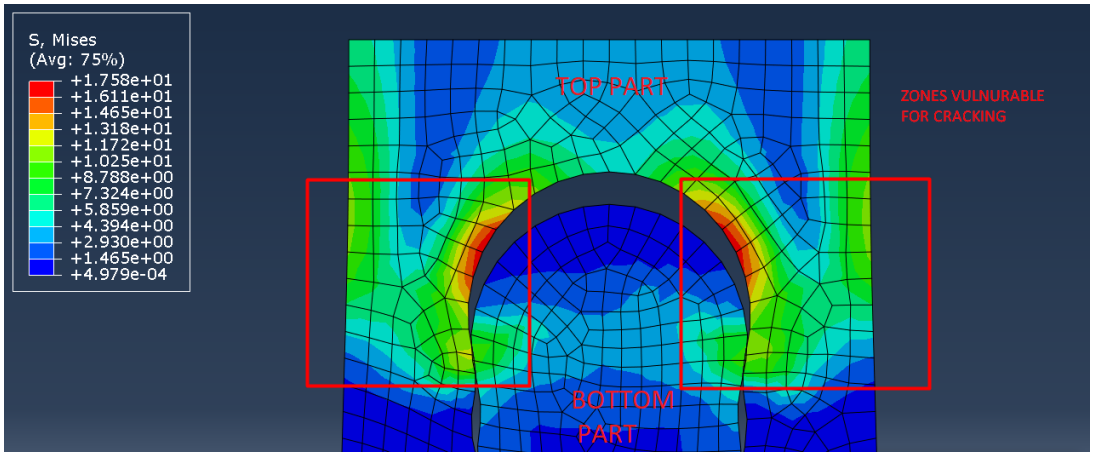

Figure 4.8: Stress concentration at the top part

4.1.5 Verification of the reference model

To verify the initial model, a comparison between the numerical and experimental reaction force-displacement graphs must be performed. The *experimental results* are plotted at the same graph as the numerical results to make the comparison clearer.

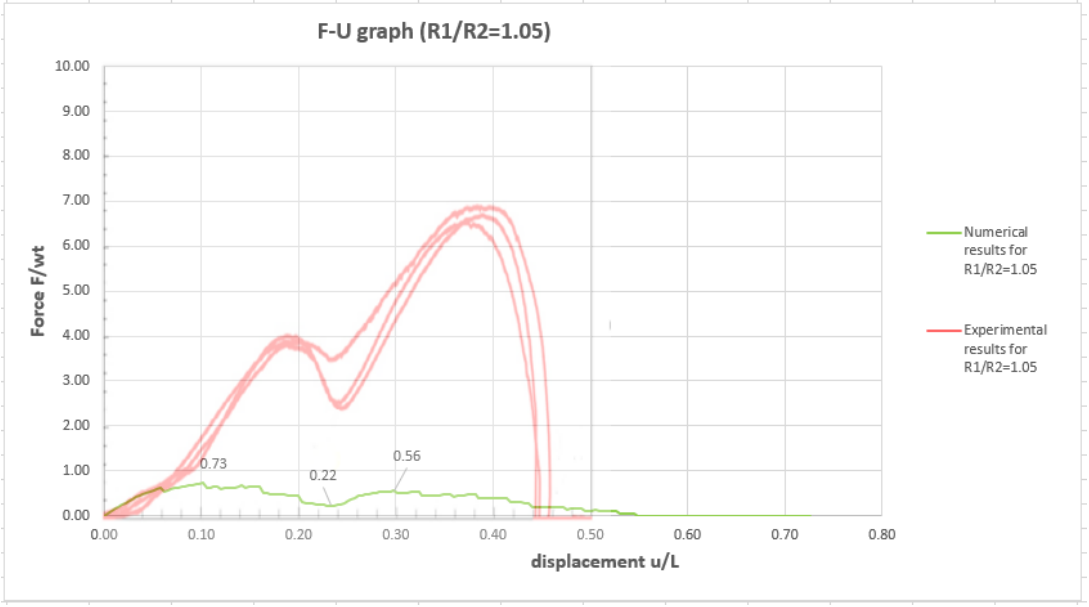

Figure 4.9: Experimental- Numerical results comparison

First curve/peak comparison:

The numerical curve presents similarities with the experimental curve. The shape they follow is quite similar. The major difference is that the values derived from the numerical simulation are lower than the experimental ones. The first peak value is approximately five times lower in the numerical curve. The location of the first peak appears to be sooner at the numerical curve than in the experimental one.

Kink comparison:

The kink location is almost identical, at 0.24 u/L. The numerical results correspond to a lower value compared to the experimental results, as it was before.

Second curve/peak comparison:

The values differ from the experimental values, they appear lower, again. The second peak value is approximately 12 times lower at the numerical results. The location of the second peak in the numerical results is located before the one of the experimental curve.

The main observations of the comparison between the 2 graphs, show that the results of the analysis following the experiments were partially satisfying. There are a lot of similarities but also a lot of differences between the experimental and numerical results.

The trend of the graphs seems similar in both cases, following almost the same shape. Both graphs start from zero, with two peaks and a kink in the middle to separate them, that represents the second equilibrium position, namely the interlock position. Additionally, the kink's position is the same almost in both the experimental & numerical analysis, a good indication for the validation of the model.

The major difference concerns the values. The experimental F/wt values are much higher. This can be attributed to many factors, some of them presented below:

- The material model assumed was *linear elastic*, and this can affect the strain values since in such a model the strains are smaller. And also the stresses are proportional to the strains. Nonlinear effects were not included and as satisfactory the assumption of linear elasticity may be, it remains a simplification of the physical model.
- The *complexity* of the analysis was high and although at the analysis nonlinear effects were included with the NLGEOM option, the way the load was applied, and the complex contact of the two surfaces can create differences with the numerical simulation and the experiment.

Another difference between the F-U graph from the experiment and the numerical analysis concerns the peaks. There are two peaks in each graph. *The second peak is higher at the experimental results and the first one at the numerical results* (see figure 4.9). In terms of mechanical stability, it is beneficial if the second peak is higher than the first.

4.2 Contact stiffness influence

4.2.1 Modelling of contact

Interface modelling is a challenging subject, since there are many crucial parameters that have to be considered to model sufficiently a mechanical interface problem. The physical problem in this research is governed by **frictional contact**. The parameter of interest is the **stiffness of the interface** (in addition to contact pressure and friction). Six simulations were performed in this subchapter, to highlight how changing these parameters affects the total response.

4.2.2 Simulation 2- Decreased contact stiffness

Simulation 2 was created with parameters identical as those of simulation 1 (reference model), except for the *lower contact stiffness* of the interface **(1000MPa** instead of 1700). All the parameters are shown in figure 4.10.

Simulations	Parameters				
Number of simulation	Geometry (R1/R2 ratio)	Contact stifness of interface (MPa)	Friction coefficient of interface	Contact Pressure (MPa)	Material model
1	**1.05**	**1700**	**0.35**	-	linear elastic
2	1.05	1000	0.35	-	
3	1.05	3000	0.35	-	
4	1.05	1.7E+10	0.35	-	
5	1.05	1.7E+10	0.35	124.5 (literature)	
6	1.05	1.7E+10	0.35	1.245E+11	
7	1.05	1.7E+10	1	1.245E+11	
8	1.00	1700	0.35	-	
9	1.10	1700	0.35	-	
10	1.05	1700	0.15	-	
11	1.05	1700	0.55	-	

(a) Basic parameters

Parameters	Geometry 1	Geometry 2	Geometry 3
θ1 (degrees)	**15**	15	18
θ2 (degrees)	**8.02**	14.89	3.02
R1 (mm)	**1.05**	1.00	1.10
R2 (mm)	**1.00**	1.00	1.00
R1/R2	**1.05**	1.00	1.10
w (mm)	**3.96**	3.86	3.99
L (mm)	**3.44**	3.55	3.60

(b) Basic parameters

Figure 4.10: Parameters used for simulation 2

The obtained Force-Displacement graph is shown below in comparison with the reference model's results.

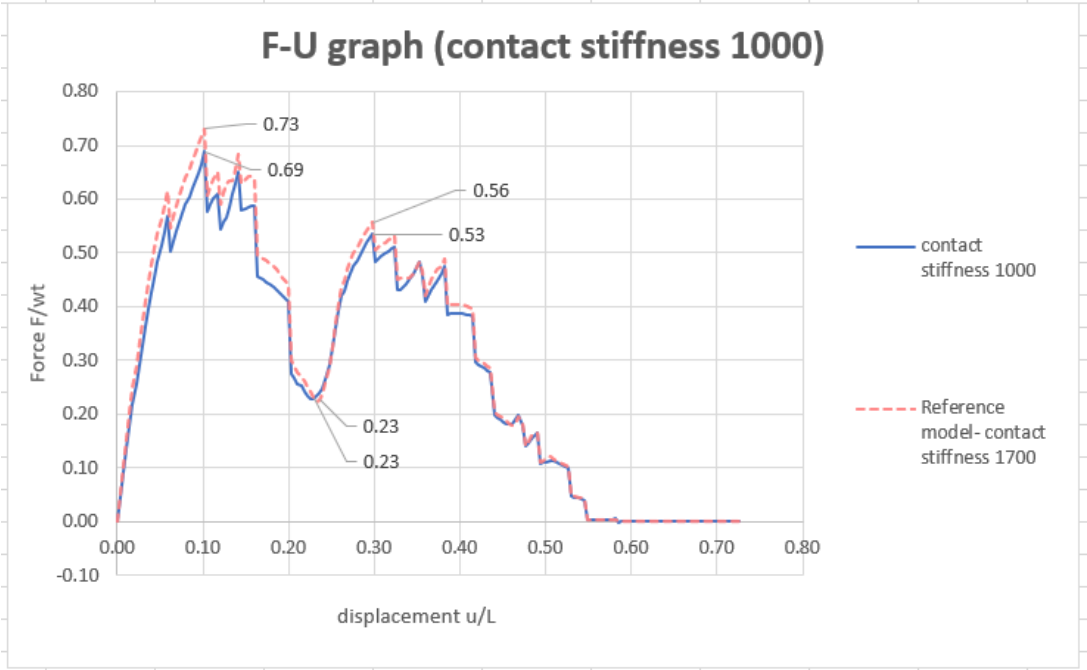

Figure 4.11: Force - Displacement plot normalized- Simulation 2

4.2.3 Simulation 3- Increased contact stiffness

Simulation 3 was created with parameters identical as simulation 1, except for the *higher contact stiffness* of the interface **(3000MPa** instead of 1700). All the parameters are shown in figure 4.12.

Simulations	Parameters				
Number of simulation	Geometry (R1/R2 ratio)	Contact stifness of interface (MPa)	Friction coefficient of interface	Contact Pressure (MPa)	Material model
1	**1.05**	**1700**	**0.35**	-	linear elastic
2	1.05	1000	0.35	-	
3	1.05	3000	0.35	-	
4	1.05	1.7E+10	0.35	-	
5	1.05	1.7E+10	0.35	124.5 (literature)	
6	1.05	1.7E+10	0.35	1.245E+11	
7	1.05	1.7E+10	1	1.245E+11	
8	1.00	1700	0.35	-	
9	1.10	1700	0.35	-	
10	1.05	1700	0.15	-	
11	1.05	1700	0.55	-	

(a) Basic parameters

Parameters	Geometry 1	Geometry 2	Geometry 3
θ1 (degrees)	**15**	15	18
θ2 (degrees)	**8.02**	14.89	3.02
R1 (mm)	**1.05**	1.00	1.10
R2 (mm)	**1.00**	1.00	1.00
R1/R2	**1.05**	1.00	1.10
w (mm)	**3.96**	3.86	3.99
L (mm)	**3.44**	3.55	3.60

(b) Basic parameters

Figure 4.12: Parameters used for simulation 3

The obtained Force-Displacement graph is shown below in comparison with the reference model's results.

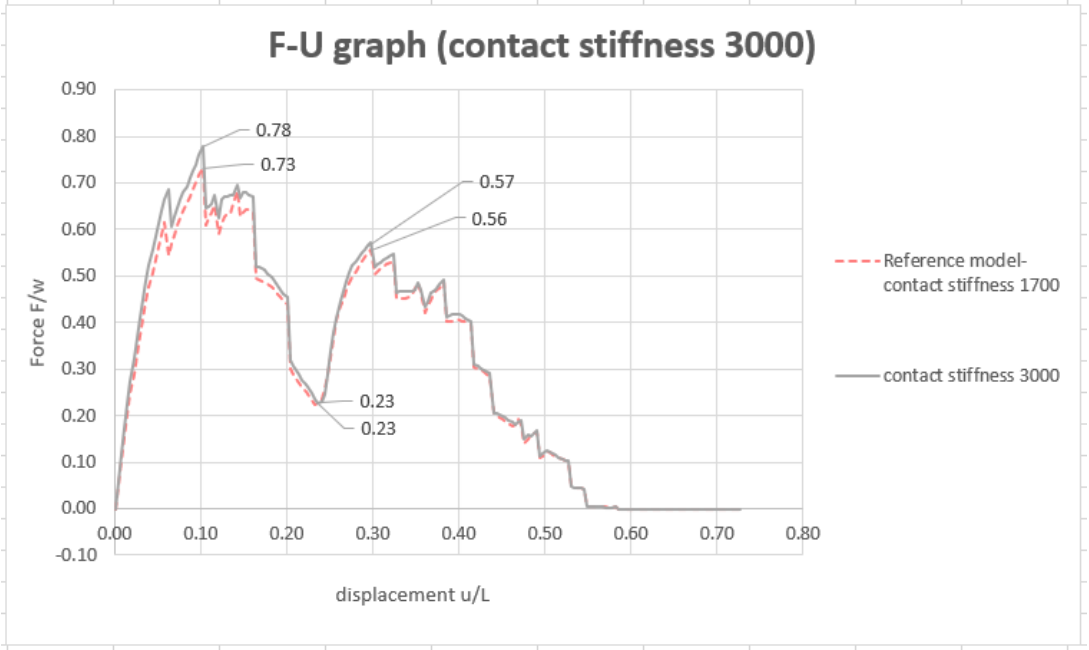

Figure 4.13: Force - Displacement plot normalized- Simulation 3

4.2.4 Simulation 4- Penalty stiffness & no contact pressure

Simulation 4 was created with parameters identical as simulation 1, except that penalty stiffness was used at the interface **(1.7E10 MPa** instead of 1700). All the parameters are shown in figure 4.14.

Simulations	Parameters				
Number of simulation	Geometry (R1/R2 ratio)	Contact stifness of interface (MPa)	Friction coefficient of interface	Contact Pressure (MPa)	Material model
1	**1.05**	**1700**	**0.35**	-	linear elastic
2	1.05	1000	0.35	-	
3	1.05	3000	0.35	-	
4	1.05	1.7E+10	0.35	-	
5	1.05	1.7E+10	0.35	124.5 (literature)	
6	1.05	1.7E+10	0.35	1.245E+11	
7	1.05	1.7E+10	1	1.245E+11	
8	1.00	1700	0.35	-	
9	1.10	1700	0.35	-	
10	1.05	1700	0.15	-	
11	1.05	1700	0.55	-	

(a) Basic parameters

Parameters	Geometry 1	Geometry 2	Geometry 3
θ1 (degrees)	**15**	15	18
θ2 (degrees)	**8.02**	14.89	3.02
R1 (mm)	**1.05**	1.00	1.10
R2 (mm)	**1.00**	1.00	1.00
R1/R2	**1.05**	1.00	1.10
w (mm)	**3.96**	3.86	3.99
L (mm)	**3.44**	3.55	3.60

(b) Basic parameters

Figure 4.14: Parameters used for simulation 4

The obtained Force-Displacement graph is shown below in comparison with the reference model's results.

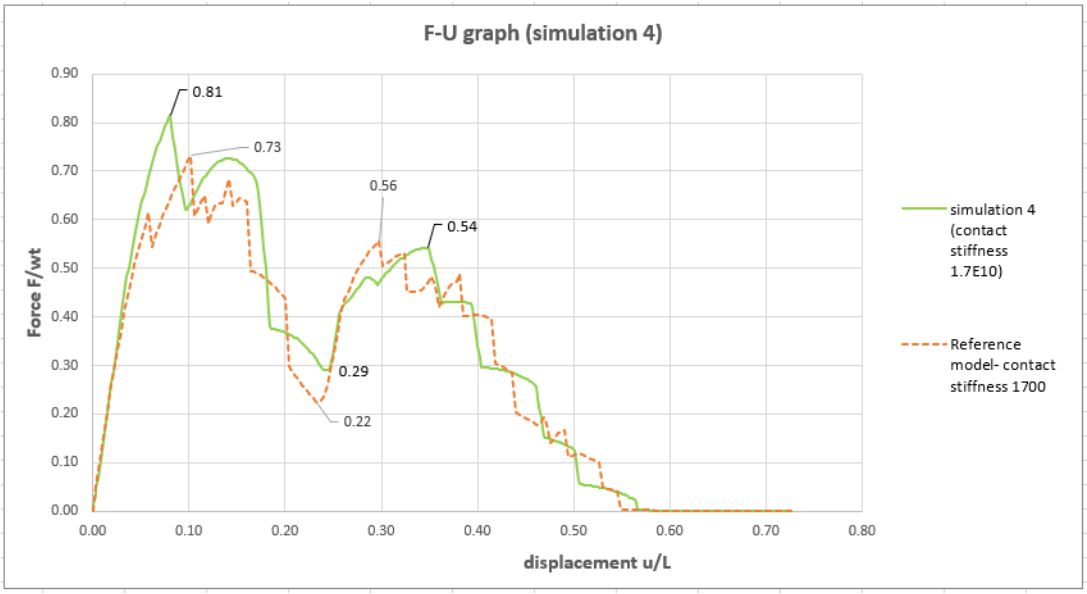

Figure 4.15: Force - Displacement plot normalized- Simulation 4

4.2.5 Simulation 5- Penalty stiffness & contact pressure

Simulation 5 was created with parameters identical as simulation 1, except that penalty stiffness was used at the interface **(1.7E10 MPa** instead of 1700) and the additional input of **maximum contact pressure**. The value of 124.5 MPa was added as it was measured in the paper (Mirkhalaf and Barthelat, 2017). All the parameters are shown in figure 4.16.

Simulations	Parameters				
Number of simulation	Geometry (R1/R2 ratio)	Contact stifness of interface (MPa)	Friction coefficient of interface	Contact Pressure (MPa)	Material model
1	**1.05**	**1700**	**0.35**	-	linear elastic
2	1.05	1000	0.35	-	
3	1.05	3000	0.35	-	
4	1.05	1.7E+10	0.35	-	
5	1.05	1.7E+10	0.35	124.5 (literature)	
6	1.05	1.7E+10	0.35	1.245E+11	
7	1.05	1.7E+10	1	1.245E+11	
8	1.00	1700	0.35	-	
9	1.10	1700	0.35	-	
10	1.05	1700	0.15	-	
11	1.05	1700	0.55	-	

(a) Basic parameters

Parameters	Geometry 1	Geometry 2	Geometry 3
θ1 (degrees)	**15**	15	18
θ2 (degrees)	**8.02**	14.89	3.02
R1 (mm)	**1.05**	1.00	1.10
R2 (mm)	**1.00**	1.00	1.00
R1/R2	**1.05**	1.00	1.10
w (mm)	**3.96**	3.86	3.99
L (mm)	**3.44**	3.55	3.60

(b) Basic parameters

Figure 4.16: Parameters used for simulation 5

The obtained Force-Displacement graph is shown below in comparison with the reference model's results.

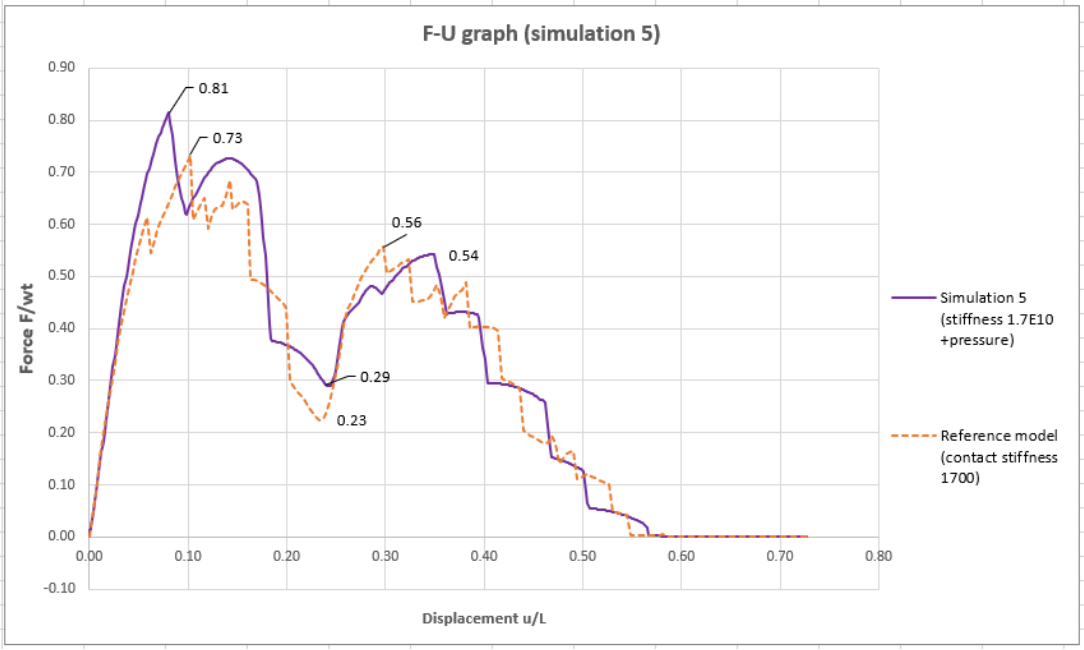

Figure 4.17: Force - Displacement plot normalized- Simulation 5

4.2.6 Simulation 6- Penalty stiffness & increased contact pressure

Simulation 6 was created with parameters identical as simulation 1, except that penalty stiffness was used at the interface **(1.7E10 MPa** instead of 1700) and also the additional input of **maximum contact pressure** of 1.245E11 MPa was added, which was 10^9 more than the one measured in the paper (Mirkhalaf et al., 2016). All the parameters are shown in figure 4.18.

Simulations	Parameters				
Number of simulation	Geometry (R1/R2 ratio)	Contact stifness of interface (MPa)	Friction coefficient of interface	Contact Pressure (MPa)	Material model
1	**1.05**	**1700**	**0.35**	-	linear elastic
2	1.05	1000	0.35	-	
3	1.05	3000	0.35	-	
4	1.05	1.7E+10	0.35	-	
5	1.05	1.7E+10	0.35	124.5 (literature)	
6	1.05	1.7E+10	0.35	1.245E+11	
7	1.05	1.7E+10	1	1.245E+11	
8	1.00	1700	0.35	-	
9	1.10	1700	0.35	-	
10	1.05	1700	0.15	-	
11	1.05	1700	0.55	-	

(a) Basic parameters

Parameters	Geometry 1	Geometry 2	Geometry 3
θ1 (degrees)	**15**	15	18
θ2 (degrees)	**8.02**	14.89	3.02
R1 (mm)	**1.05**	1.00	1.10
R2 (mm)	**1.00**	1.00	1.00
R1/R2	**1.05**	1.00	1.10
w (mm)	**3.96**	3.86	3.99
L (mm)	**3.44**	3.55	3.60

(b) Basic parameters

Figure 4.18: Parameters used for simulation 6

The obtained Force- Displacement graph is shown below in comparison with the reference model's results.

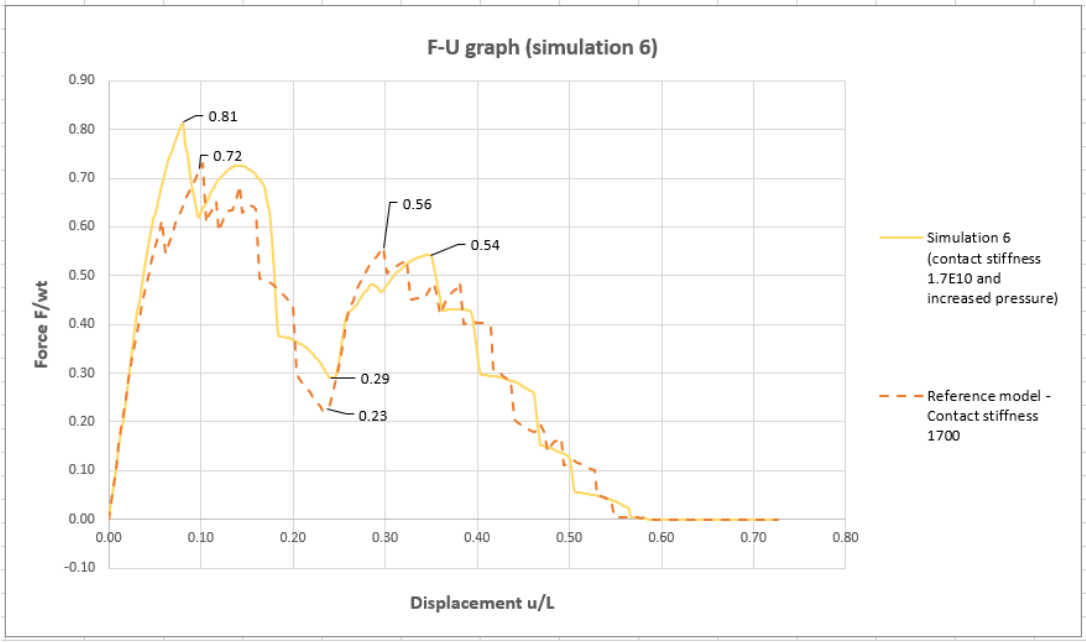

Figure 4.19: Force - Displacement plot normalized- Simulation 6

4.2.7 Simulation 7- Penalty stiffness & increased contact pressure & increased friction coefficient

Simulation 7 was created with parameters identical as simulation 1, except that penalty stiffness was used at the interface **(1.7E10 MPa** instead of 1700) and also the additional input of **maximum contact pressure** of 1.245E11 MPa was added and the **friction coefficient** was increased to 1.0. This value of contact pressure was 10^9 more than the one measured in the paper (Mirkhalaf et al., 2016) and the friction coefficient is also larger (in the paper was 0.35). All the parameters are shown in figure 4.20.

Simulations	Parameters				
Number of simulation	Geometry (R1/R2 ratio)	Contact stifness of interface (MPa)	Friction coefficient of interface	Contact Pressure (MPa)	Material model
1	**1.05**	**1700**	**0.35**	-	linear elastic
2	1.05	1000	0.35	-	
3	1.05	3000	0.35	-	
4	1.05	1.7E+10	0.35	-	
5	1.05	1.7E+10	0.35	124.5 (literature)	
6	1.05	1.7E+10	0.35	1.245E+11	
7	1.05	1.7E+10	1	1.245E+11	
8	1.00	1700	0.35	-	
9	1.10	1700	0.35	-	
10	1.05	1700	0.15	-	
11	1.05	1700	0.55	-	

(a) Basic parameters

Parameters	Geometry 1	Geometry 2	Geometry 3
θ1 (degrees)	**15**	15	18
θ2 (degrees)	**8.02**	14.89	3.02
R1 (mm)	**1.05**	1.00	1.10
R2 (mm)	**1.00**	1.00	1.00
R1/R2	**1.05**	1.00	1.10
w (mm)	**3.96**	3.86	3.99
L (mm)	**3.44**	3.55	3.60

(b) Basic parameters

Figure 4.20: Parameters used for simulation 7

The obtained Force- Displacement graph is shown below in comparison with the reference model's results.

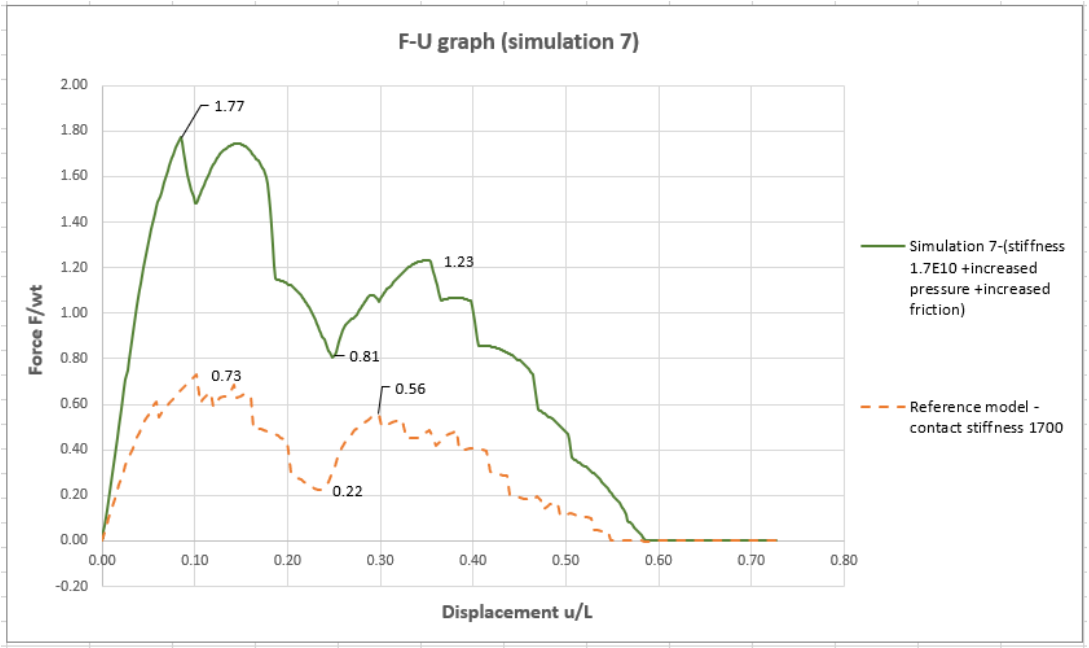

Figure 4.21: Force - Displacement plot normalized- Simulation 7

4.2.8 Comparison of simulations with different interface parameters

The normalized force-displacement graphs extracted from the simulations 1, 2, 3 are presented below. *Simulation 1* (initial model) was created with the same contact stiffness at the interface as the rest of the material, namely **1700 MPa**. *Simulation 2* was created with lower contact stiffness at the interface (**1000 MPa**) and *simulation 3* had higher contact stiffness at the interface (**3000 MPa**).

Simulation 2 with the lowest contact stiffness at the interface (1000 MPa), was also the one with the lowest reaction forces exerted in the graph 4.22 (blue line). This result shows that with a weaker (”less stiff”) interface the reaction forces from the pull-out test extracted at the top of the suture were also smaller, meaning that it was easier to pull out and displace the parts of such a model than simulation 1 (contact stiffness 1700 MPa) and simulation 3 (contact stiffness 3000 MPa).

The higher the interface stiffness the higher the forces extracted, see figure 4.22. This observation is true for almost all the points of the graph, except the reaction force value at the kink, which was unaffected by the change in stiffness. As the stiffness of the interface was increased from 1000 to 1700 and then to 3000 MPa the kink positions (for model 1, 2, 3) shifted slightly to the right, benefiting the strain hardening behavior locally as the system would require more displacement to reach the second equilibrium position but the strain at the end is almost the same. The position of the kink is located approximately at 0.22 $\approx$0.24 u/L.

A general observation is that additional stiffness at the interface can be helpful by making the system harder to transform but a very large increase in stiffness could also result in brittle failure of the tab.

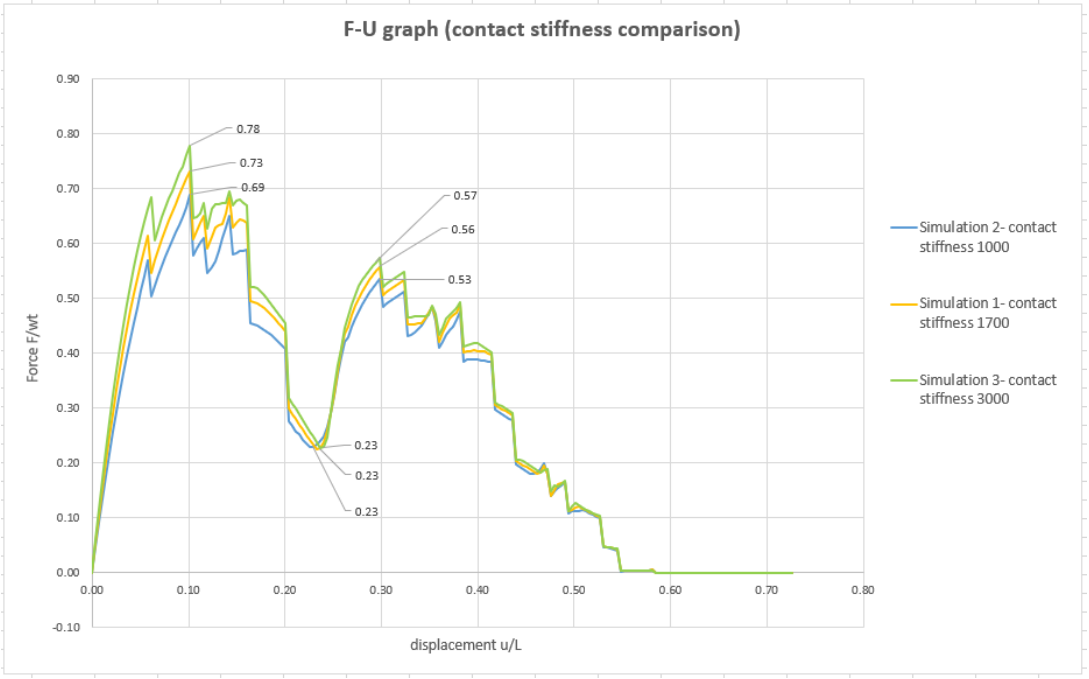

Figure 4.22: Comparison of models 1,2,3- Different contact stiffnesses

To obtain the ”higher” reaction forces according to the experimental results of (Mirkhalaf and Barthelat, 2017) penalty contact stifness of 1.7E10 was applied at the interface as mentioned before. The results of the simulations with penalty contact stiffness (dotted lines) in comparison to the ”normal” stiffness values (continuous lines) are given below.

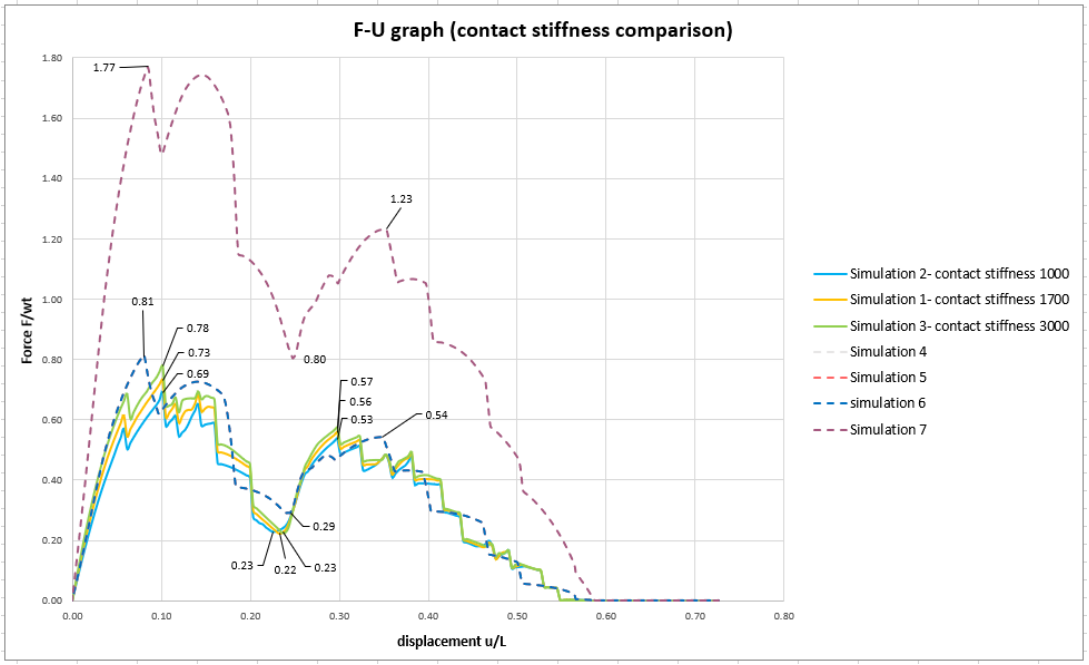

Figure 4.23: Comparison of models with penalty and normal stiffness

The results do not present as high peaks as it was the case at the experimental results, however with the penalty stiffness and increased friction (simulation 7), the forces at the first and second peak become more than double. The additional input of contact pressure did not contribute to the increase since simulations 4, 5, 6 have identical curve. In the end, the friction coefficient increase from 0.35 to 1.0 (simulation 7) has the largest effect at the total response. This result shows that even with very high contact stiffness and friction at the interface the reaction forces will not increase more than a point. Also the danger of brittle failure of the tabs is higher.

4.3 Geometry of the tab

The geometry of the tabs is very important for the bistable interlock effect. By fine tuning the interlocking angles and radii, the response of the system can change greatly. At this subchapter, a comparison of sutures with higher and lower interlocking radii ratios is performed.

4.3.1 Simulation 8- R1/R2=1.00

Simulation 8 was created with parameters similar to the reference model (simulation 1). For this case the geometry differs as *geometry 2* was used **(R_1/R_2=1.00** instead of 1.05 of the initial model- see fig. 4.24b). Geometry 2 is based on a different R_1/R_2 ratio and this influences also θ_1, θ_2 angles and the width and height of the sample according to the formulas (2.1), (2.2), (2.3). All the other parameters were kept the same (friction coefficient and contact stiffness of the interface) and they are presented in detail in the figure 4.24.

Simulations	Parameters				
Number of simulation	Geometry (R1/R2 ratio)	Contact stifness of interface (MPa)	Friction coefficient of interface	Contact Pressure (MPa)	Material model
1	**1.05**	**1700**	**0.35**	-	linear elastic
2	1.05	1000	0.35	-	
3	1.05	3000	0.35	-	
4	1.05	1.7E+10	0.35	-	
5	1.05	1.7E+10	0.35	124.5 (literature)	
6	1.05	1.7E+10	0.35	1.245E+11	
7	1.05	1.7E+10	1	1.245E+11	
8	1.00	1700	0.35	-	
9	1.10	1700	0.35	-	
10	1.05	1700	0.15	-	
11	1.05	1700	0.55	-	

(a) Basic parameters

Parameters	Geometry 1	Geometry 2	Geometry 3
θ1 (degrees)	15	**15**	18
θ2 (degrees)	8.02	**14.89**	3.02
R1 (mm)	1.05	**1.00**	1.10
R2 (mm)	1.00	**1.00**	1.00
R1/R2	1.05	**1.00**	1.10
w (mm)	3.96	**3.86**	3.99
L (mm)	3.44	**3.55**	3.60

(b) Geometry parameters

Figure 4.24: Parameters used for simulation 8

The obtained Force-Displacement graph is shown below in comparison with the reference model's results.

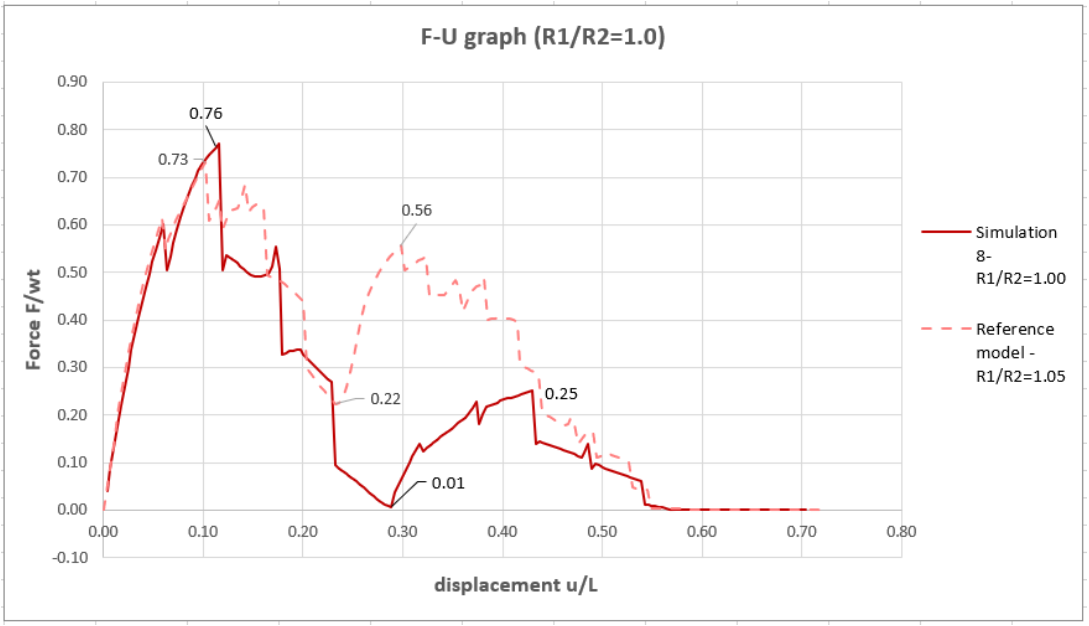

Figure 4.25: Force - Displacement plot normalized- Simulation 8

4.3.2 Simulation 9- R1/R2=1.10

Simulation 9 was created with parameters similar to the initial model (simulation 1). For this case the geometry differs as *geometry 3* was used **(R_1/R_2=1.10** instead of 1.05 as in the initial model- see fig. 4.26b). Geometry 3 is based on a different R_1/R_2 ratio and this influences also θ_1, θ_2 angles and the width and height according to the formulas (2.1), (2.2), (2.3). All the other parameters were kept the same (friction coefficient, contact stiffness of the interface) and they are presented in detail in figure 4.26.

Simulations	Parameters				
Number of simulation	Geometry (R1/R2 ratio)	Contact stifness of interface (MPa)	Friction coefficient of interface	Contact Pressure (MPa)	Material model
1	**1.05**	**1700**	**0.35**	-	linear elastic
2	1.05	1000	0.35	-	
3	1.05	3000	0.35	-	
4	1.05	1.7E+10	0.35	-	
5	1.05	1.7E+10	0.35	124.5 (literature)	
6	1.05	1.7E+10	0.35	1.245E+11	
7	1.05	1.7E+10	1	1.245E+11	
8	1.00	1700	0.35	-	
9	1.10	1700	0.35	-	
10	1.05	1700	0.15	-	
11	1.05	1700	0.55	-	

(a) Basic parameters

Parameters	Geometry 1	Geometry 2	Geometry 3
θ1 (degrees)	15	15	**18**
θ2 (degrees)	8.02	14.89	**3.02**
R1 (mm)	1.05	1.00	**1.10**
R2 (mm)	1.00	1.00	**1.00**
R1/R2	1.05	1.00	**1.10**
w (mm)	3.96	3.86	**3.99**
L (mm)	3.44	3.55	**3.60**

(b) Geometry parameters

Figure 4.26: Parameters used for simulation 9

The obtained Force-Displacement graph is shown below, in comparison with the reference model's results.

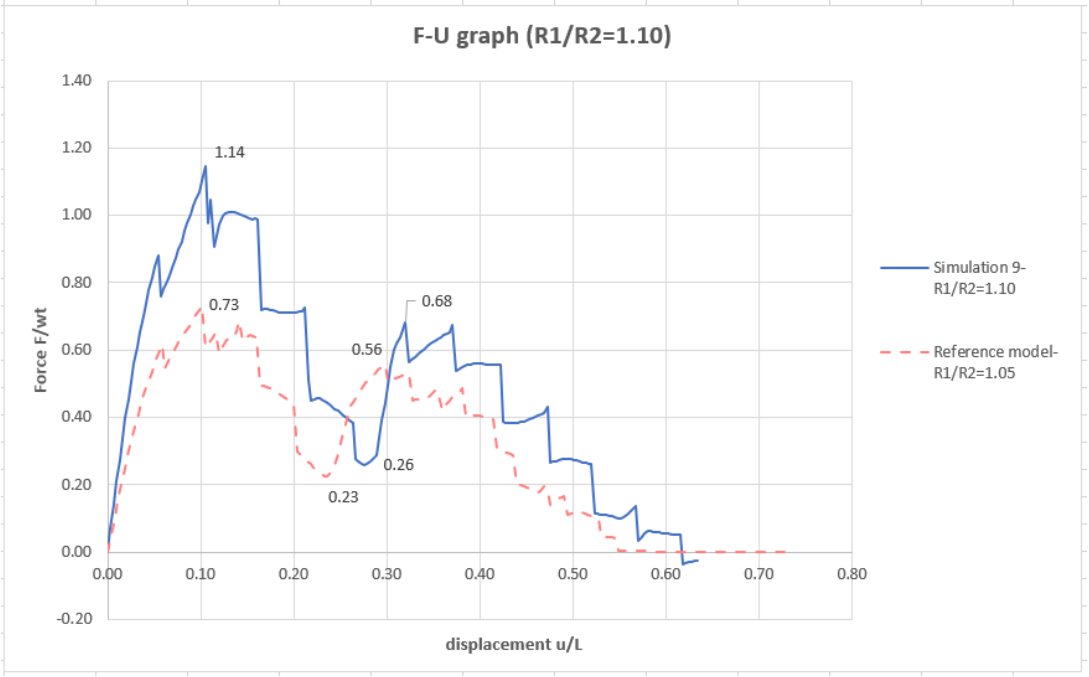

Figure 4.27: Force - Displacement plot normalized- Simulation 9

4.3.3 Comparison of simulations with different geometry parameters

In the paper (Mirkhalaf and Barthelat, 2017) experimental results for R_1 / R_2=1.00 and 1.05 are presented (figure 4.28) and these results are going to be compared with the equivalent ones from the numerical models:

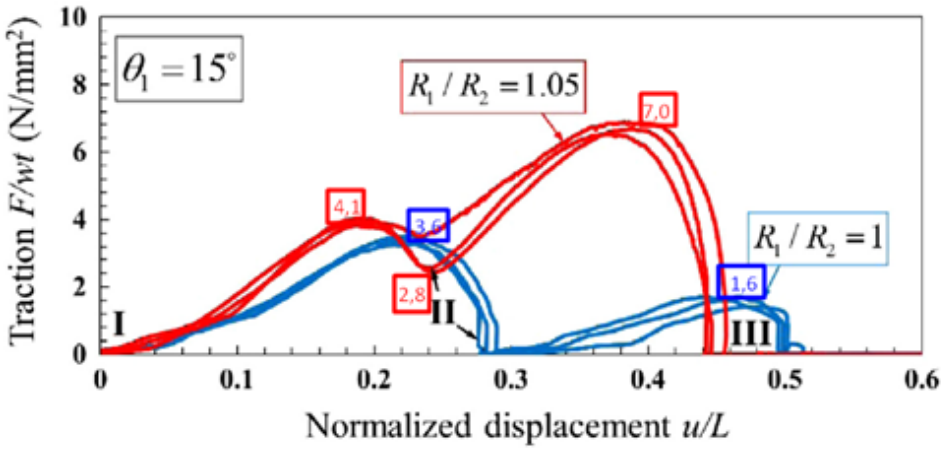

Figure 4.28: Results taken from the paper (Mirkhalaf and Barthelat, 2017)

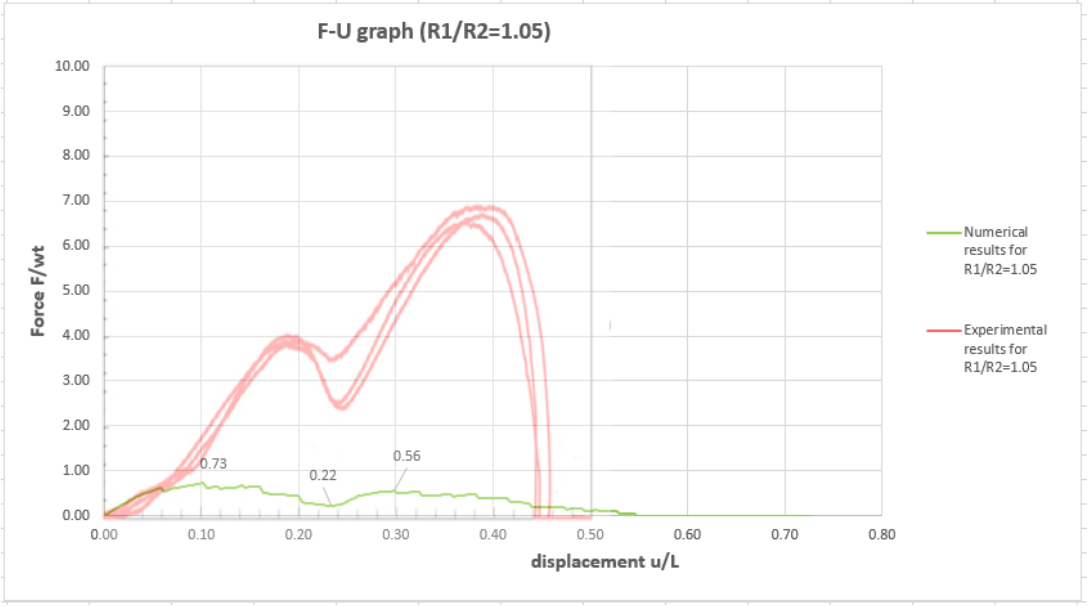

Figure 4.29: Experimental- Numerical results comparison R1/R2=1.05

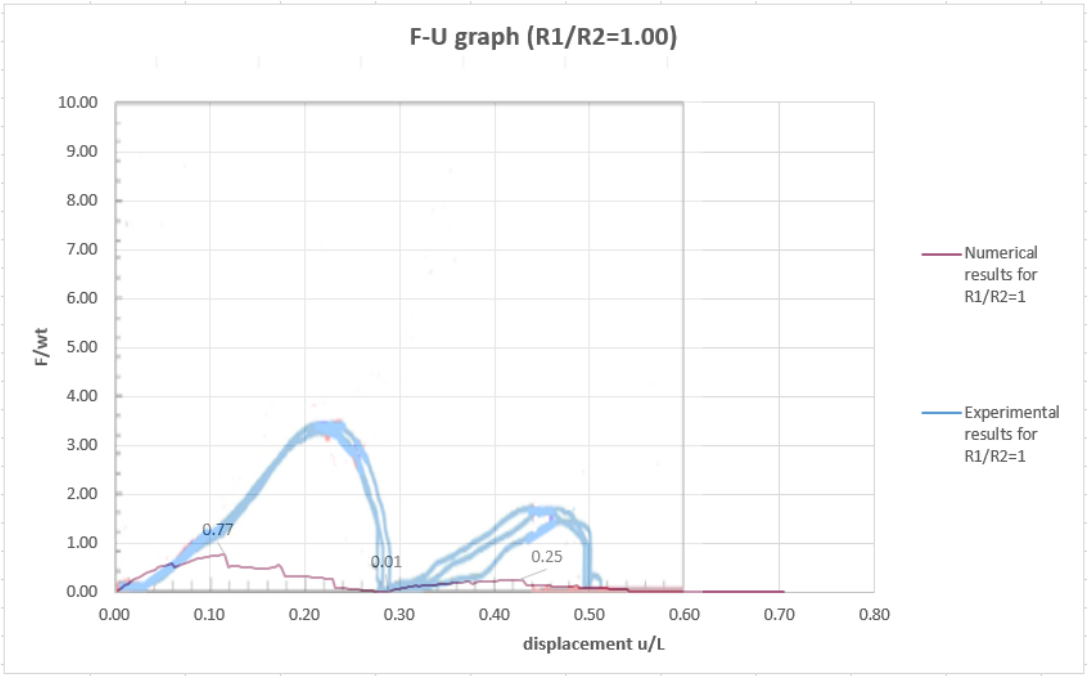

Figure 4.30: Experimental- Numerical results comparison R1/R2=1.00

The *red* curve was already compared with *simulation 1* with R_1/R_2=1.05 (see subchapter 4.1.5) and the *blue* curve can be compared with *simulation 8* with R_1/R_2=1.00.

So a verification for simulation 8 can occur since there are experimental data to compare this simulation with.

For **model 1** (R_1/R_2=1.05) as mentioned in the subchapter 4.1.5 the major difference between the F-U graph from the experimental and numerical analysis concerns the peaks. The second peak is higher in the experimental results while the first one at the numerical results (see figure 4.29). A desirable outcome would be to have a higher second peak since it adds to the overall mechanical stability of the system. When the first peak is higher, the system is less stable since it would be easier for the tabs to get pulled out from the second equilibrium position that the first. This effect could reduce the ductility of a system comprised of a lot of these sutures. Regarding the kink position, it is almost the same.

For **model 8** (R_1/R_2=1.00) the numerical and experimental results show more similarities than the aforementioned model 1. In both experimental and numerical results the first peak is higher than the second and the kink is at zero stress (due to the specific geometry with equal R_1 & R_2, this part fits without stresses at the pull-out). The kink's location is almost at the same value of u/L in both experiment and numerical analysis (see figure 4.30). The values (as in model 1) are lower than those of the experimental results. This simulation can be verified since the curve is quite close to the one corresponding to the experimental results.

Another variation of the geometry was performed in **model 9** (R_1/R_2=1.10). A higher interlocking radii ratio results in higher forces and the kink appeared later than the R_1/R_2=1.05 curve, which can have a positive effect on the overall ductility of the system. However, in this model, since the difference in the first and second radius is larger, the danger of fracture of the tabs (a failure mode unwanted for the specific model) is higher. This was also tested in the experiments and highlighted in the paper (Mirkhalaf and Barthelat, 2017).

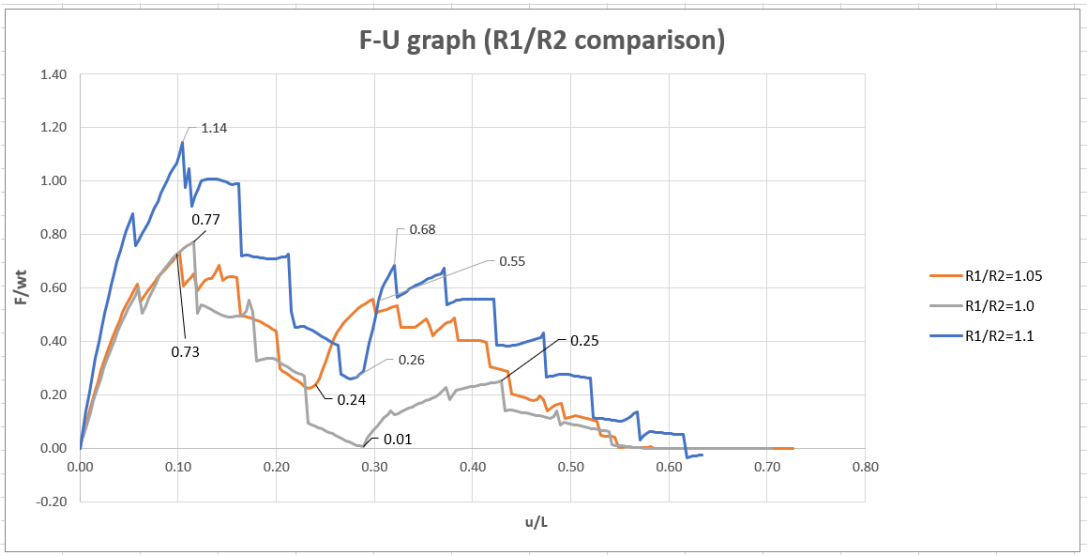

Figure 4.31: Comparison of models 1,8,9- Different geometry parameters

The results of the three models are quite different. What could be observed from the comparison amongst them is that a *higher* interlocking radii ratio *enhances* the interlocking effect but could also cause brittle failure due to the excessive stresses at the tab. The R_1/R_2=1 model

does not offer high mechanical stability compared to the other simulations since the second peak is much lower than the first. The R_1/R_2=1.05 model presents higher reaction forces than R_1/R_2=1, but the kink (2nd equilibrium position) comes earlier (at smaller developed strains), in this way it does not delay the strains as effectively as the other 2 models.

The geometry of the system and specifically the R_1/R_2 ratio is a *very sensitive parameter* that affects the mechanical response the most compared to θ_1, the friction coefficient, and material parameters (Hu et al., 2018). The R_1/R_2 ratios are picked from an admissible domain (see figure 2.4) and the change in the ratio also affects the angles θ_1, θ_2 to make the interlocking effect feasible. That being said, a small change in the ratio can affect the response a lot and it would be optimal if a lot of different models with different geometry parameters were constructed to draw more accurate conclusions at this part.

4.4 Friction at the interface

During the pull out of the suture, the top and bottom parts are sliding away from one another. Stresses develop to oppose this motion and these are normal and tangential (frictional) stresses, correlated with the friction coefficient. In this subchapter, the response of sutures with higher and lower friction coefficients is going to be compared.

4.4.1 Simulation 10- Decreased friction coefficient

Simulation 10 was created with parameters same as those of simulation 1, except for the *lower friction coefficient* **(0.15** instead of 0.35). The geometry is the same as the initial model **(geometry 1)**. All the parameters are shown in figure 4.32.

Simulations	Parameters				
Number of simulation	Geometry (R1/R2 ratio)	Contact stifness of interface (MPa)	Friction coefficient of interface	Contact Pressure (MPa)	Material model
1	**1.05**	**1700**	**0.35**	-	linear elastic
2	1.05	1000	0.35	-	
3	1.05	3000	0.35	-	
4	1.05	1.7E+10	0.35	-	
5	1.05	1.7E+10	0.35	124.5 (literature)	
6	1.05	1.7E+10	0.35	1.245E+11	
7	1.05	1.7E+10	1	1.245E+11	
8	1.00	1700	0.35	-	
9	1.10	1700	0.35	-	
10	1.05	1700	0.15	-	
11	1.05	1700	0.55	-	

(a) Basic parameters

Parameters	Geometry 1	Geometry 2	Geometry 3
θ1 (degrees)	**15**	15	18
θ2 (degrees)	**8.02**	14.89	3.02
R1 (mm)	**1.05**	1.00	1.10
R2 (mm)	**1.00**	1.00	1.00
R1/R2	**1.05**	1.00	1.10
w (mm)	**3.96**	3.86	3.99
L (mm)	**3.44**	3.55	3.60

(b) Geometry parameters

Figure 4.32: Parameters used for simulation 10

The obtained Force-Displacement graph is shown in comparison with the reference model's results.

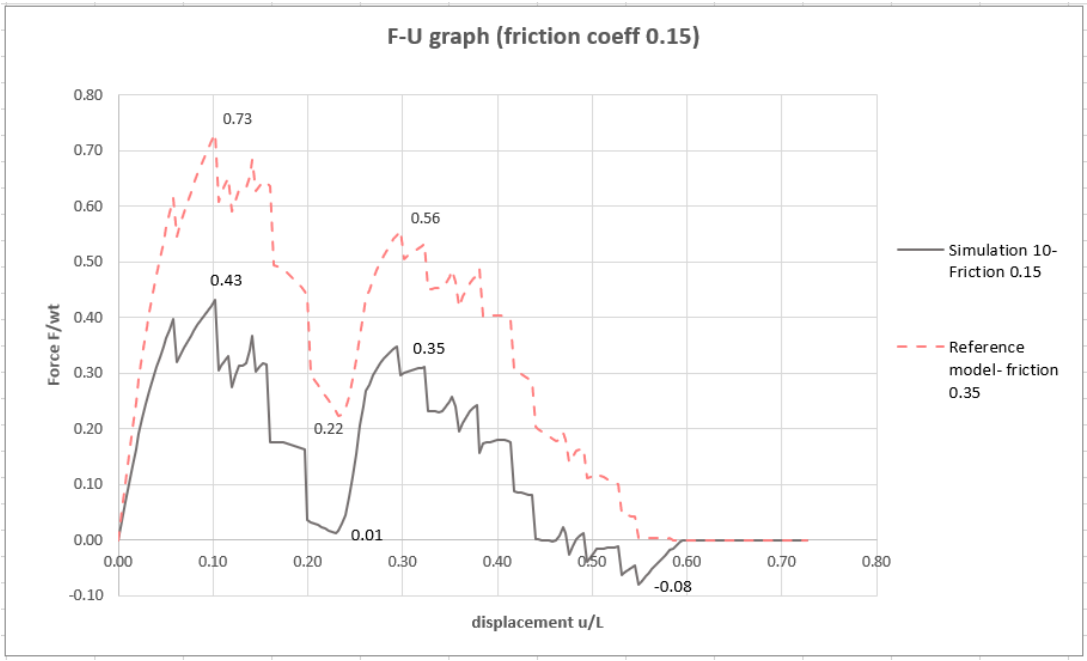

Figure 4.33: Force - Displacement plot normalized- Simulation 10

4.4.2 Simulation 11- Increased friction coefficient

Simulation 11 was created with parameters same as those of simulation 1, except the *higher friction coefficient* **(0.55** instead of 0.35). The geometry is the same as the initial model **(geometry 1)**. All the parameters are shown in figure 4.34.

Simulations	Parameters				
Number of simulation	Geometry (R1/R2 ratio)	Contact stifness of interface (MPa)	Friction coefficient of interface	Contact Pressure (MPa)	Material model
1	**1.05**	**1700**	**0.35**	-	linear elastic
2	1.05	1000	0.35	-	
3	1.05	3000	0.35	-	
4	1.05	1.7E+10	0.35	-	
5	1.05	1.7E+10	0.35	124.5 (literature)	
6	1.05	1.7E+10	0.35	1.245E+11	
7	1.05	1.7E+10	1	1.245E+11	
8	1.00	1700	0.35	-	
9	1.10	1700	0.35	-	
10	1.05	1700	0.15	-	
11	1.05	1700	0.55	-	

(a) Basic parameters

Parameters	Geometry 1	Geometry 2	Geometry 3
θ1 (degrees)	**15**	15	18
θ2 (degrees)	**8.02**	14.89	3.02
R1 (mm)	**1.05**	1.00	1.10
R2 (mm)	**1.00**	1.00	1.00
R1/R2	**1.05**	1.00	1.10
w (mm)	**3.96**	3.86	3.99
L (mm)	**3.44**	3.55	3.60

(b) Geometry parameters

Figure 4.34: Parameters used for simulation 11

The obtained Force-Displacement graph is shown below in comparison with the reference model's results.

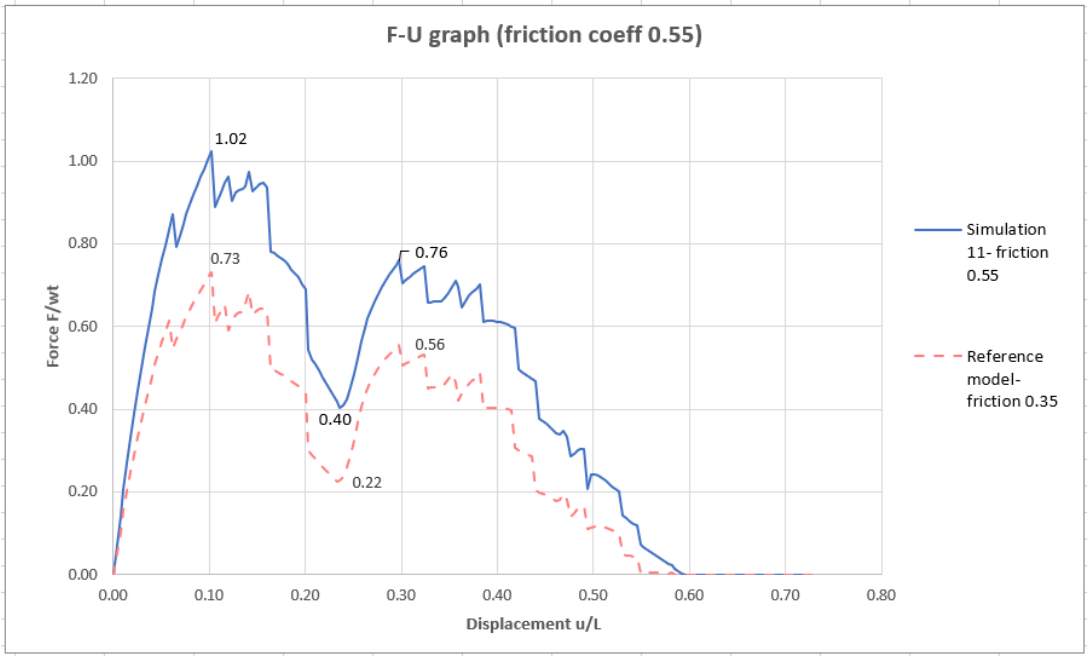

Figure 4.35: Force - Displacement plot normalized- Simulation 11

4.4.3 Comparison of simulations with different friction coefficients

For model 1 (reference) the friction coefficient from the paper (Mirkhalaf et al., 2016) **(f=0.35)** was used. Model 10 and model 11 were 2 variations of the initial model with friction coefficients f=0.15 and f=0.55 respectively, to test how the friction coefficient affects the system's response to the pull-out test.

The results show that with lower friction at the interface **(f=0.15)** the forces extracted are lower. An interesting fact is the appearance of negative forces (Model 10- friction coefficient 0.15) at the end of the curve that could be related to a bounce-back effect.

The first peak is highly influenced by the increase in the friction coefficient. For friction coefficient 0.15, the peaks 1 and 2 have a 24% difference while for f=0.35 the first peak has 28% higher maximum value than the second and the 0.55 curve had 30% difference at the first and second peak.

In the case of lower friction coefficient the kink reaches almost *zero* force. This is an interesting result as it means the friction coefficient heavily influences the locking position, there are almost no stresses there due to the low friction.

A higher coefficient of friction, according to parametric research, can help with strength, stiffness, and energy absorption (Malik et al., 2017). However, high tensile stresses in the contact areas are also produced by the high friction at the interface, and these stresses have the potential to cause the tabs to fracture. On the contrary, a low friction coefficient allows for higher interlocking angles to be used without the tabs cracking, which in turn results in increased stiffness and strength. Low friction coefficients also reduce the tensile stresses in the contact zones [(Mirkhalaf and Barthelat, 2017)]. However, this is not what it is depicted in the figure

4.36. The friction coefficient increase has a positive influence on the strength and energy absorption for the values examined (f=0.15, 0.35, 0.55), but the increase should be moderated to avoid brittle failure of the tabs.

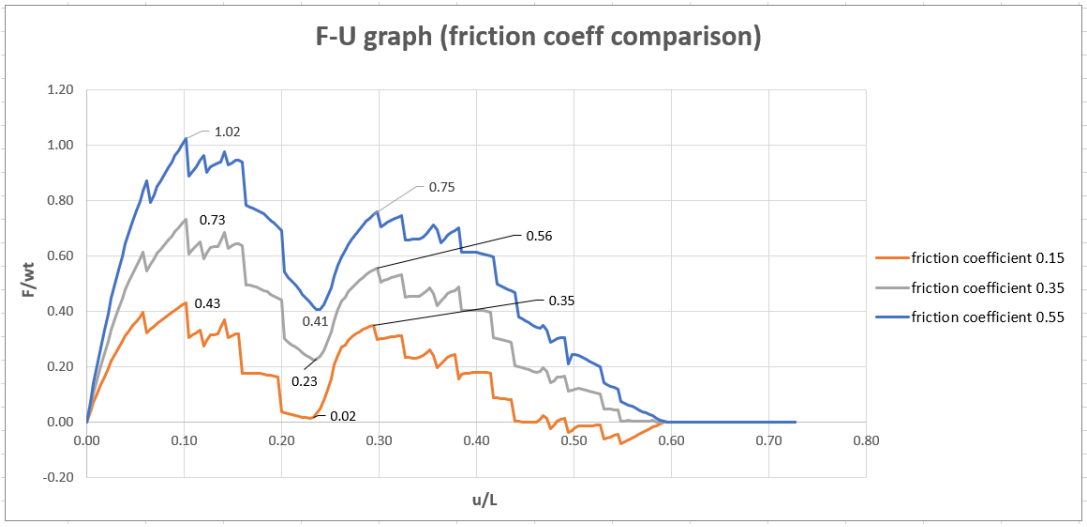

Figure 4.36: Comparison of models 1,6,7- Different friction coefficients

4.5 Material model study

In this subchapter, the obtained results from the elastic, elastic-brittle and elastoplastic material models will be compared. In the end a sensitivity analysis concerning the elastoplastic material will be performed to determine the influence of the change in the constitutive relations on the total response.

4.5.1 Elastic material model

Assumption: The material performs elastically and there is no modelling of cracks. The strains are in the linear elastic regime.

The results following this material model are presented below:

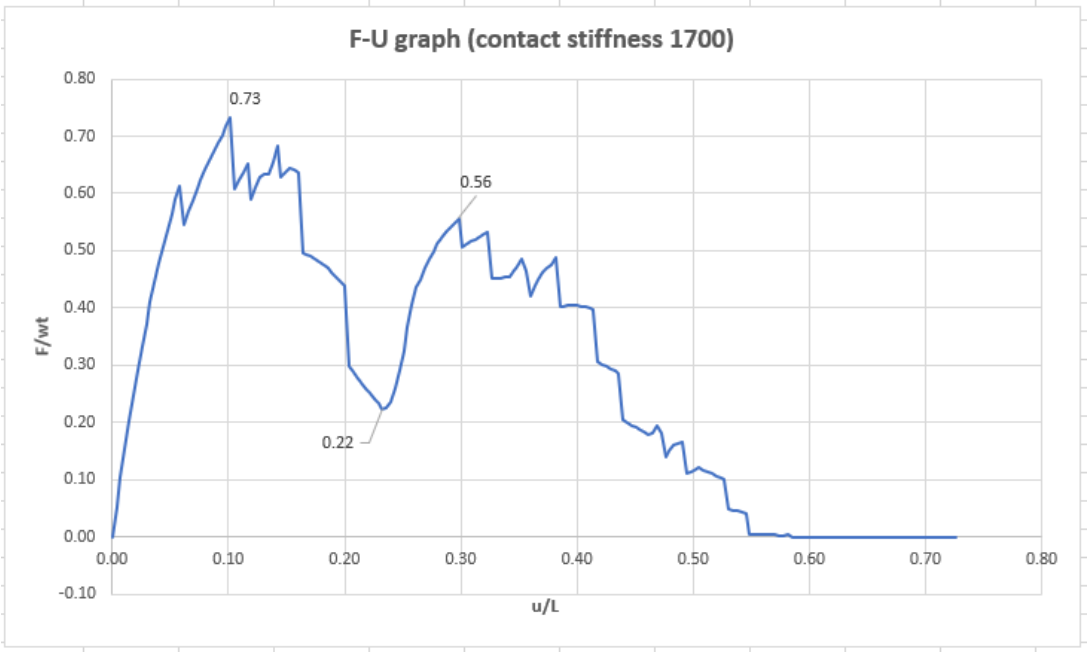

Figure 4.37: Analysis results with linear elastic material model

4.5.2 Elastic-brittle material model

For the material model that included cracking, the same parameters were used as the elastic model. The density of the ABS used was $1.07E-09$ ton/mm3, the Young's modulus was 1700 MPa and the Poisson's ratio $\nu = 0.2$. The only difference was that the property brittle cracking was added to the material model to capture the brittle failure of ABS.

With the elastic-brittle material model, the force-displacement plots were very different from the experimental ones and not many conclusions could be drawn nor a clear comparison with the experimental results could be performed.

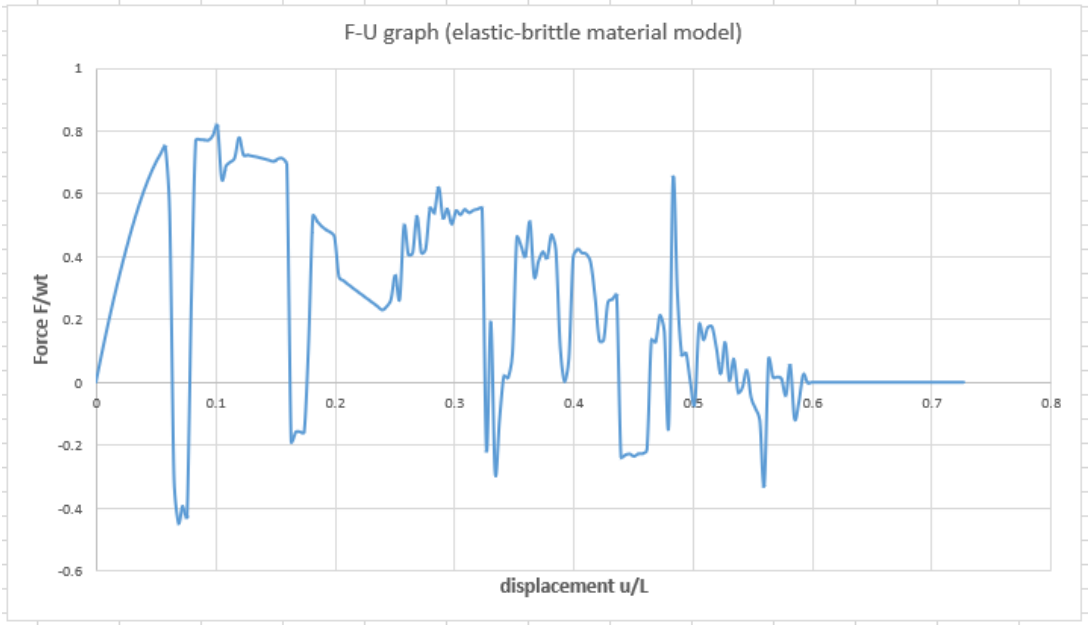

Figure 4.38: Analysis results with elastic-brittle material model

The results from the analysis of the elastic-brittle material model, were quite distorted. The modelling of cracks adds more complexity to the model. The kinks at the graph (loading-unloading phases) suggest the opening of cracks.

At the same model, analyses with *smaller time period* were performed and the trend of the graph showed similarities with the experimental results. This is related to the time of the crack initiation that mostly took place after the locking position. These results are presented below for an analysis with time period of t=100 (instead of the regular t=500 that was used for simulations 1-11). However with t=100, the suture did not undergo the complete pull-out, the analysis was completed after the interlocking position but while the top and bottom part were still in contact.

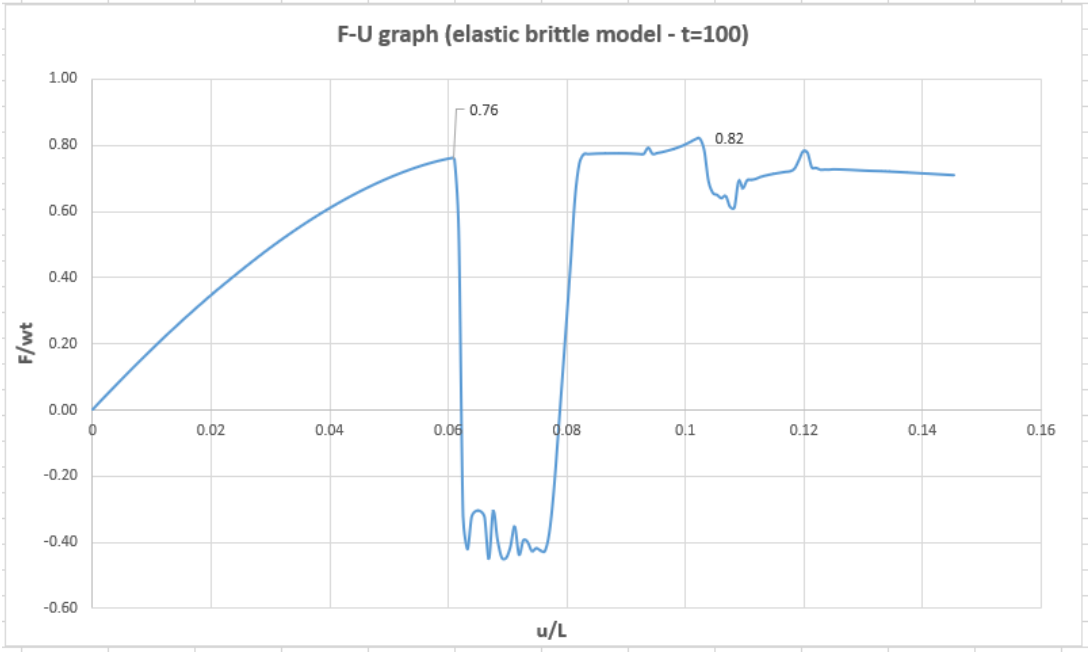

Figure 4.39: Analysis with t=100 and elastic-brittle material model

This curve presents similarities with the experimental results. The trend of the curve presents the first peak and a sudden drop with a following plateau (where it would be the kink's position) and then a second spike. A contour plot of the stresses at the end of the analysis is also shown in figure 4.40 to illustrate the opening of the cracks.

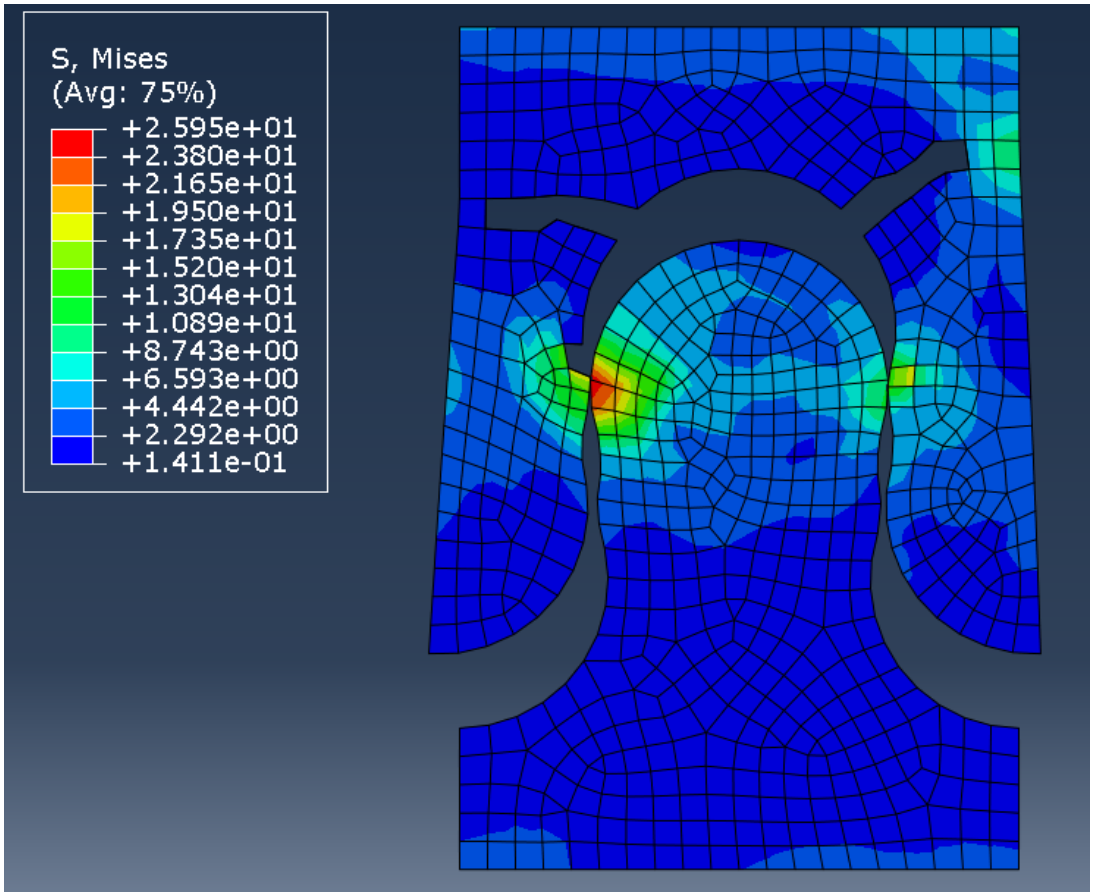

Figure 4.40: Stresses and crack formation (elastic-brittle material model)

4.5.3 Elastoplastic material model

The added plastic regime to the material model (see subchapter 3.3.3) gave the following output:

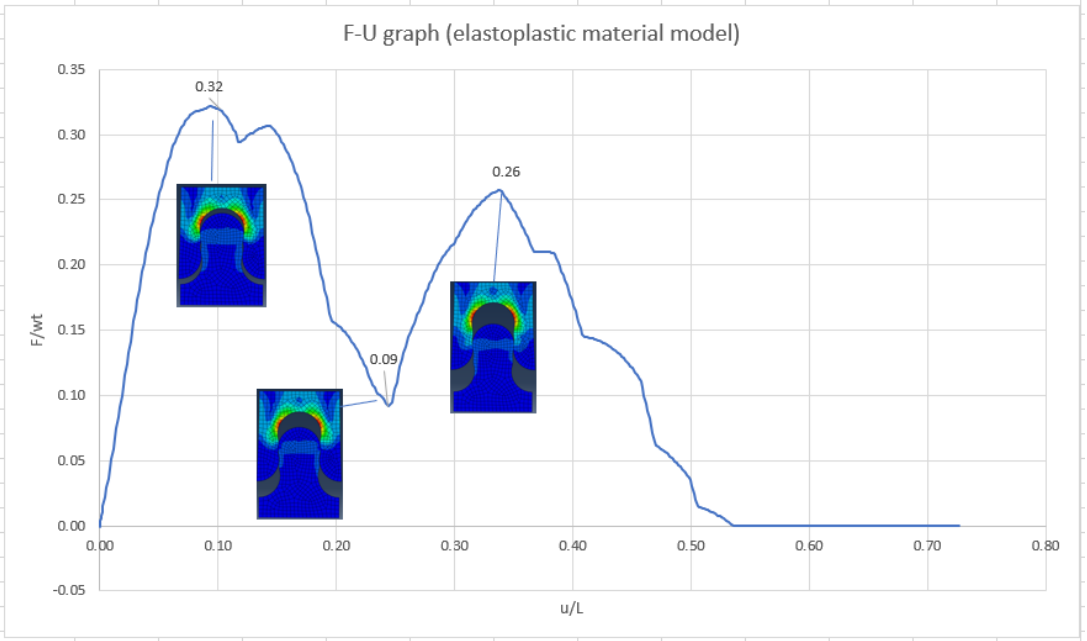

Figure 4.41: Force - Displacement plot for elastoplastic material model

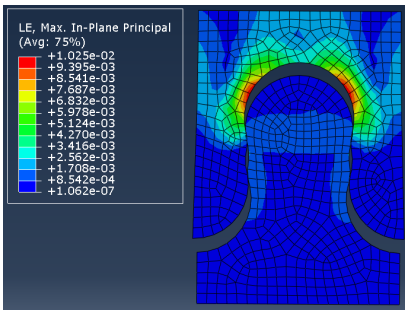

(a) Strain at the first peak

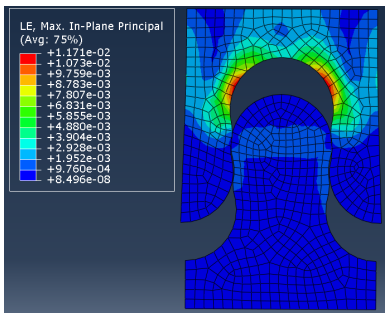

(b) Strain at the kink

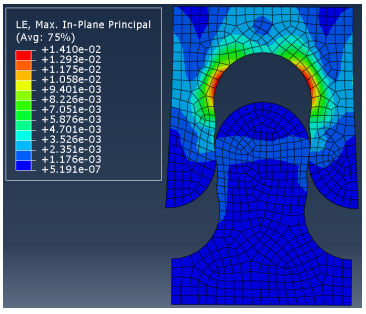

(c) Strain at the second peak

Figure 4.42: Strain contours at characteristic locations of the F-U curve

The F-U graph of the elastoplastic constitutive relation results in lower reaction forces, as expected. The redistribution of stresses and plastic deformations in a ductile material can have this effect compared to a more brittle material.

4.5.4 Comparison of the response with different material models

To compare all the material models and understand which one gives the best results, the following graph was plotted. Limitations need to be taken into account here. The models are not fully comparable since the elastoplastic material model was analysed with static analysis but the elastic brittle cracking model could only be analysed with dynamic explicit analysis due to the nature of the brittle cracking property's time dependency:

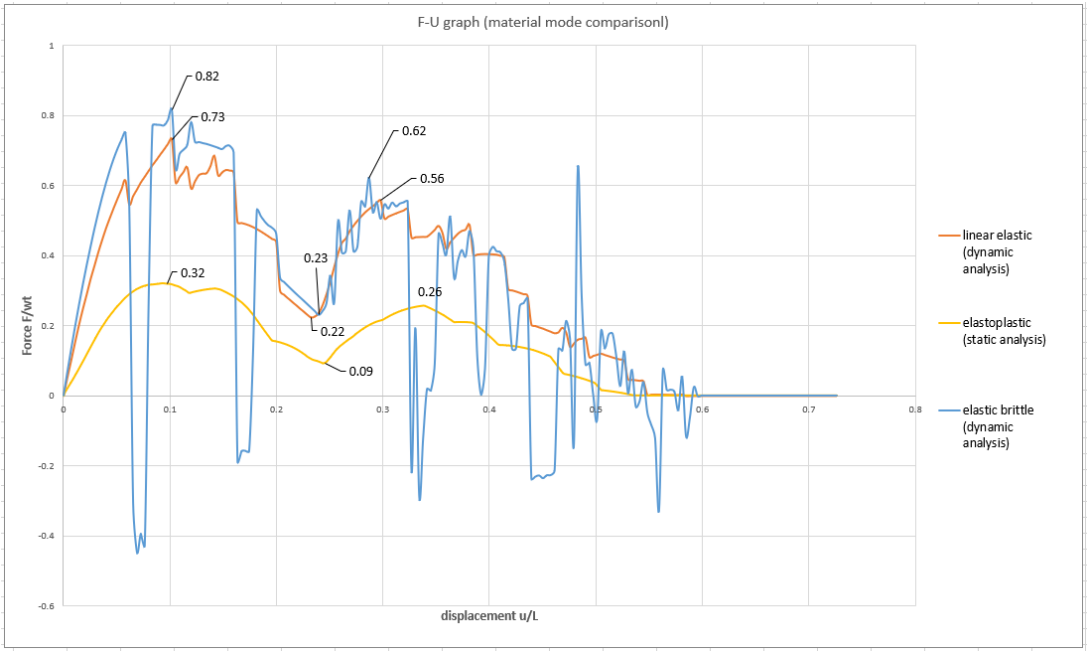

Figure 4.43: Force - Displacement comparison for elastic & elastoplastic material model

As mentioned before the linear elastic material under dynamic loading had the optimal response. The forces extracted were the highest, except for the elastic-brittle model that had slightly higher peaks but with a lot of distortions along the graph. The elastic and elastic brittle models seem to follow the same shape (except for the kinks indicating the formation of cracks). Now, comparing the linear elastic and elastoplastic material, the linear elastic presents almost double reaction forces at the peaks and kink, it is subsequently stronger than the elastoplastic material.

4.5.5 Sensitivity analysis of elastoplastic material model

At this part, 7 variations of the **elastoplastic material model** were performed (according to the paper (Mirkhalaf and Barthelat, 2017)), to quantify the influence of the stresses at charac-

teristic points and E modulus, on the response of the suture. The abovementioned material model for the sensitivity analysis will be referred to as **reference model**.

At the table 4.44 all the parameters describing the constitutive relations for the different variations are shown. The two main models implemented a **bi-linear plastic model** (reference model & variations 1, 2, 6, 7) and a **multi-linear plastic model** (variations 3, 4, 5). The parameters chosen for these variations are in proportion to the parameters given at the paper (Mirkhalaf and Barthelat, 2017).

	Initial material model	Variation 1	Variation 2	Variation 3	Variation 4	Variation 5	Variation 6	Variation 7
Yield stress:	109.8 MPa	1098 MPa	10980 MPa	109.8 MPa	1098 MPa	10980 MPa	109.8 MPa	109.8 MPa
Yield strain:	6.65%	6.65%	6.65%	6.65%	6.65%	6.65%	6.65%	6.65%
Intermediate stress:	-	-	-	118 MPa	1180 MPa	11800 MPa	-	-
Intermediate strain:	-	-	-	9%	9%	9%	-	-
Stress at failure:	118 MPa	1180 MPa	11800 MPa	118 MPa	1180 MPa	11800 MPa	118 MPa	118 MPa
Strain at failure:	11.2%	11.2%	11.2%	11.2%	11.2%	11.2%	11.2%	11.2%
E-modulus:	1700	1700	1700	1700	1700	1700	1800	1900

Figure 4.44: Elastoplastic material model variations

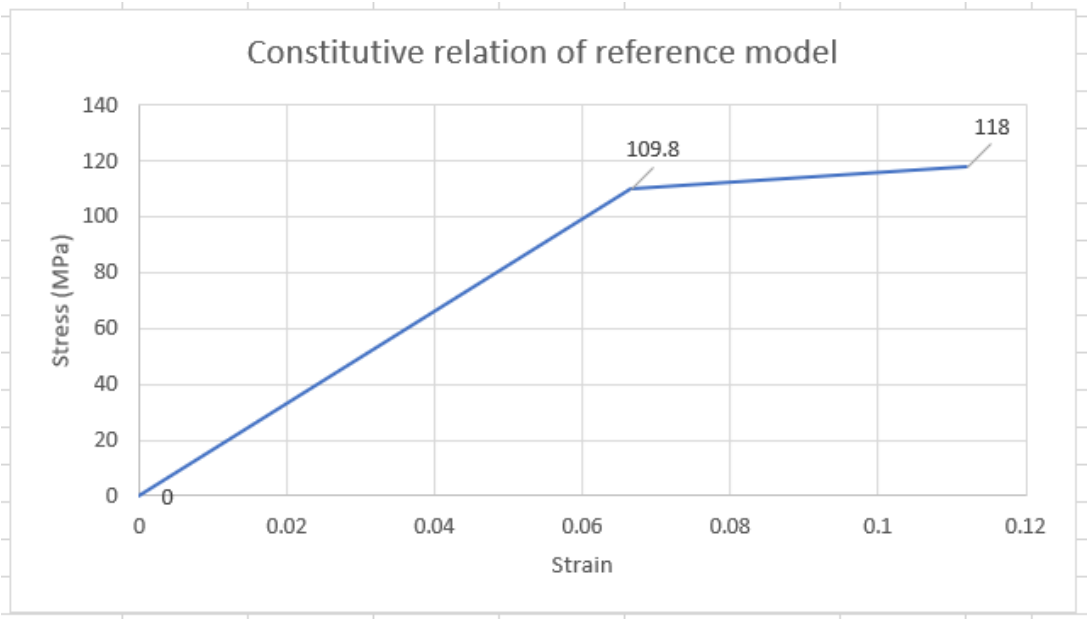

Figure 4.45: Reference model constitutive relation

Variations 1,2

To make the results easier to analyse, the variations of the reference model can be categorized. Variation 1 has 10 times the stresses at yielding and fracture points, while variation 2 has 100 times the stresses at yielding and fracture points (see figure 4.46). These variations were performed to evaluate the influence of the increase of stress at characteristic points at the response of the suture.

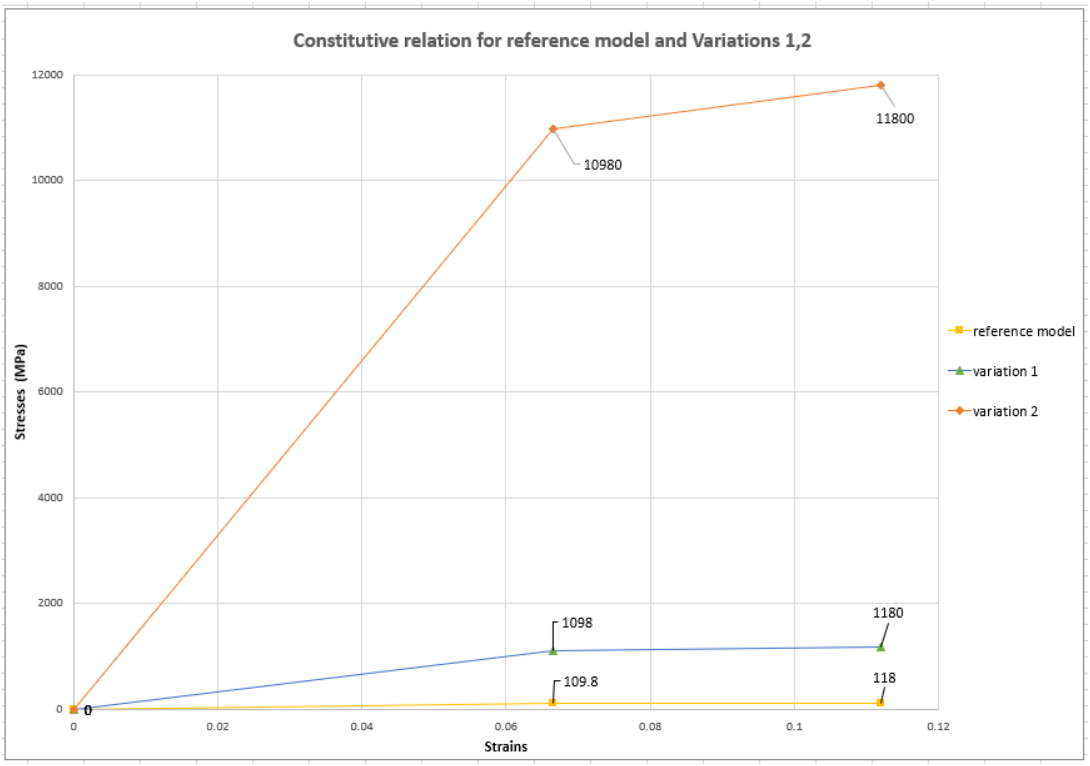

Figure 4.46: Constitutive relation of reference model and variations 1,2

The results of these 3 different models are shown below:

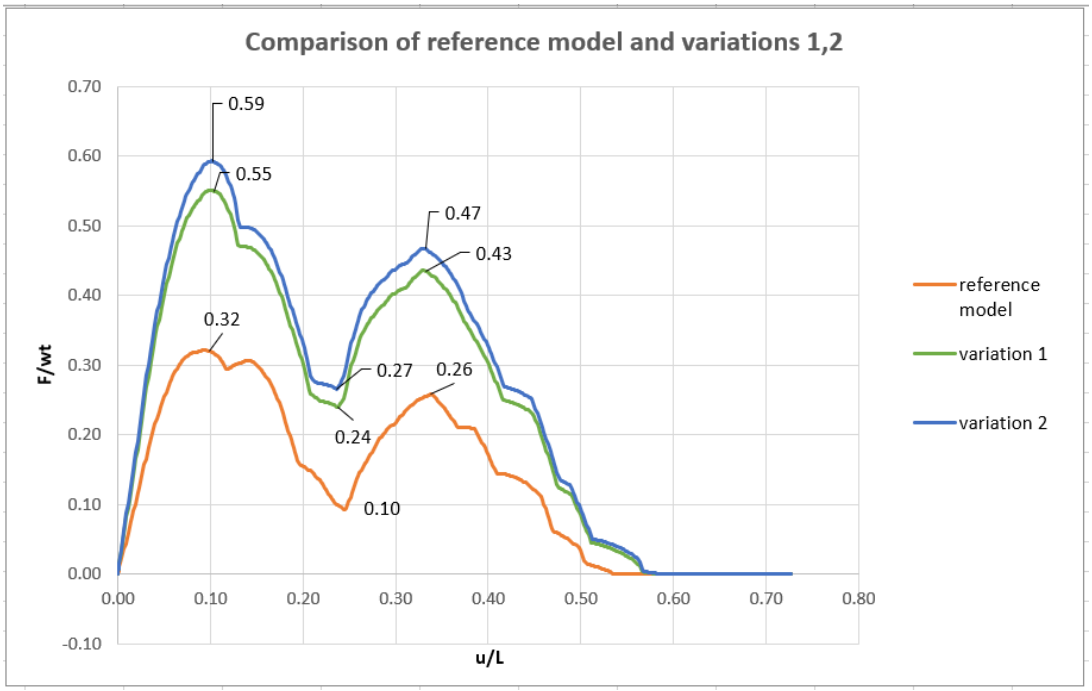

Figure 4.47: F-U graph of reference model and variations 1,2

In general, the increase of stress enhances the overall response. A first observation is that the tenfold increase of stress (variation 1) has a significant impact on the response while the 100fold increase of stress (variation 2) does not differ much from the tenfold increase. Specifically, an increase of strength of 100 times will increase the reaction forces extracted at the 1st and second peak less than twice. At the kink, the increase is larger due to the stronger contact in the position of the kink where the top part is locked at the cavity of the bottom part.

Variations 3,4,5

Variations 3, 4, 5 have a multi-linear constitutive relation with one intermediate point added at the stress strain diagram and then constant stress after this point. This is shown in figure 4.48. Variation 3 has the same stresses and strains at yielding and fracture as the reference model, variation 4 and 5 have 10 and 100 times the stresses at yielding and fracture respectively. These variations were performed to evaluate the influence of the stresses at the response of the suture with a different constitutive model that is still close to the one used at the experiments.

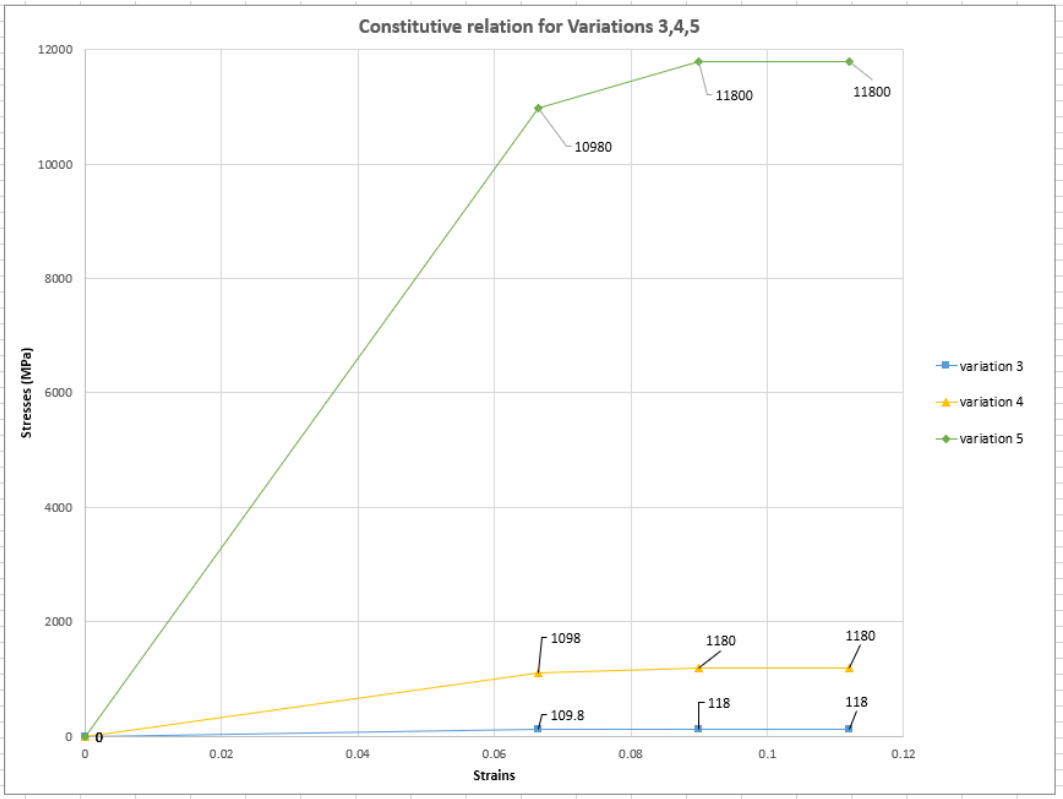

Figure 4.48: Constitutive relation for variations 3,4,5

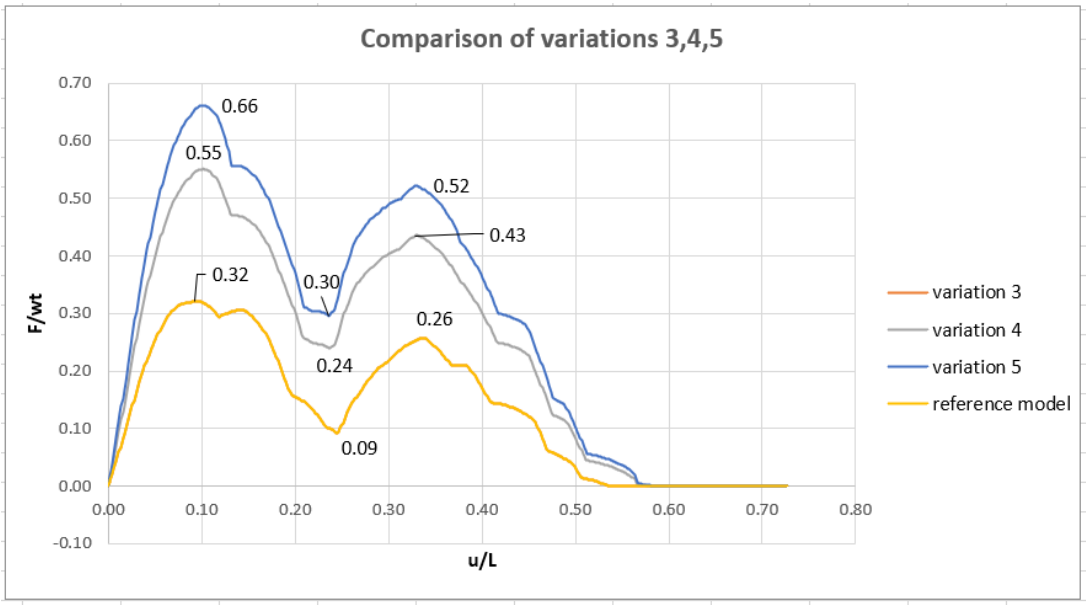

Figure 4.49: F-U graph of reference model and variations 3,4,5

A point of importance following the figure 4.49 is that changing the constitutive model had almost zero influence in the response. The response following the bi-linear plasticity of the reference model is the exact same as variation 3 (multi-linear model). However, with this new constitutive model, increasing the stress 100 times caused a larger increase of stresses at the peaks and at the kink. Specifically, now, at the first peak the stress is 0.66 while it was 0.59 for the previous material model. At the kink it increased from 0.27 to 0.3 and at the second peak from 0.47 to 0.52. So larger stresses can extract higher reaction forces with the multi-linear material model.

Variations 6,7

In the paper (Mirkhalaf and Barthelat, 2017) the E modulus of ABS was measured as 1.7 ± 0.2 GPa, so it is important to test the increase of the value of E modulus to discover its influence in the response of the suture. The E modulus of the reference model was 1700MPa, in variation 6 it was increased to 1800MPa and in variation 7 to 1900MPa.

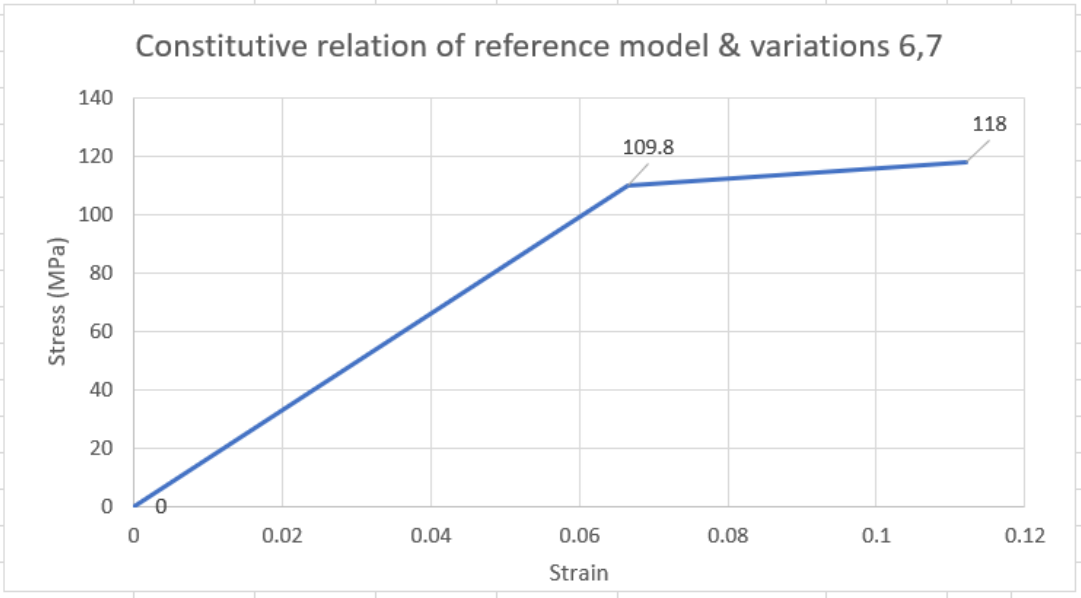

Figure 4.50: Constitutive relation for variations 6,7

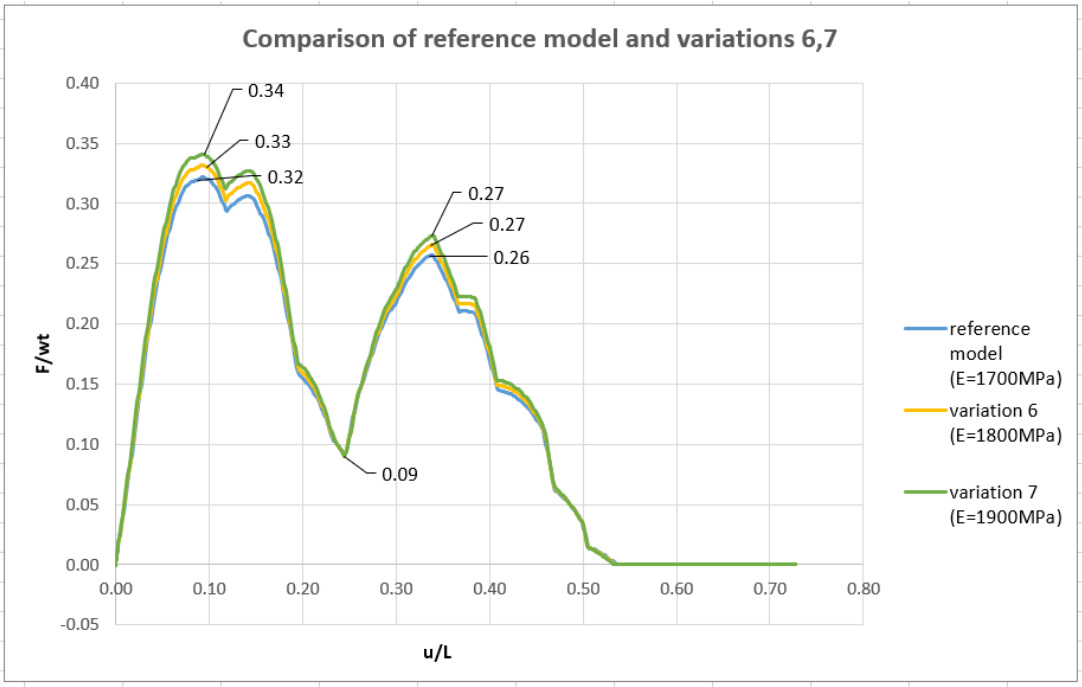

Figure 4.51: F-U graph of reference model and variations 6,7

As expected the reaction forces extracted with higher stiffness are also higher. Additionally the stiffness of the material seems to be a more sensitive parameter than the stresses at characteristic points. With an increase of 5.71% from 1700MPa (reference model) to 1800MPa (variation 6) there is an increase in stress of 3.1 % at the first peak, no influence at the kink and 5.6 % a the second kink. With the same magnitude increase of stresses the difference in the response is almost zero.

4.6 Mesh study

The different mesh sizes used were a coarse mesh with 0.2 global seed size, a finer mesh with global seed size 0.1 and a locally refined mesh.

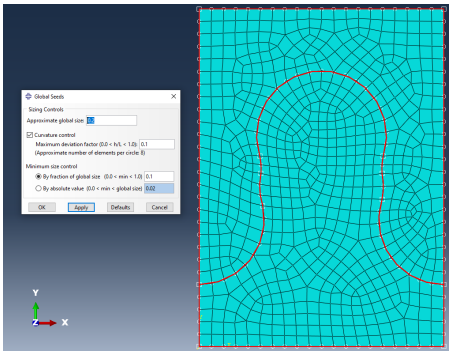

(a) coarse mesh with global seed size 0.2

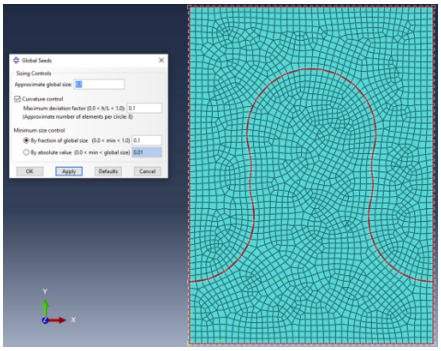

(b) fine mesh with global seed size 0.1

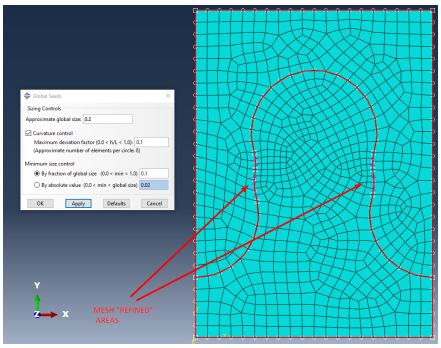

(c) Locally refined mesh

Figure 4.52: Mesh Variations

The results with finer mesh (see figure 4.52b) in comparison to a normal (coarse) mesh (see figure 4.52a) are presented below:

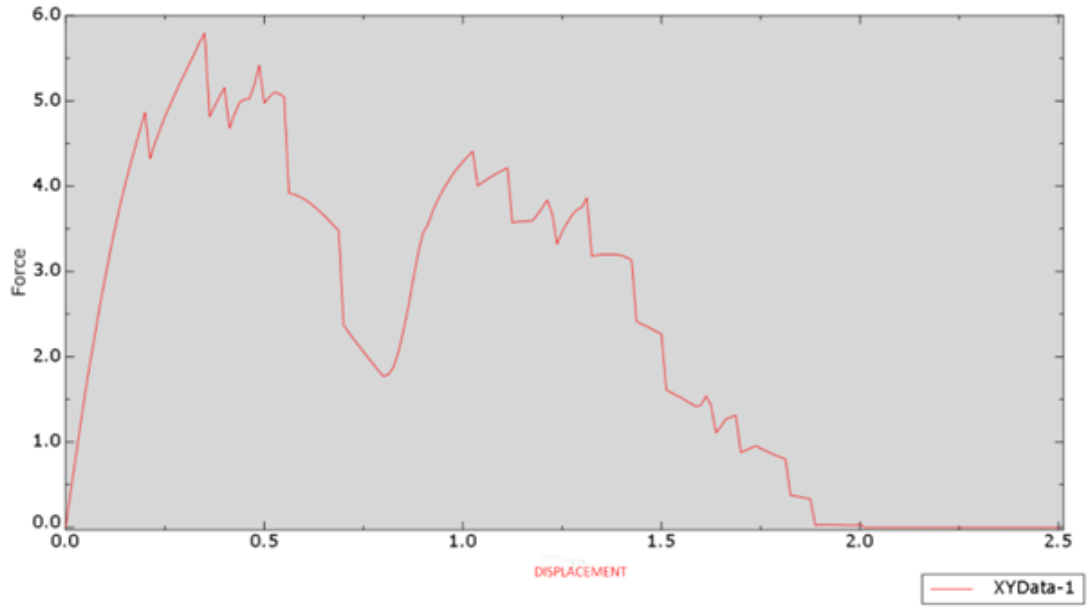

(a) Results with coarse mesh (global seed size 0.2)

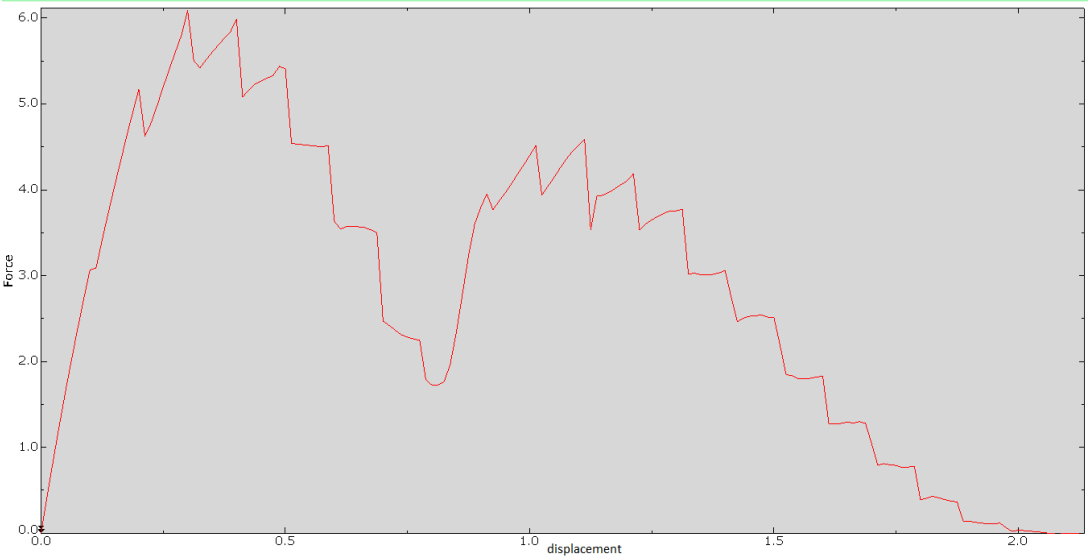

(b) Results with fine mesh (global seed size 0.1)

Figure 4.53: Comparison of results with coarse and fine mesh

The final results obtained with fine and coarse mesh were quite similar. The kink position is almost identical. The forces exerted at the peaks are slightly higher (5.13 % at the first peak and 4.44% at the second) for the finer mesh. The kinks along the F-U curve were expected to be smoothed out with finer mesh, and partially this is true since it is obvious that the number of kinks is bigger (due to the increase of elements and nodes) which makes the curve appear slightly smoother.

The distribution of values on the curve also appears to be more Gaussian-like (the maximum value appears almost at the middle of the curve) instead of the "steeper" shape that they had with the coarse mesh (the maximum values appeared at the beginning of the curve). This result shows that with a mesh refinement the results could be enhanced in regard to the position of the maximum value at the peaks.

4.7 Loading procedure

Although dynamic analysis was used for most simulations to capture the non linear effects related with time, it was interesting to discover what results a static analysis would give. The displacement rate applied in the paper (Mirkhalaf and Barthelat, 2017) was 5μm/sec which is a constant and it could be a sufficient assumption to use static analysis for this problem. Additionally, the use of computational time is a very important parameter and it can severely be improved with static analysis.

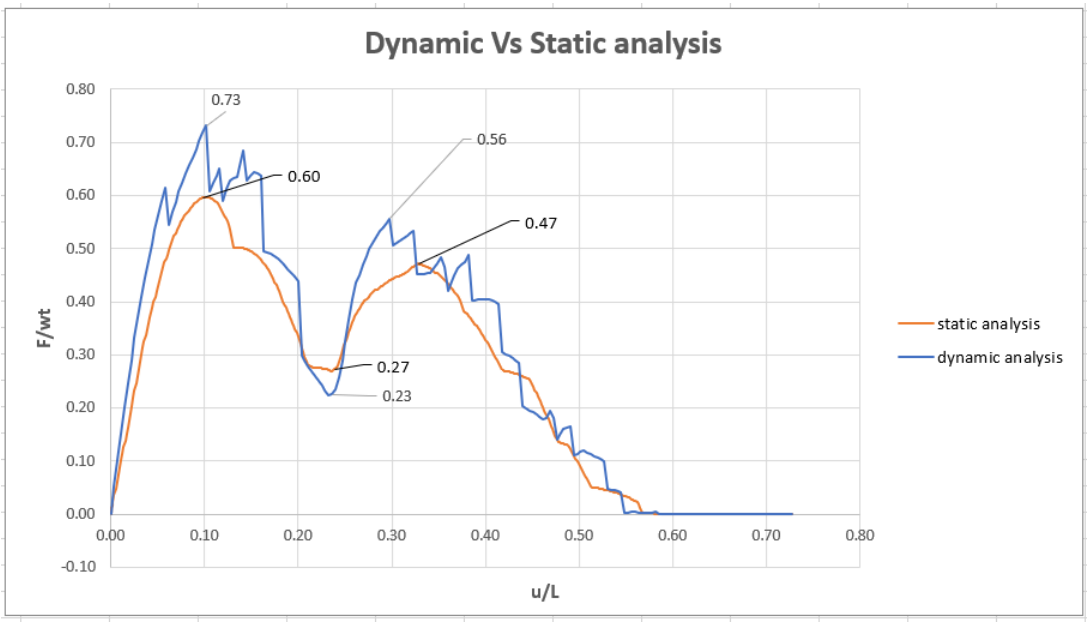

Figure 4.54: Dynamic vs Static analysis results

The static analysis performed had the same parameters as the dynamic analysis. The time period used, was 500 seconds and the final displacement 2.5 mm, according to the applied displacement rate of 5μm/sec. The curve corresponding to the static analysis appears smoother, result reasonable since the dynamic effects add complexity to the model since the non linearities could result in such kinks along the curve.

The reaction forces extracted with dynamic analysis were higher. The difference in values of static and dynamic analysis of the first peak was in the order of 19.5% and at the second peak 17.5 %.

4.8 Sutured line model

After investigating the behaviour of an isolated suture with a single tab, a more complex model of a bistable interlocked material was created with *multiple interlocked sutures*. The purpose of this model is to once again investigate the mechanical response under application of the same tensile force applied as a displacement rate of 5 μm. Specifically what is expected to be seen is a force-displacement curve as such:

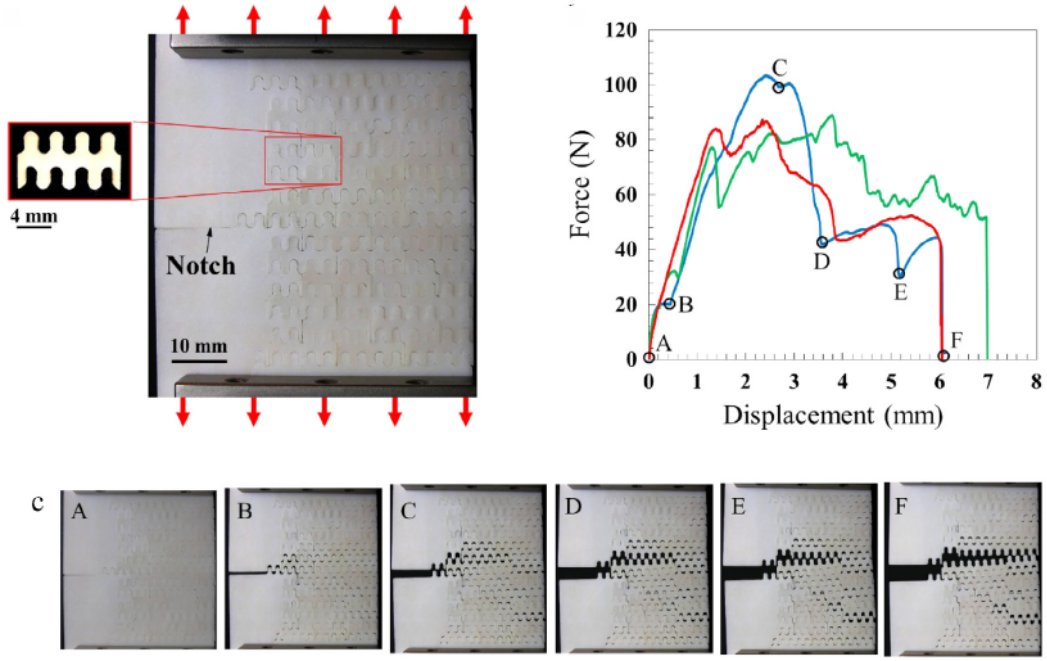

Figure 4.55: Typical tensile response of a bistable interlocked material shown in Phases A-F (Mirkhalaf and Barthelat, 2017)

In figure 4.55 the force-displacement curve reveals the force that is extracted when the test sample is subjected to tensile forces (Mirkhalaf and Barthelat, 2017). Letters *(A-F)* are assigned to specific points of the force-displacement graph to make a connection between points of interest of the graph with the physical test.

In the beginning, the tensile forces induce the increase in force as the top and bottom part slid apart. *Point B* reveals a small drop in the force due to the transformation of the parts next to the notch. After this, the deformations are spreading throughout the sample as it is visible in figure 4.55 (points C and D). The propagation of the crack is progressing but the sample is still able to resist deformation *(points C, D, E)* until it fails *(Point F)*. This mechanism can severely enhance the fracture toughness (obtained by the division of the area under the curve to the area corresponding to the uncracked connection) up to 10 times compared to plain ABS (Mirkhalaf and Barthelat, 2017).

The numerical model created to be subjected to tensile test had **2 layers** for simplicity and usage of less computational time, in contrast with the more complex model presented in the

paper (Mirkhalaf and Barthelat, 2017) in figure 4.55, which was comprised of 48 building blocks.

Model 8 was constructed with the same parameters as model 1 presented below:

- $\mathbf{R_1/R_2 = 1.05}$ for all tabs of the suture,
- $\boldsymbol{\theta_1 = 15}\ ^\circ$,
- **contact stiffness 1700 MPa**,
- **friction coefficient f=0.35**.

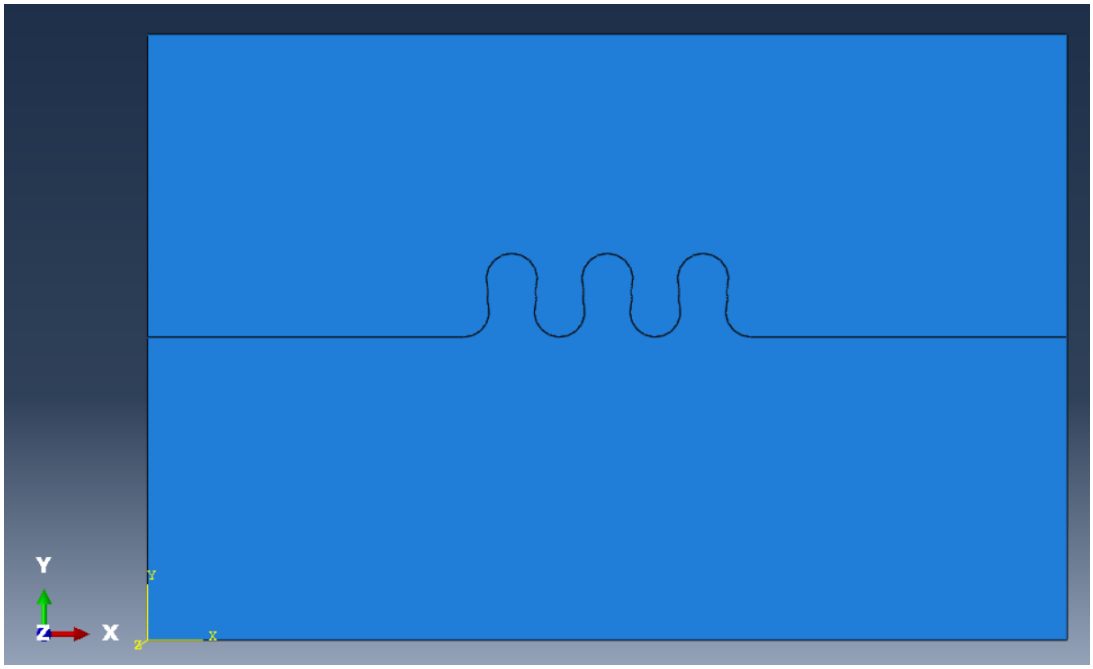

Figure 4.56: Sutured line sample assembly

After being subjected to the tensile forces, the concentration of stresses around the curved parts was high (depicted with red and yellow colors in figure 4.57).

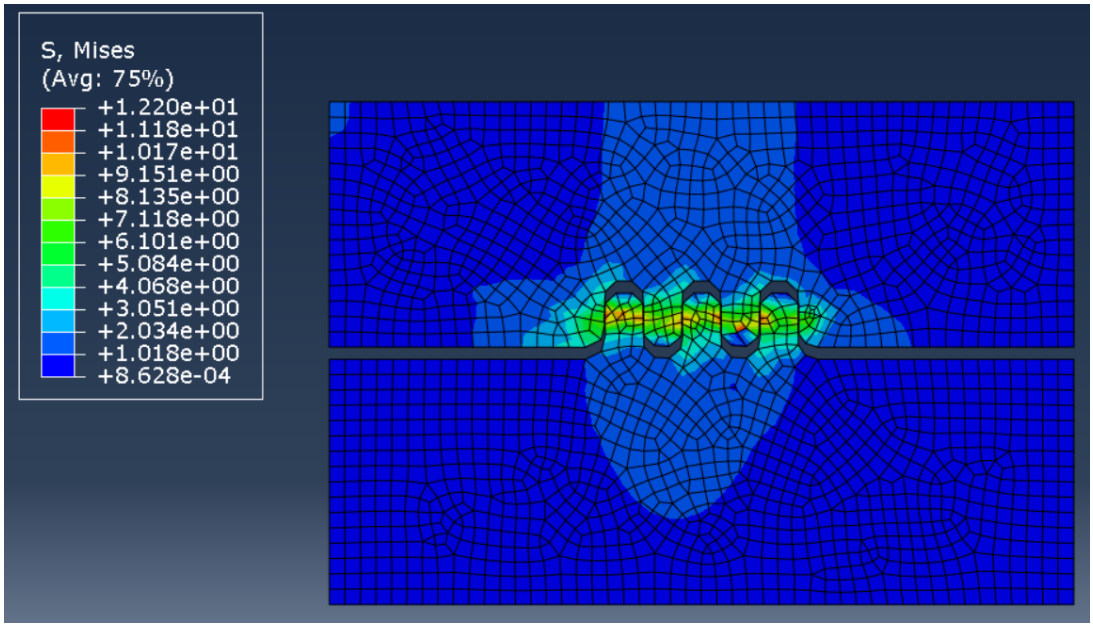

Figure 4.57: Sutured line sample stresses

The results of the analysis performed in Abaqus are summarized in the following graph:

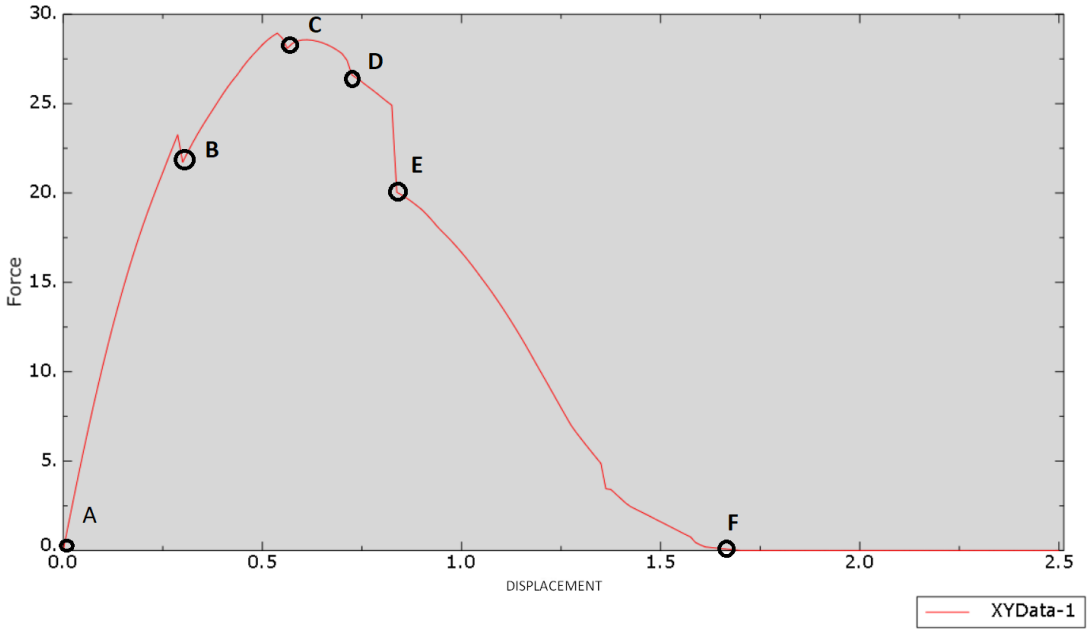

Figure 4.58: Force- Displacement graph for sutured line sample

The obtained result resembles a lot the shape of the experimental results (figure 4.55). The

kinks are present and the points of interest are noted with letters A-F. However a major difference is that the ”plateau” regime (point D-E-F) that indicates the delay of failure/transformation of the suture is almost nonexistent in figure 4.58. In the numerical model, the failure is more brittle in the sense that from point D to E and E to F rapid drops of force happen while the suture is under tension. More detailed documentation is presented in the subchapter (5.4)

5 Discussion

5.1 General remarks

The numerical models gave mostly satisfactory results. The results demonstrate that the interlocking effect could delay the strain localization and offer a mechanism of energy dissipation in the system, adding ductility. The comparison of the numerical results with the experimental results from the paper (Mirkhalaf and Barthelat, 2017) showed similarities concerning the Force-displacement development.

5.2 Results for R1/R2=1.05 - Reference model

The highest reaction forces *in magnitude* are extracted in frame 4 of the analysis (before the II equilibrium position) and at frame 11 (after the II equilibrium position) and there are almost same in magnitude (3.22 and 3.13 respectively) with a difference of 2.8%. However when it comes to the summation of the reaction forces with the displacement incrementation the first curve is higher than the second. On the contrary, in the experimental results, the first peak is lower than the second and this enhances the overall stability of the system as it delays strains and offers ductility in the whole system. This result needs more exploration.

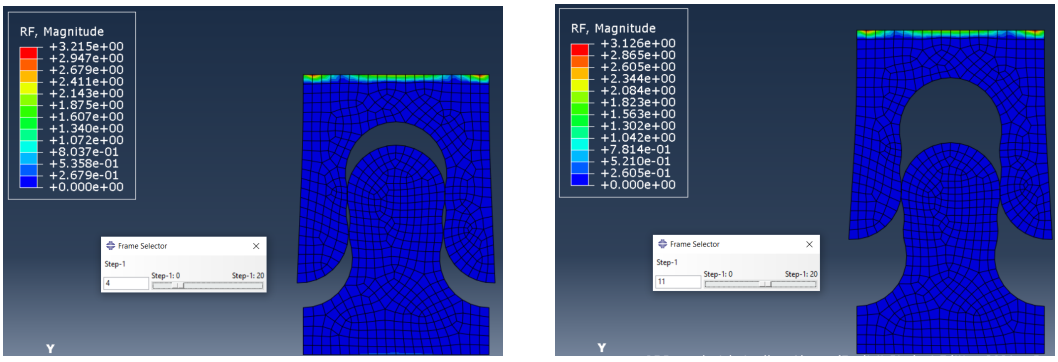

(a) Reaction forces-frame 4

(b) Reaction forces-frame 11

Figure 5.1: Magnitude of reaction forces at frames 4 and 11 of the analysis

One of the reasons that could have resulted in this, could be the following. The first peak in the curve happens before the interlock position (equilibrium position II). The maximum value (summation of reaction forces) appears due to the increase of friction and normal forces during the process of pulling out the suture. At this moment (see figure 5.1a) there are 2 pairs of contact points that resist that movement. The maximum of the second peak appears

when the system has passed the interlock position and only one pair of contact points (see figure 5.1b) resists the movement. So this could have resulted in a ”higher” first peak and a ”lower” second peak. The experiment and numerical analysis present different assumptions for the modelling of the interface and the material behavior so this could have an effect on the interchange of the peaks of the curve.

Additionally, the complexity of the analysis was high, and although in the analysis module nonlinear effects were included with the NLGEOM option, the way the load was applied and other parameters (regarding material or interface) can create differences between the numerical simulation and the experiment. It was already shown how a finer mesh affected the appearance of the maximum value of the curve making it more Gaussian-like than the one with a coarse mesh.

The kink's position was almost identical at 0.24 u/L, which implies that the main assumptions behind the model were okay.

When it comes to value comparison, the values derived from the numerical simulation are quite smaller than the experimental ones. The location of the first peak appears sooner at the numerical curve than in the experimental one. It has to be taken into account that the material model assumed was linear elastic, and this can affect the strain values since in such a model the strains are usually smaller. Nonlinear effects were not included in the material model and as satisfactory the assumption of linear elasticity may be, it is still a simplification of the physical model.

5.3 Results for R1/R2=1.00

Simulation 8 was created with R_1/R_2=1.00 and at the comparison with the experimental results there were many similarities. In both experimental and numerical results the first peak is higher than the second and the kink is at zero stress (due to the specific geometry during the pull-out this part fits without any stresses) and is almost at the same value of u/L. The values are lower than those of the numerical analysis. This was explained before as it can be related to the linear elastic material model assumption. This simulation seems a satisfactory model for this experiment since the results are quite close to the experimental results.

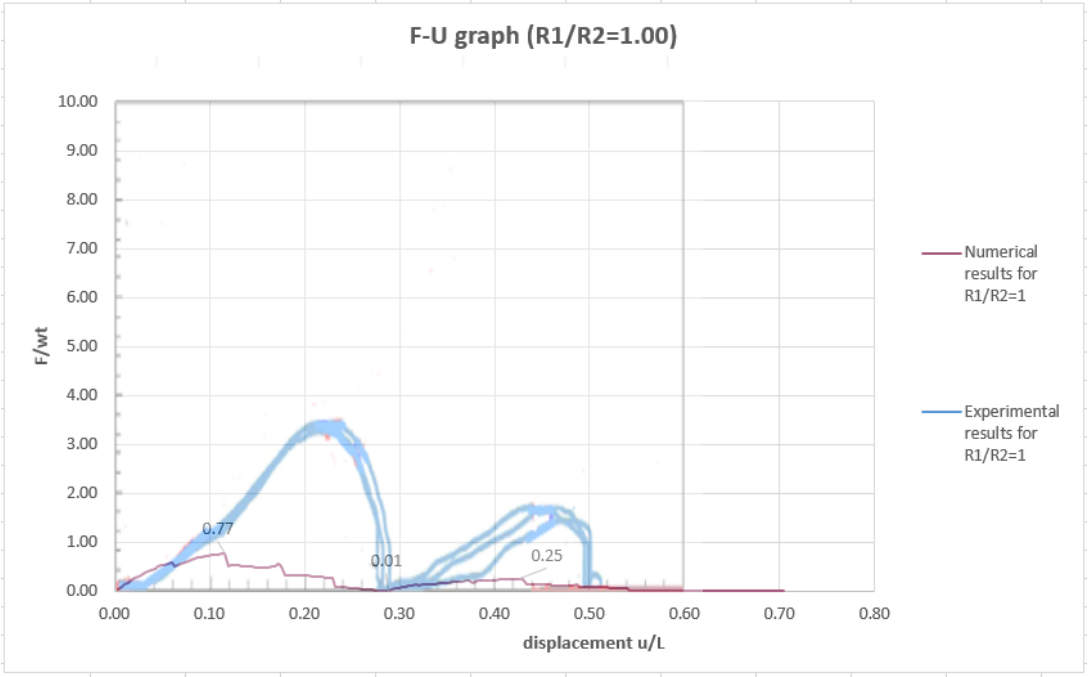

Figure 5.2: Experimental- Numerical results comparison R1/R2=1.00

The increase of the contact stiffness of the interface and of the friction coefficient seems to benefit the system since larger reaction forces were required for the pull-out.

When it comes to the contact stiffness an increase of 100% (from 1000MPa to 3000MPa) results to an increase of 10.95 % of the maximum reaction force needed to move the system to the second equilibrium position and 5.9 % of the maximum force required to completely pull out the suture from the second equilibrium position. Such an increase delays the strain that the system reaches the second equilibrium position by 8.7 %.

In regard to the friction coefficient, an increase of 114% (from 0.15 to 0.55) results to an increase of 81.4 % of the maximum reaction force needed to move the system to the second equilibrium position and 74% of the maximum force required to completely pull-out the suture from the second equilibrium position. Such an increase delays the strain that the system reaches the second equilibrium position by 4%.

This shows that the increase of friction coefficient is more efficient to make the system resist the tensile forces.

5.4 Results for sutured line model

In general, the obtained result is quite similar to the experimental graph (figure 4.55). The points of interest are noted with the letters A-F. A major difference although, is that the ”plateau” regime (point D-E-F) that indicates the delay of failure or a complete transformation of the suture is almost nonexistent in figure 4.58. This is explored further below.

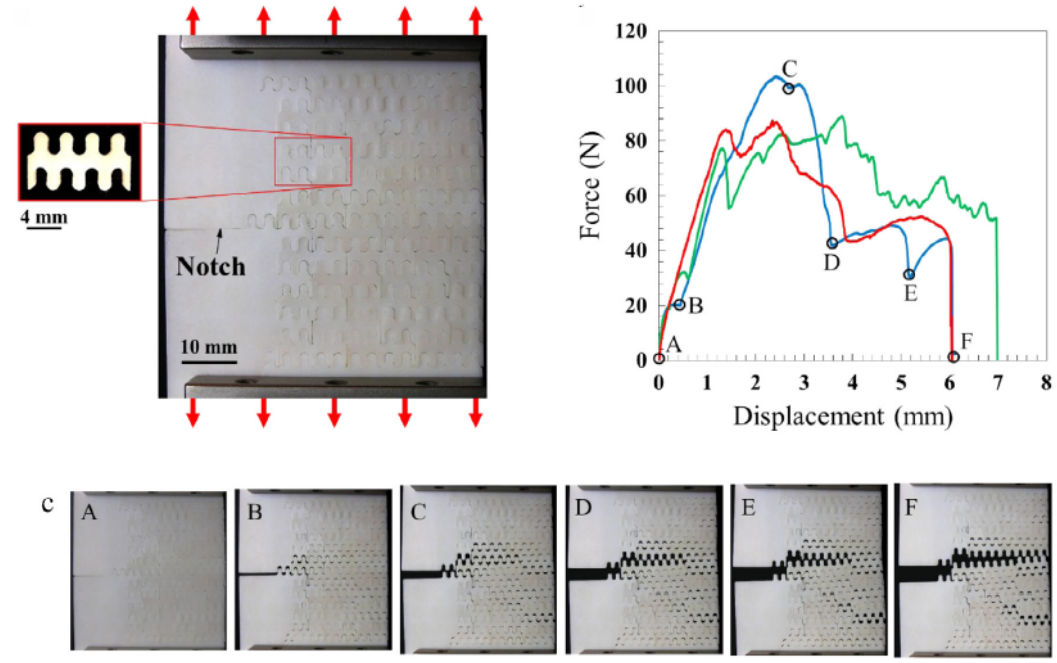

(a) Tensile response of a bistable interlocked material shown in Phases A-F (Mirkhalaf and Barthelat, 2017)

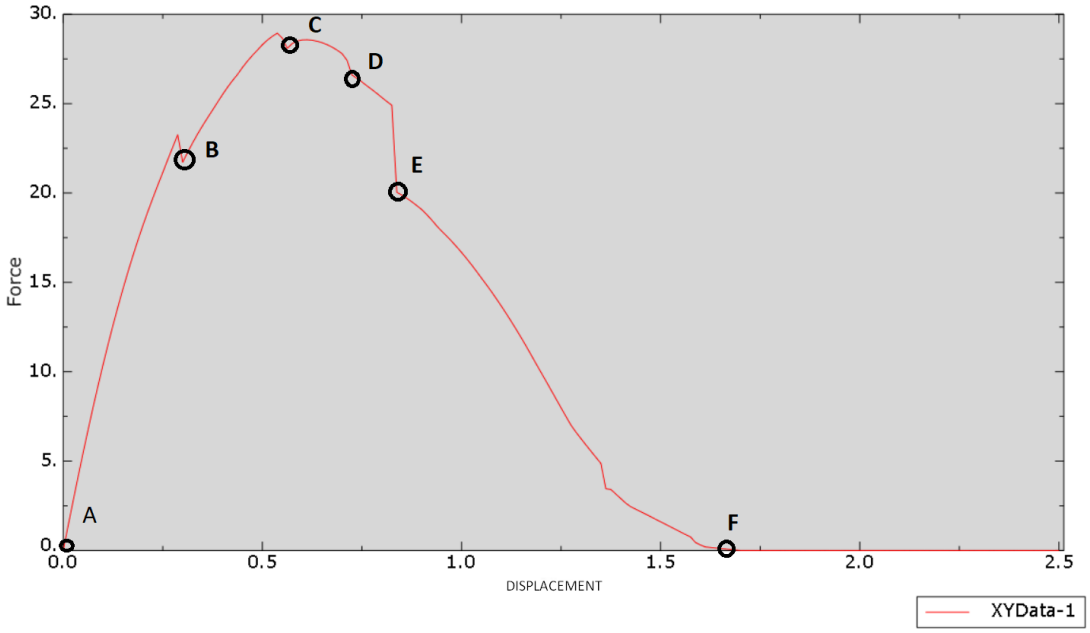

(b) Numerical results for R_1/R_2=1.0

Figure 5.3: Force-Displacement graph for sutured line sample

In the numerical model, the mechanical behavior seems more brittle. The plateau regime that

delays the failure/transformation of the sutured line associated with the points D, E, F is not present. Of course, this result could be attributed to many factors, some of them are named below:

- **Number of layers**: The more layers that are implemented in the model, the higher the delay in strain localization. So having only two layers could result in a more brittle mechanism in comparison to the 48 layers presented in (Mirkhalaf et al., 2016).
- **Material model**: The material model used was linear elastic without taking into account non linear deformation. This assumption can give satisfactory results for the simulations but up to a point - necking and fracture are not accurately captured, so the points E (stable point before fracture and F (fracture) can look very different from the experiment.
- **Mesh size**: Since the mesh used was coarse to shorten the computation time, it affected the stresses and the force-displacement diagram. The local stress concentrations could go unnoticed in a coarse mesh as nodes are further apart from point of load application, while in a finer mesh the stress localizations are pronounced. Although, this might be a secondary cause since in the initial model two different mesh sizes were compared without showing a large increase of stresses for the finer mesh.

6 Conclusions and Recommendations

In this research, the benefits of bistable interlock in connections made from ABS were investigated. Eight numerical models were built to simulate sutures made by ABS and tested under tensile force application.

The results were compared with the experimental results of the paper (Mirkhalaf and Barthelat, 2017). Some of these models were closer to the experimental results, some of them presented differences. For these simulations the influence of **contact stiffness in the interface**, **friction between the sutured parts** and differences in **geometry** were investigated.

Following the main conclusions are presented:

- The experimental results for R_1/R_2= 1.0 and 1.05 can be partially verified with the numerical models built for this research. Comparing the F-U graphs there are a lot of similarities especially for R_1/R_2= 1.0. For R_1/R_2= 1.05 some alterations in the assumptions used for the model could take place to get more similar results to the experiment.
- *Contact stiffness of the interface* is a very important parameter, as seen in subchapter 4.22. Higher contact stiffness of the interface results in higher reaction forces and it delays the system from reaching the second equilibrium position, meaning that it makes the system more stable. It does not show the delay in strain for failure/complete transformation of the suture (end of the analysis). The implementation of *penalty stiffness* at the interface did not result in major increase in forces but combined with a higher friction coefficient increased the peak values more than twice.
- *Geometry of the tabs* is the most sensitive parameter and even a slight change of R_1 can affect the results a lot. From an R_1 increase of 1.05 to 1.1 there was a large increase at the reaction forces, but since the friction is higher having a larger R_1 is not always beneficial for ductility since the tab could be easily fractured.
- The strength and energy absorption are positively impacted by the increase of *friction coefficient*, however, this increase should happen carefully. If the friction coefficient exceeds a threshold the amplitude of the strains rises to a point where the tabs could fracture.
- Following the *material model study* the linear elastic material presented the best response. Adding plasticity to the material model resulted in lower reaction forces making the suture less strong. Increasing the strength ten times in the elastoplastic material would result in a similar response of the linear elastic material. The stiffness is contributing more to the increase of the reaction forces at the total response.
- The *mesh refinement* offers benefits to the response by making the curve shape more Gaussian-like and closer to the experimental one. The reaction forces extracted did not vary much.

Some recommendations based on the results of the research are the following:

- Alterations in the initial model with R_1/R_2=1.05 could enhance the obtained results. Changing the material model assumptions to add non linear effects, or refining the contact more could lead to a more similar F-u curve with the experimental one.
- Since crack modelling is not added to the reference model, there is not mesh dependency on crack formation and the mesh refinement does not have a major role except in smoothing the F-U curve. The force and strain values increase slightly with a finer mesh. However a finer mesh at the perimeter of the curved parts could be an interesting alteration and could be beneficial for the final results.
- The geometry, and specifically the R_1/R_2 ratio as mentioned before, affects the system a lot. More geometry variation models should be explored than the 3 investigated in this research (R_1/R_2=1.0, 1.05, 1.10), so a clearer image of how the geometry influences the mechanism would be obtained. For the 3 variations explored, there was not a clear pattern on how the radii ratio affects the mechanical response, since a higher ratio makes the reaction forces larger on one hand but for the first peak of the case R_1/R_2 =1.0 and 1.05 there was almost no difference.
- Regarding the sutured line simulation (model 8) the addition of more layers, could have a positive effect on the overall ductility of the system (the deformations would be spread over larger volumes, so even when some tabs transform, the others can delay the deformations and failure).
- It is important to modify the initial model (using ABS) to a model using a form of ductile concrete as the main material and to additionally explore the size effect of different samples in the overall response of the system. This is also the goal of this research, to make the bi-stable interlock connections applicable so they can be used in construction with a widely used material as concrete to add ductility and spread deformations.

7 Appendix

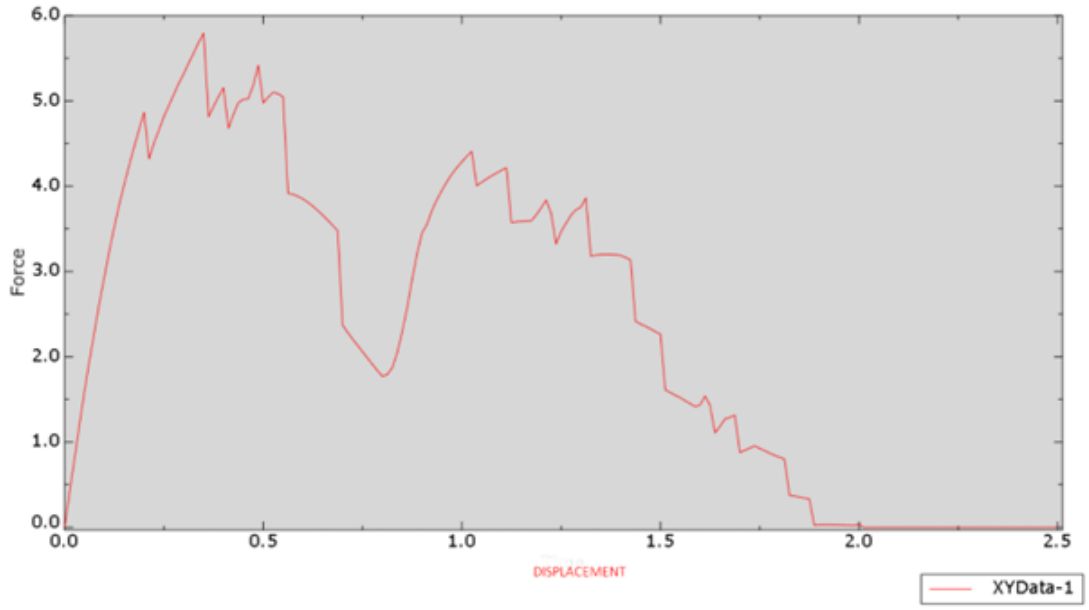

Figure 7.1: Force - Displacement plot (Abaqus)

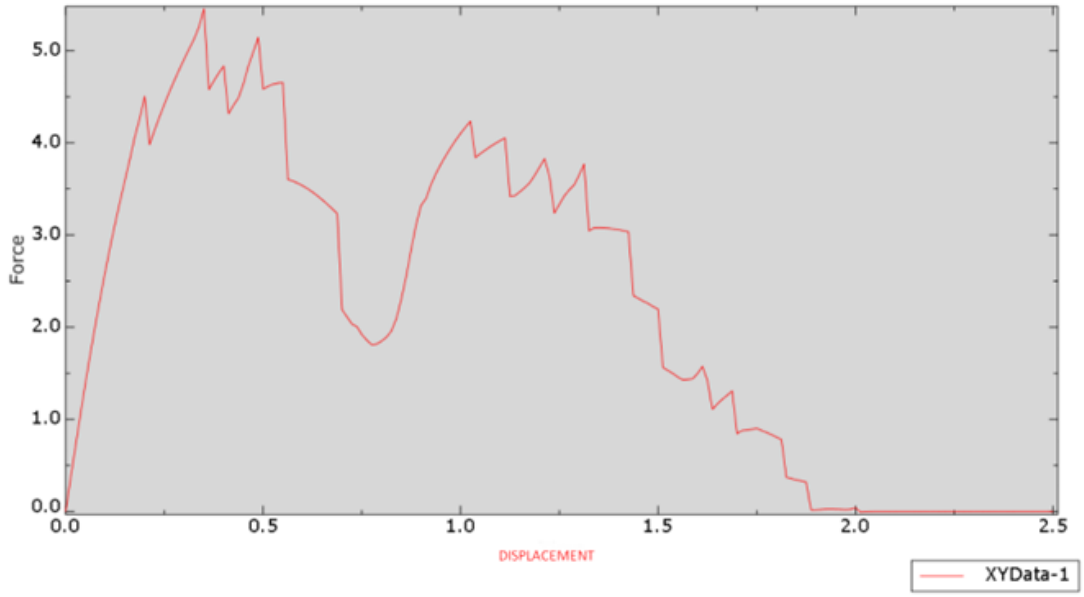

Figure 7.2: Force - Displacement plot (Abaqus) -Simulation 2

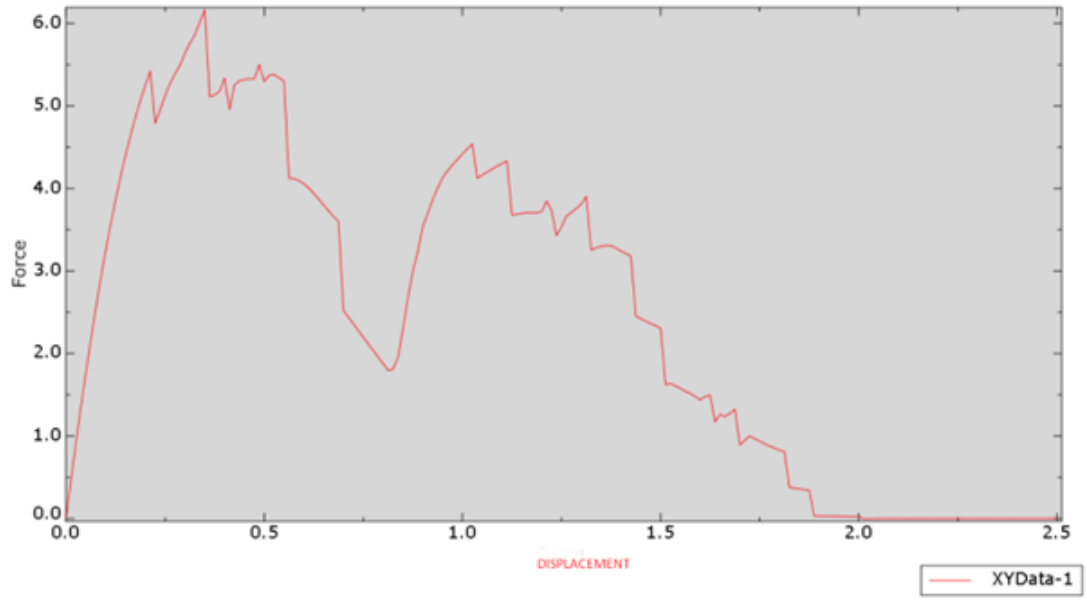

Figure 7.3: Force - Displacement plot (Abaqus)- Simulation 3

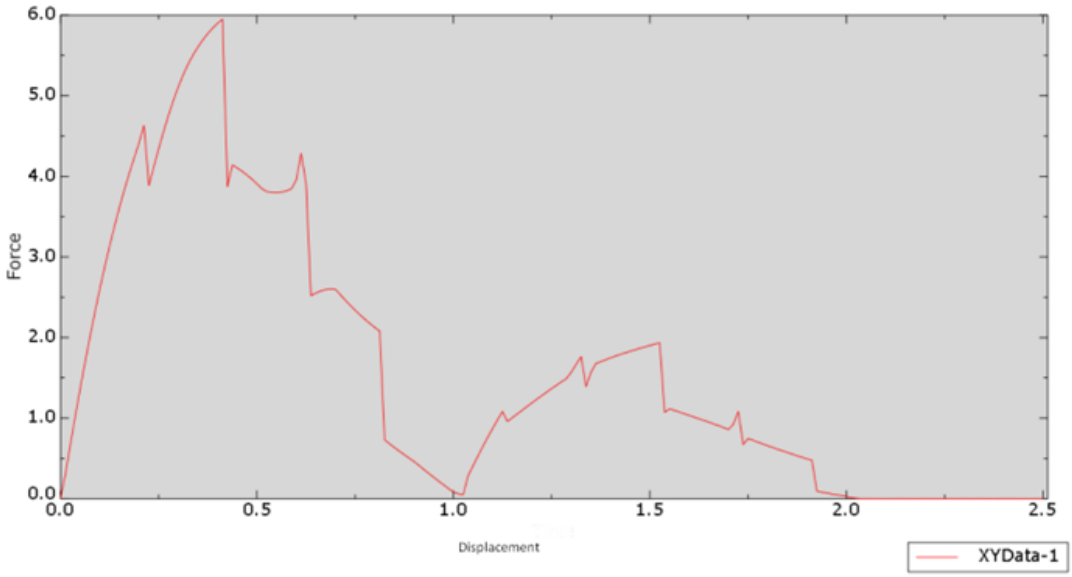

Figure 7.4: Force - Displacement plot (Abaqus)- Simulation 4

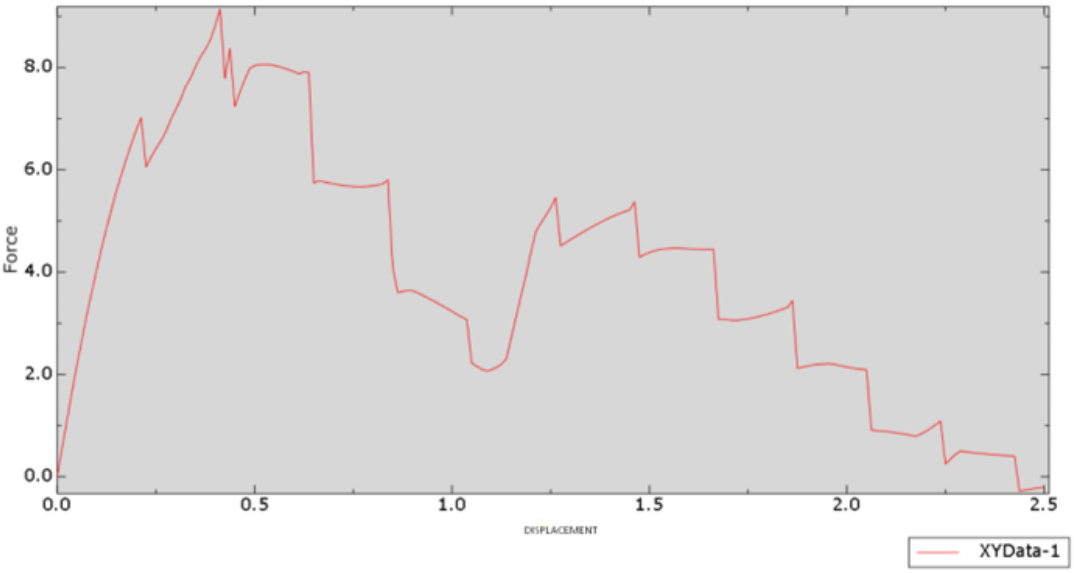

Figure 7.5: Force - Displacement plot (Abaqus)- Simulation 5

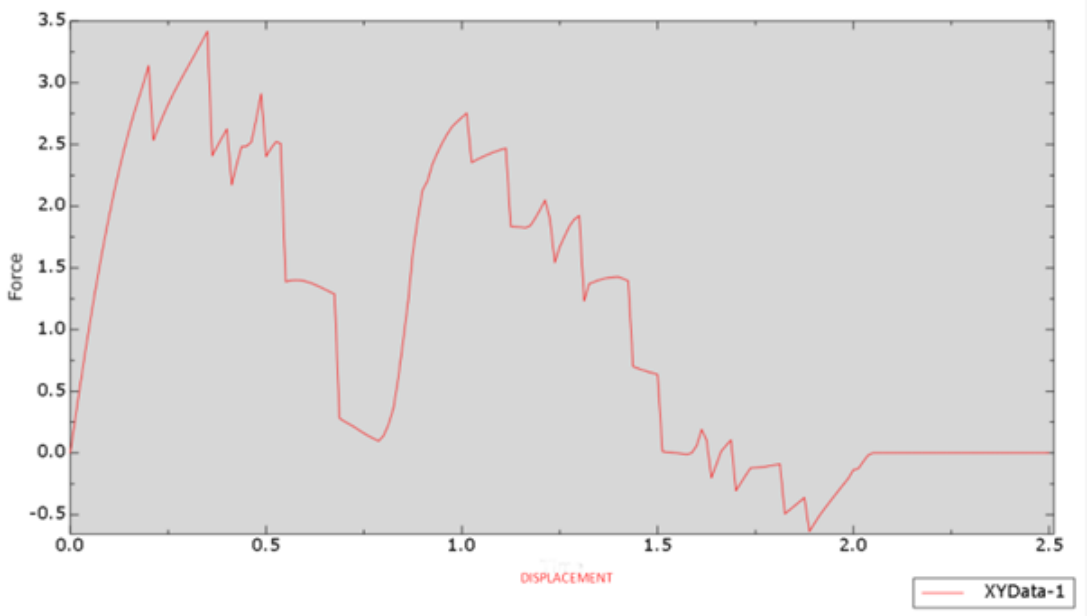

Figure 7.6: Force - Displacement plot (Abaqus)- Simulation 6

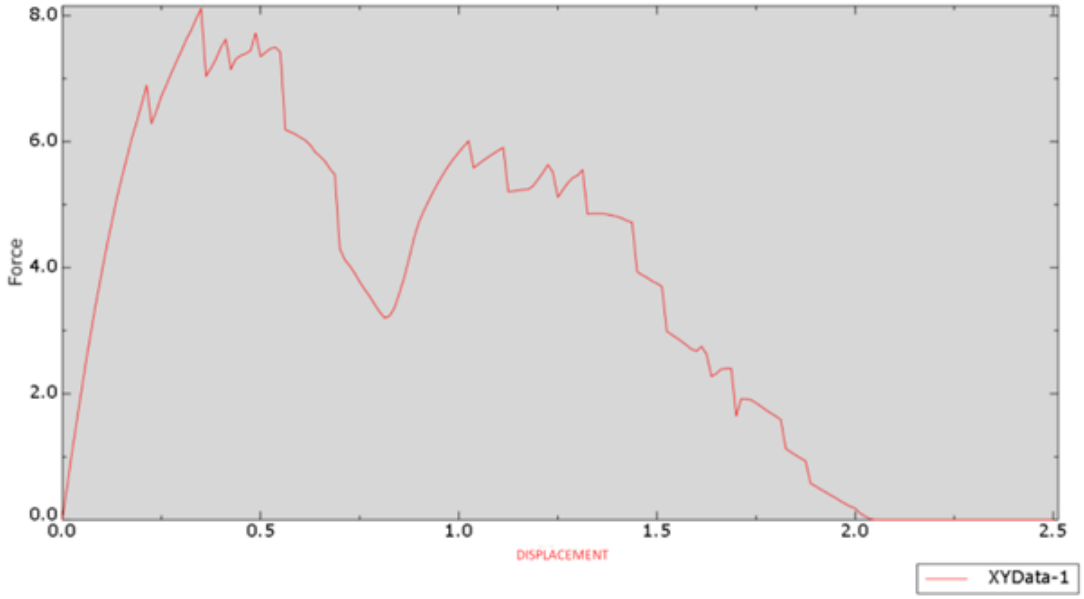

Figure 7.7: Force - Displacement plot (Abaqus)- Simulation 7

Bibliography

Alheit, B., Bargmann, S., and Reddy, B. (2021). Dynamic mechanical behaviour of suture interfaces as inspiration for architectured hierarchical interlocking composites. *Journal of the Mechanics and Physics of Solids*, 157:104620.

Banjanin, B., Vladić, G., Pál, M., Balos, S., Dramicanin, M., Rackov, M., and Knežević, I. (2018). Consistency analysis of mechanical properties of elements produced by fdm additive manufacturing technology. *Matéria (Rio de Janeiro)*, 23.

Hu, W., Mengzhu, Y., and Yufan, W. (2018). Closed-loop optimization and investigation of bistable interlocked structure. *International Journal of Mechanical Sciences*, 144:10–23.

Malik, I., Mirkhalaf, M., and Barthelat, F. (2017). Bioinspired j̈igsaw¨like interlocking sutures: Modeling, optimization, 3d printing and testing. *Journal of the Mechanics and Physics of Solids*, 102:224-238.

Mirkhalaf, M. and Barthelat, F. (2017). Design, 3d printing and testing of architectured materials with bistable interlocks. *Extreme Mechanics Letters*, 11:1-7.

Mirkhalaf, M., Tanguay, J., and Barthelat, F. (2016). Carving 3d architectures within glass: Exploring new strategies to transform the mechanics and performance of materials. *Extreme Mechanics Letters*, 7:104–113. Mechanics in Extreme Manufacturing.

Mirkhalaf, M., Zhou, T., and Barthelat, F. (2018). Simultaneous improvements of strength and toughness in topologically interlocked ceramics. *Proceedings of the National Academy of Sciences*, 115(37):9128-9133.

Olivera, S., Muralidhara, H. B., Venkatesh, K., Gopalakrishna, K., and Vivek, C. S. (2016). Plating on acrylonitrilebutadienestyrene (abs) plastic: a review. *Journal of materials science*, 51(8):3657-3674.

Restrepo, D., Mankame, N. D., and Zavattieri, P. D. (2015). Phase transforming cellular materials. *Extreme Mechanics Letters*, 4:52–60.

Systemes, D. (2008). Abaqus Keywords Reference Manual (v6.8).

Systemes, D. (2015). Abaqus Analysis User's Guide (2016).

Systemes, D. (2022a). About Contact Interactions - SIMULIA User Assistance 2022.

Systemes, D. (2022b). Contact Constraint Enforcement Methods in Abaqus/Explicit - SIMULIA User Assistance 2022.

Systemes, D. (2022c). Contact Formulations in Abaqus/Standard - SIMULIA User Assistance 2022.

Systemes, D. (2022d). Explicit Dynamic Analysis - SIMULIA User Assistance 2022.

Systemes, D. (2022e). Free meshing with quadrilateral and quadrilateral-dominated elements - SIMULIA User Assistance 2022.

Systemes, D. (2022f). Frictional Behavior - SIMULIA User Assistance 2022.

Systemes, D. (2022g). Mass Scaling - SIMULIA User Assistance 2022.

Systemes, D. (2022h). Meshing independent and dependent part instances - SIMULIA User Assistance 2022.

Systemes, D. (2022i). What are mesh seeds? - SIMULIA User Assistance 2022.

Vukasovic, T., Vivanco, J., Celentano, D., and Garcia-Herrera, C. (2019). Characterization of the mechanical response of thermoplastic parts fabricated with 3d printing. *The International Journal of Advanced Manufacturing Technology*, 104:1–12.

Wang, K., Li, S., Rao, Y., Wu, Y., Peng, Y., Yao, S., Zhang, H., and Ahzi, S. (2019). Flexure behaviors of abs-based composites containing carbon and kevlar fibers by material extrusion 3d printing. *Polymers*, 11(11).

Colophon

This document was typeset using LaTeX, using the KOMA-Script class `scrbook`. The main font is Palatino.